AD-A040 669 PENNSYLVANIA STATE UNIV UNIVERSITY PARK APPLIED RESE--ETC F/G 13/13
ACOUSTIC FAIRING - AN APPLICATION TO BEAM REINFORCED PLATES.(U)
AUG 73 G F LIN N00017-73-C-1418
UNCLASSIFIED TM-73-196 NL

1 OF 2
AD
A040669

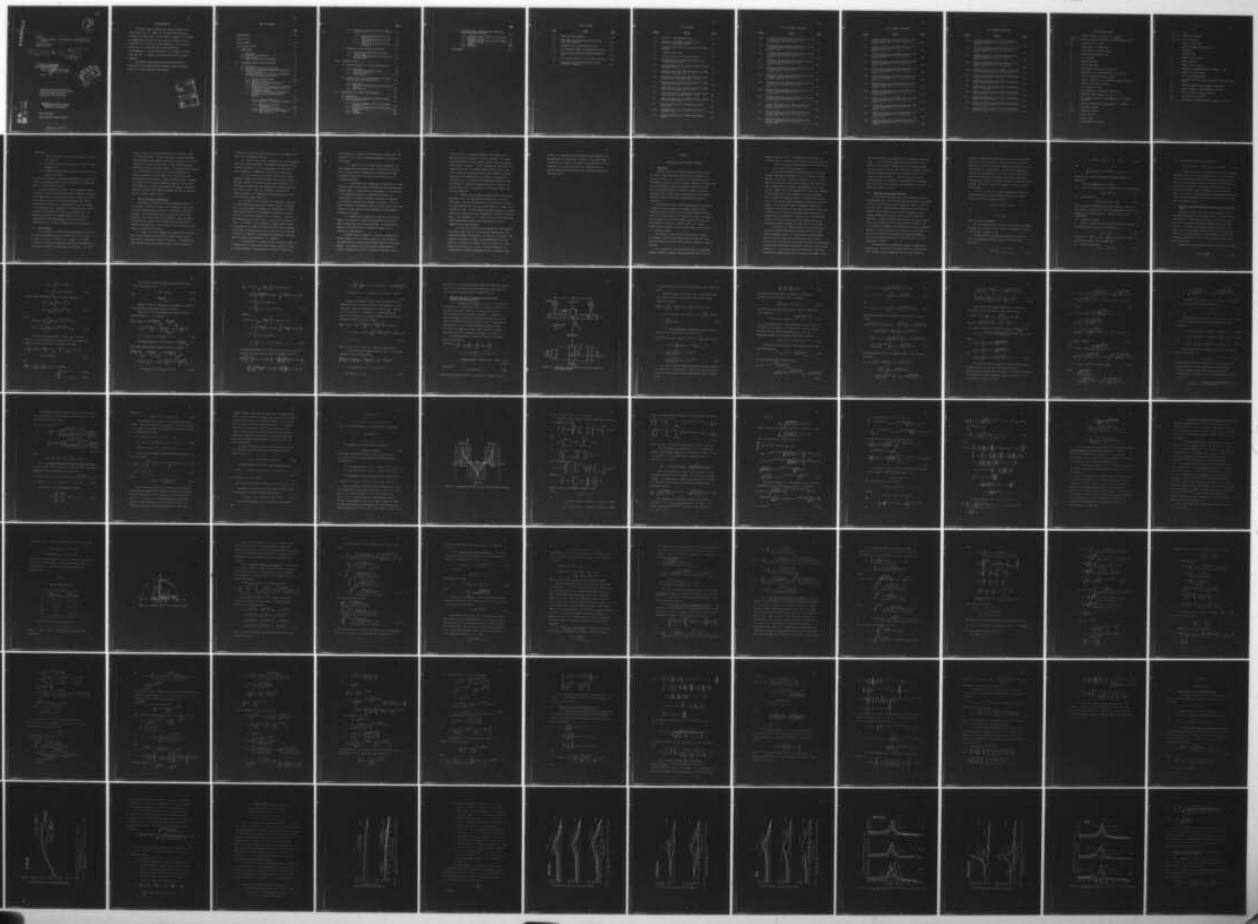

(2)

P. S.

(6) ACOUSTIC FAIRING - AN APPLICATION TO BEAM REINFORCED PLATES.

(10) Gau F. Lin

(9) Doctoral thesis,

(11) 23 Aug 73

(12) 178p.

(14) Technical Memorandum
~~File No.~~ TM-73-196
August 23, 1973
Contract No. N00017-73-C-1418
(15)
Copy No. 1

The Pennsylvania State University
Institute for Science and Engineering
APPLIED RESEARCH LABORATORY
University Park, Pennsylvania

APPROVED FOR PUBLIC RELEASE
DISTRIBUTION UNLIMITED

NAVY DEPARTMENT

NAVAL ORDNANCE SYSTEMS COMMAND

ACKNOWLEDGMENTS

The author wishes to express his sincere gratitude to his thesis advisor, Dr. S. I. Hayek, for his guidance and assistance throughout the entire study. He also wishes to thank Dr. J. M. Lawther for suggesting the problem, for his supervision during Dr. Hayek's sabbatical leave and for many helpful discussions. He also wishes to thank Dr. A. D. Stuart for many helpful discussions. Acknowledgments are also due to Professors V. H. Neubert, R. Vierck, N. Davids, and E. J. Skudrzyk for serving on the author's doctoral committee.

This study has been supported by the Applied Research Laboratory of The Pennsylvania State University under the contract with the U.S. Naval Ordnance Systems Command.

TABLE OF CONTENTS

Page

Page

LIST OF TABLES

LIST OF FIGURES

LIST OF FIGURES (CONTINUED)

LIST OF FIGURES (CONTINUED)

LIST OF FIGURES (CONTINUED)

LIST OF MAJOR SYMBOLS

D	bending stiffness of the plate ($D = \frac{Eh^3}{12(1-\nu^2)}$)
$H_o^{(1)}, (2)$	Hankel functions of first and second kind of degree zero
I_n	an integral (n = number)
J_o	Bessel function of degree zero
c	phase velocity of acoustic medium
F_o	amplitude of the applied force
h	plate thickness
i	imaginary unit $\sqrt{-1}$
k_o	acoustic wavenumber
m	mass density of the plate, per unit area
M	mass density of the attached beam, per unit length
p	acoustic pressure in the fluid medium
k_c	acoustic wavenumber at the classical coincidence frequency
r	radius in cylindrical coordinate
t	time variables, seconds
z	axial component in cylindrical coordinates
Ω	normalized radial frequency ($\Omega = \frac{\omega}{\omega_o}$)
ω	radial angular frequency, radians/second ($e^{-i\omega t}$ assumed throughout)
ω_o	classical coincidence radial frequency ($\omega_o = c^2\sqrt{M/D}$)
$\delta(x)$	Dirac delta function
k_x, k_y	bending wave numbers
E	Young's modulus
N	acoustic power
N_o	driving power of the plate

γ	$M/\rho_o h^2$
(R, ϕ, θ)	spherical coordinates
(r, θ, z)	polar coordinates
v	velocity of the plate
$\tilde{v}$	Fourier transform of plate velocity
ε	loss factor
ν	Poisson's ratio
ρ_o	density of fluid medium
ρ	density of plate
$\bar{\phi}$	fluid-velocity potential
σ	reciprocal of normalized radial frequency ($\sigma = \frac{1}{\Omega}$)
I, I_b	moment of inertia of beam
b	width of the attached beam
d	distance between spring-mass system and the attached beam at x=0
m_1	distributed mass per unit length in y-direction
k_1	uniform stiffness per unit length in y-direction
ϕ	testing function; velocity potential
c_p	plate velocity ($c_p = \sqrt{E/\rho}$)
I_j^o	non-dimensional integral defined in Chapter II (j=1,2,3)

CHAPTER I

INTRODUCTION

1.1 Background

The analysis of most marine structures has been known to be extremely complicated and difficult. Thus, it becomes essential for one to idealize marine structures by simple configurations so that an approximate and yet reasonable estimate of a ship's vibration and acoustic radiation can be made. For instance, the motion of a ship hull reinforced by the framing elements can be qualitatively treated as that of a plate or a shell reinforced by beam or ring elements. Likewise, a vibrating machine mounted on the beam of a ship hull can be idealized as a time-harmonic point force excitation on a beam-reinforced plate.

Vibrating machines have been known to be supported by foundations attached to the reinforcing beams of a ship hull. This is obviously dictated by the necessity of providing a good structurally strong member to distribute the static load of the machine. This procedure of attaching machinery to reinforcing beams has proven to be an effective method for reducing the hull vibration and the resulting radiated noise. This is due to the fact that the impedance termination, as seen by the machine, is higher when it is attached to reinforcing beam than when attached to the softer ship plating. The reduction in the radiated noise when a vibrating machine is attached to the reinforcing beam rather than the

plate has not been analytically proven, though it has been intuitively known and shown in some experimental studies.

In order to achieve a reduction in the radiated noise from reinforced plates and shells, it is proposed to attach suitably chosen and judiciously located discontinuities in the proximity of reinforcement, either to effect sources' mutual destructive interference or to change the acoustic character of the sources. This new approach will be referred to as "Acoustic Fairing." It is anticipated that the radiated noise from a structure with a structural discontinuity would be influenced by the application of acoustic fairing.

To effect a reduction of the radiated noise from structures with structural discontinuities by the application of acoustic fairing, one must first obtain a better understanding of the role a structural discontinuity plays in the radiated noise from reinforced structures. Thus, one must obtain estimates of the radiated noise from a representative structure with a typical structural discontinuity such as a plate reinforced by a beam. And then, the method of "Acoustic Fairing" can be applied to that structure.

1.2 Statement of the Problem

For the exploration of the essential physical features of the "Acoustic Fairing" studies, two specific, typical problems are investigated within this thesis.

The first problem is to investigate the radiated noise from an infinite elastic plate reinforced by an infinite beam excited by a time-harmonic point force located on the beam. An attached beam can be considered to act as a structural discontinuity of the

following type:

(1) a mass discontinuity, which will normally act as a line mass impedance,

(2) an elastic discontinuity which acts as a path of energy propagation, and

(3) a beam-like discontinuity which acts as an elastic as well as mass discontinuity.

The theoretical derivation and numerical computations of this problem provide the background material for the assessment of radiated noise due to a coupled beam-plate system.

The second problem is to devise a simple mathematical model of acoustic fairing by attaching an additional infinitely long, line spring-mass system to the left and the right of the beam and to study their interaction with the existing attached beam. The radiated sound pressure and power from a beam-reinforced plate are computed for various values of the sprung mass, the spring stiffness and the distance of the systems with respect to the attached beam. The analytic solution for this problem together with the numerical computations yields an understanding of the role the physical parameters play in a successful application of acoustic fairing.

1.3 Basic Approach

The derivation of a single governing differential equation for the basic beam-reinforced plate is partially based on the works of G. Lamb, Jr. [1] and E. E. Ungar [2]. It begins with writing, separately, the equations representing the flexural displacements of a beam and a thin plate from their equilibrium positions. The fluid

pressure acting on the beam-reinforced plate is expressed in terms of a velocity potential. By employing Fourier transform techniques, taking advantage of the symmetry property and by making the reasonable assumption of a narrow attached beam, a single coupled governing differential equation is finally obtained. The integral representations of the sound pressure and power are set up by substituting the continuity equation at the interface of fluid and plate into the governing differential equation. Again, integral transform techniques are employed on the governing differential equation. The far-field acoustic pressure is obtained with the help of asymptotic techniques. Numerical solutions for the radiated pressure and power are made with the aid of digital computer IBM 370.

1.4 Review of Previous Investigations

The studies of vibration and acoustic radiation properties of isotropic, homogeneous structures such as membranes, plates, and shells have been extensively carried out in the field of structural acoustics. Many publications, related to this area of structural acoustics, can be easily found in the literature. Thus, the review of this section is confined only to those papers dealing with the effects of discontinuities or non-uniformities on the vibration of and acoustic radiation from structures.

G. L. Lamb, Jr. [1] has analyzed the vibration of an infinite elastic beam attached to an acoustically unloaded infinite elastic plate which is excited by an harmonic point force. He expressed the input impedance of the beam reinforced plate in terms of degree of

coupling of the beam to the plate and the ratio of wavelength in the plate to the wavelength in the bar.

E. E. Ungar [2] has studied the transmission of plate flexural waves across reinforcing beams. He developed the equations for the beam-plate interaction in vacuo and expressed the plate motion in terms of reflection, transmission, and near-field coefficients.

In R. Lyon's work [3] on the sound radiation from a beam-reinforced infinite, thin plate, he computed the acoustic radiation resistance caused by an incident flexural wave in the plate. He used Ungar's results [2] for the reflected and transmitted amplitude for a plate in vacuo. Thus, the influence of the near-field acoustic pressure on the reflectivity and transmissibility of the attached beam was totally neglected.

E. L. Shenderov [4] has obtained the transmission coefficient of sound through a thin plate with interjacent supports. He found that, for certain angles of incidence of a sound wave on the plate, a substantial decrease of the transmission coefficient will result and that the acoustic transmissibility of structures is smaller at low frequencies than at high, which is valid because the supports are rigid. D. D. Plakhov [5] has considered a similar problem; namely, the transmission of a plane sound wave through an infinite laminated ribbed plate. He claimed that when the mass of the ribs is increased to infinity, the results of calculating the transmission coefficient agree with the results published by E. L. Shenderov.

I. I. Klyukin and Y. D. Sergeev [6] have studied the problem of a flexural wave in a plate without fluid loading scattered by point antivibration systems. They showed that the radius of influence of

the antivibrator, inside which the attenuation is greater than 3 dB, is about 0.3 to 0.4 times the flexural wavelength in the plate for antivibrators.

V. T. Lyapunov [7] has discussed the wave propagation in a liquid-loaded plate with an obstruction. He has shown in this work that the energy transfer through the liquid depends on the angle of incidence of the wave and the ratio of its frequency to the coincidence frequency.

I. P. Konovalguk [8] has investigated the reflection of a plane sound wave from an elastic plate reinforced with many infinitely long stiffness members. He mentioned that the dependence of the potential on the impedances of each rib, in transverse and rotational vibration mode, has a distinct resonance character; the sharpness of the resonance depends on the thickness of the plate. Also, the flexural impedance of each member plays an important part in the total reflection of sound from the plate, especially for large angles of incidence on the plate.

V. N. Romanov [9] has analyzed the influence of reinforcing beams on the radiation of sound by an infinite plate driven by a field of random line forces between the beams. He showed that the pressure of the beams yields a considerable increase in the radiation at low frequencies.

G. Maidanik and E. M. Kerwin, Jr. [10] have considered the acoustic radiation from an infinite orthotropic plate and from the multipanel-structure, including fluid-loading effects and structural damping. They pointed out that heavy fluid loading reduces the acoustic radiation from a point- or line-driven orthotropic plate.

It also shifts the resonance frequencies of the panels in the multipanel structures downward. Structural damping, if it exceeds radiation damping, can reduce acoustic radiation from free-wave and panel-resonance responses. In their considerations, they dealt with average values only, for instance, under the assumption that when a typical spacing of the ribs is smaller than the flexural wavelength in the plate, the ribbed plate is considered as a homogeneous, orthotropic plate. And when they discussed the radiation efficiency of the panels, a statistical approach was adopted. Therefore, the specific effects of the individual ribs on the sound radiation was not fully understood.

E. S. Jarmul [11] has studied the sound radiation from simple and ribbed plates. He experimentally verified that a structural discontinuity, such as a stiffening rib in a finite plate, increases the sound radiation from such a plate when excited by a randomly time varying point force. He also indicated that one component of the sound radiation of a finite plate can be attributed to a Helmholtz resonator effect. This component, as D. S. Pallett [12] put it, may arise under certain circumstances because of the interaction of the force component and the edge component.

M. S. Howe and M. Heckl [13] have examined the sound radiation from infinite plates due to the interaction of bending waves with density and stiffness fluctuations in the material of the plate. They regarded the variation in density and bending stiffness as random functions of position on the plate. They also assumed that for low frequency excitation, i.e., below the coincidence frequency, the random density and bending stiffness constitute a stationary random

process. They concluded that the radiation losses brought about by the phenomenon of scattering due to density and bending-stiffness fluctuations are relatively very small at low frequencies, but are comparable to loss factors caused by other mechanisms such as internal damping and energy transfer into supporting structures at high frequencies.

CHAPTER II

MATHEMATICAL MODEL OF ACOUSTIC FAIRING

2.1 Assumptions

The basic, specific structure considered in this thesis is an infinite fluid loaded plate reinforced with an infinite beam excited by a point force. Of course, it is known that infinite plate-beam systems do not exist in reality. However, the justification for considering the plate and the beam to be of infinite extent lies in the assumption that the structural damping of the beam-reinforced plate is sufficient to render boundary-reflected waves negligible compared to the waves propagating from the point of excitation.

Throughout this study, it will be assumed that the plate and the beam are thin, homogeneous and isotropic, and obey linear constitutive equations [14]. For the structure (plate and beam), stress is a linear function of the strain, which will be considered much less than unity, and for the fluid, pressure deviations from the hydrostatic pressure are a linear function of the density change, and thus acoustic pressure is just a small variation from the hydrostatic pressure.

Since acoustic motions in the inviscid fluid are always irrotational, even if viscosity effects are considered [15], the problem of wave motion in the fluid thus can be solved by a velocity potential.

At the interface of the structure and fluid, the fundamental boundary condition is given by equating the normal velocity of the

plate to that of the fluid. No conditions are enforced on the tangential velocity component in front of the thin viscous layer at the boundaries for the case of small-amplitude periodic motion, this thin layer acts like an ideal lubricant [16].

In most physical problems posed properly by a set of given boundary conditions, there would exist only one physical solution. However, in some cases, so-called "paradoxes" occur; i.e., it may appear that there exists more than one solution. For instance, the path of integration in the integral representation of a solution may pass through a pole of the integrand on the real axis, resulting in an unbounded value for the integral in the strict Riemanian sense. Although the integral may exist in Cauchy-Principle-value sense, it does not necessarily represent the solution of a physical problem. This situation is often a consequence of unrealistic assumptions, usually made when the complete equations have been found too difficult to solve, and an approximate,oversimplified set of equations has been substituted. In dealing with such difficulties, the physical system is often assumed to be damped, and then the solution is obtained by taking a limiting value of zero damping.

In this thesis, the classical plate equation will be used to develop the governing differential equations of the point force excited beam-plate system. As is well known, the classical plate equation does not account for shear and rotary inertia effects. Though it may not be accurate for the high frequencies, it nevertheless will adequately illustrate the analytical formulation and the physical phenomena [17]. The width of the attached beam and/or distributed masses will be assumed smaller than the flexural wave length so that

they can be considered as mathematically concentrated stiffness and masses. The formulated governing differential equations for the vibration of and acoustic radiation from a beam-reinforced plate excited by a point force are those involving the singularity functions. The desired generalized solutions will be obtained by the use of integral transform techniques. These solutions are valid for distributed masses and stiffnesses, distributed over a vanishingly small width, but can be considered as good approximate solutions to a thin beam attached to a plate.

2.2 Classical and Generalized Solutions

The solutions of boundary value problems which are assumed to be sufficiently smooth and to satisfy the equation at each point inside the region of definitions of these problems are termed as "classical solutions" [18]. Physical phenomena involving discontinuities which characterize the intensity of the external perturbation can be treated conveniently and directly by the use of the singularity functions. In order to formulate these problems, one must not always insist on the smoothness of the solution inside the region. Thus, it is necessary to introduce the "generalized functions" to generalize the idea of a derivative and idea of a function. The solutions of the physical problems involving singularity functions obtained by the use of generalized functions (or distributions) are called "generalized solutions."

The foundations of the mathematical theory of generalized functions were laid by Dirac [19] and developed by Laurent Schwartz [20]. Viewing the narrow application for the class of analytic

functions, Schwartz has extended the concept of classical functions and proposed a method called the "Theory of Distributions" which justifies not only the use of the δ-function, but also the use of all derivatives of the δ-function [21]. He considered a generalized function (or a distribution) as a continuous linear functional on the space of testing functions which are continuous, have continuous derivatives of all orders, and vanish identically outside some finite interval. In order to clarify this thought, one needs to define the following:

(i) $F(\phi)$ is said to be a linear functional on the space of testing functions if, to every testing function $\phi(x)$, a real or complex number $F(\phi)$ is assigned such that

$$F(\phi_1 + \phi_2) = F(\phi_1) + F(\phi_2)$$

and

$$F(\lambda\phi) = \lambda F(\phi) \quad ,$$

where λ is any complex number.

(ii) A functional $F(\phi)$ is said to be continuous if the sequence of numbers $F(\phi_n)$ converges to zero, whenever the sequence of testing functions $\phi_n(x)$ converges to zero.

The following are some important properties of a specific family of singularity functions [22] which are conventionally expressed as:

$$H(x) = \begin{cases} 0 \ , & \text{for } x < 0 \\ 1 \ , & \text{for } x > 0 \ , \end{cases} \qquad (2.1)$$

$$H^{n+1}(x) = \delta^n(x) = 0 \quad \text{if} \quad x \neq 0 \tag{2.2}$$

and

$$\int_{-\infty}^{\infty} \delta^n(x)\, f(x)\, dx = (-1)^n\, f^{(n)}(0) \quad , \quad n=0,1,2,\ldots, \tag{2.3}$$

where $f(x)$ is a function possessing the requisite number of derivatives.

Some useful properties of δ-function:

(1) A delta (δ) function acts as a derivative of a unit step function

$$\delta(x) = \frac{d}{dt}\{H(x)\} \tag{2.4}$$

(2) Sifting property

$$\int_{-\infty}^{\infty} f(x)\, \delta(x-x_o)\, dx = f(x_o) \tag{2.5}$$

This is the most important property of the δ-function. Note that this property is satisfied for all $f(x)$ independent of the fact that $f(x)$ has to be a testing function. However, $f(x)$ has to be differentiable.

(3) Equivalence property

Let $\Delta_1(x)$ and $\Delta_2(x)$ be two expressions involving δ-functions and ordinary space functions; then by definition,

$$\Delta_1(x) = \Delta_2(x) \quad , \tag{2.6}$$

if and only if $\int_{-\infty}^{\infty} f(x)\, \Delta_1(x)\, dx = \int_{-\infty}^{\infty} f(x)\, \Delta_2(x)\, dx$ for all space functions $f(x)$ for which the integrals exist.

(4) Even and odd property

$$\delta^n(x) = (-1)^n\, \delta^n(-x) \ . \tag{2.7}$$

(5) Higher order δ-function sifting property

$$\int_{-\infty}^{\infty} \delta^n(x)\ f(x)\ dx = (-1)^n\ f^n(x)\Big|_{x=0} = (-1)^n\ f^n(0) \quad . \qquad (2.8)$$

To summarize this section, generalized functions can be handled algebraically as if they were ordinary functions, provided that their use can be justified by recourse to their functional representation. Also, it is to be understood that if an equation involving generalized functions is multiplied by an arbitrary continuous function f(x), which has a sufficient number of derivatives, and then integrated from $-\infty$ to ∞, with the functional property of the generalized functions used to evaluate the integrals, the result will be a correct equation involving ordinary functions.

2.3 Derivation of Governing Differential Equation for a Beam-Plate System

Consider an infinite thin elastic plate, Figure (2.1),with a thickness h and density ρ lying in the plane z=0. The top half-space of the plate $z < 0$ is a vacuum, while the bottom half-space of the plate $z > 0$ is occupied by an acoustic fluid of density ρ_o, sound velocity c. An infinitely long beam is attached on the top of the plate at x=0. A time-harmonic point force $F_o e^{-i\omega t}\ \delta(y)$ is excited on the top of the beam, where F_o is the amplitude of the force, δ(y) is the Dirac delta function, and ω is the circular frequency of the harmonic excitation.

Starting with the wave equation for the fluid velocity potential, $\bar{\phi}$,

$$\nabla^2\bar{\phi} = \frac{1}{c^2}\ \frac{\partial^2\bar{\phi}}{\partial t^2} \quad , \qquad (2.9)$$

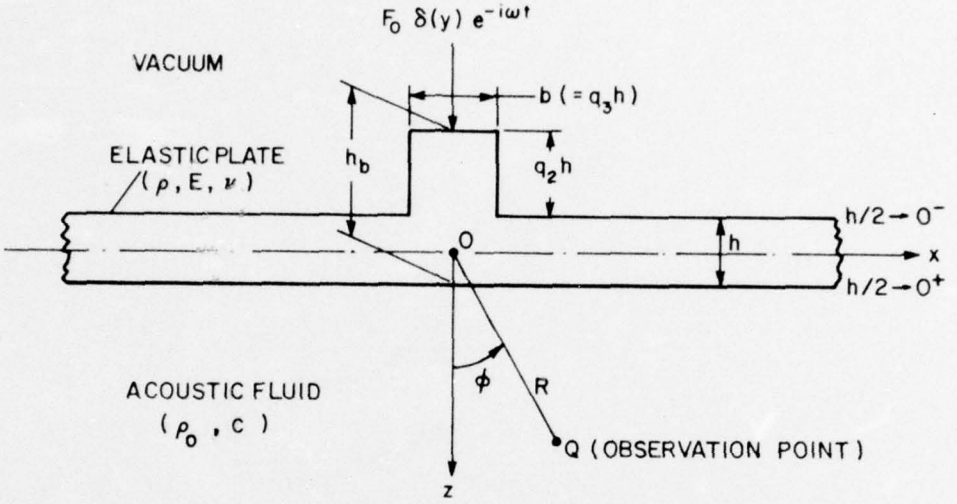

SECTION A-A

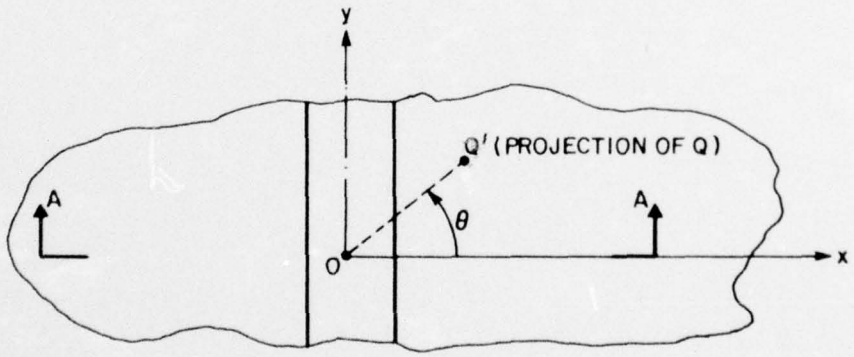

TOP VIEW

Figure 2.1 Geometry of Beam-Reinforced Plate

letting $\bar{\phi} = \phi e^{-i\omega t}$, and using the rectangular coordinate (x, y, z), Equation (2.9) can be written as follows:

$$\frac{\partial^2\phi}{\partial x^2} + \frac{\partial^2\phi}{\partial y^2} + \frac{\partial^2\phi}{\partial z^2} + k_o{}^2\phi = 0 \quad , \tag{2.10}$$

where $k_o = \omega/c$ (acoustic wave number).

The pressure can be obtained from the fluid velocity potential

$$p(x, y, z, t) = \rho_o \frac{\partial\bar{\phi}}{\partial t} = - i\omega\rho_o e^{-i\omega t} \phi \ . \tag{2.11}$$

Denoting the transverse displacements of the reinforcing beam and the plate by $\bar{U}(y, t)$ and $\bar{W}(x, y, t)$, the coupled differential equation of motion for the beam becomes [1]:

$$EI_b \frac{\partial^4\bar{U}}{\partial y^4} + M_b \frac{\partial^2\bar{U}}{\partial t^2} = - D\left[\frac{\partial}{\partial x} \nabla^2 \bar{W}\Big|_{x=0^+} - \frac{\partial}{\partial x} \nabla^2 \bar{W}\Big|_{x=0^-}\right] + F_o e^{-i\omega t}\delta(y) - bp, \tag{2.12}$$

where I_b = moment of inertia of the beam = $1/12\ bh_b^3$, see Figure 2.1,

M_b = total mass of the beam = ρbh_b ,

D, E, F_o and p were given earlier. The bracketed terms in Equation (2.12) represent the shear force applied by the plate on the beam.

The equation of motion of a plate coupled to an acoustic medium can be written as follows:

$$D\left[\frac{\partial^4\bar{W}}{\partial x^4} + 2 \frac{\partial^4\bar{W}}{\partial x^2 \partial y^2} + \frac{\partial^4\bar{W}}{\partial y^4}\right] + m \frac{\partial^2\bar{W}}{\partial t^2} = - p \ , \quad \text{for} \begin{cases} \frac{b}{2} < x < \infty & (2.13a) \\ -\infty < x < -\frac{b}{2} \ . & (2.13b) \end{cases}$$

Let us define the Fourier cosine transform pairs in one dimension x by

$$f_c(k_x') = \int_0^\infty f(x) \cos k_x' x \, dx$$

$$f(x) = \frac{2}{\pi} \int_0^\infty f_c(k_x') \cos k_x' x \, dk_x' \quad , \tag{2.14}$$

and the Fourier transform pairs for one and two dimensions by

$$\tilde{f}(k_x) = \frac{1}{\sqrt{2\pi}} \int_{-\infty}^{\infty} f(x) \, e^{-ik_x x} \, dx$$

$$f(x) = \frac{1}{\sqrt{2\pi}} \int_{-\infty}^{\infty} \tilde{f}(k_x) \, e^{ik_x x} \, dk_x \quad , \tag{2.15}$$

and

$$\tilde{f}(k_x, k_y) = \frac{1}{2\pi} \int_{-\infty}^{\infty} \int_{-\infty}^{\infty} f(x, y) \, e^{-ik_x x} \, e^{-ik_y y} \, dx \, dy$$

$$f(x, y) = \frac{1}{2\pi} \int_{-\infty}^{\infty} \int_{-\infty}^{\infty} \tilde{f}(k_x, k_y) \, e^{ik_x x} \, e^{ik_y y} \, dk_x \, dk_y \quad . \tag{2.16}$$

Differentiating Equations (2.12), (2.13a) and (2.13b) with respect to time t and removing the time factor $e^{-i\omega t}$, one obtains the flexural velocities of the beam and the plate as follows:

$$EI_b \frac{\partial^4 u}{\partial y^4} - \omega^2 M_b u = - D \left[\frac{\partial}{\partial x} \nabla^2 v \Big|_{x=0^+} - \frac{\partial}{\partial x} \nabla^2 v \Big|_{x=0^-} \right] - i\omega F_o \, \delta(y)$$

$$+ b \, \rho_o \, \omega^2 \, \phi(z=0) \tag{2.17}$$

and

$$D\left(\frac{\partial^4 v}{\partial x^4} + 2 \frac{\partial^4 v}{\partial x^2 \partial y^2} + \frac{\partial^4 v}{\partial y^4} \right) - \omega^2 m v = \rho_o \, \omega^2 \, \phi(z=0) \quad ,$$

$$\text{for} \begin{cases} \frac{b}{2} < x < \infty & (2.18a) \\ -\infty < x < -\frac{b}{2} \quad . & (2.18b) \end{cases}$$

The continuity equations between beam and plate along the line of their juncture are:

$$u(y) = v(x=0, y) \tag{2.19}$$

and

$$\left.\frac{\partial v(x, y)}{\partial x}\right|_{x=0} = 0 \quad . \tag{2.20}$$

Equation (2.20) is a consequence of the symmetrical property of the beam-plate configuration and the drive force.

Applying Fourier cosine transform for Equation (2.18a) on x for the range $\frac{b}{2} < x < \infty$, one obtains:

$$D\left[k_x'^4\, v_c(k_x', y) + k_x'^2 \left.\frac{\partial v(x, y)}{\partial x}\right|_{x=0^+} - \left.\frac{\partial^3 v(x, y)}{\partial x^3}\right|_{x=0^+} + 2\left(-k_x'^2 \frac{d^2 v_c(k_x', y)}{dy^2} - \left.\frac{\partial^3 v(x, y)}{\partial x\, \partial y^2}\right|_{x=0^+}\right) + \frac{d^4 v_c(k_x', y)}{dy^4}\right]$$

$$- \omega^2 m\, v_c(k_x', y) = \rho_o \omega^2 \phi_c(k_x', y, z = 0) \quad . \tag{2.21}$$

Rearranging Equation (2.21) and noting that $\left.\frac{\partial^3 v(x, y)}{\partial x\, \partial y^2}\right|_{x=0} = 0$, which can be deduced from the Equation (2.20), one obtains

$$D\left[\left.\frac{\partial^3 v(x, y)}{\partial x^3}\right|_{x=0^+} + \left.\frac{\partial^3 v(x, y)}{\partial x\, \partial y^2}\right|_{x=0^+}\right] = D\left[\left.\frac{\partial^3 v(x, y)}{\partial x^3}\right|_{x=0^+}\right]$$

$$= D\left[k_x'^4\, v_c(k_x', y) - 2\, k_x'^2 \frac{d^2 v_c(k_x', y)}{dy^2} + \frac{d^4 v_c(k_x' y)}{dy^4}\right]$$

$$- \omega^2 m\, v_c(k_x', y) - \rho_o \omega^2 \phi_c(k_x', y, z = 0) \tag{2.22}$$

or

$$D \frac{\partial}{\partial x} \nabla^2 \, v(x, y)\Big|_{x=0^+} = D\Bigg[k_x'^4 \int_{0^+}^{\infty} v(x, y) \cos k_x' x \, dx - 2k_x'^2 \int_{0^+}^{\infty} \frac{\partial^2 v(x, y)}{\partial y^2} \cos k_x' x \, dx + \int_{0^+}^{\infty} \frac{\partial^4 v(x, y)}{\partial y^4} \cos k_x' x \, dx\Bigg] - \omega^2 m \int_{0^+}^{\infty} v(x, y) \cos k_x' x \, dx - \rho_o \omega^2 \int_{0^+}^{\infty} \phi(x, y, z = 0) \cos k_x' x \, dx \quad . \tag{2.23}$$

Similarly,

$$- D \frac{\partial}{\partial x} \nabla^2 v(x, y)\Big|_{x=0^-} = D\Bigg[k_x'^4 \int_{-\infty}^{0^-} v(x, y) \cos k_x' x \, dx - 2 k_x'^2 \int_{-\infty}^{0^-} \frac{\partial^2 v(x, y)}{\partial y^2} \cos k_x' x \, dx + \int_{-\infty}^{0^-} \frac{\partial^4 v(x, y)}{\partial y^4} \cos k_x' x \, dx\Bigg] - \omega^2 m \int_{-\infty}^{0^-} v(x, y) \cos k_x' x \, dx - \rho_o \omega^2 \int_{-\infty}^{0^-} \phi(x, y, z = 0) \cos k_x' x \, dx \quad . \tag{2.24}$$

Substituting Equations (2.23) and (2.24) into Equation (2.17), one obtains a universal beam-plate coupled differential equation:

$$D\Bigg[k_x'^4 \Bigg\{\Bigg(\int_{-\infty}^{0^-} + \int_{0^+}^{\infty}\Bigg) v(x, y) \cos k_x' x \, dx\Bigg\} - 2k_x'^2 \Bigg\{\Bigg(\int_{-\infty}^{0^-} + \int_{0^+}^{\infty}\Bigg) \frac{\partial^2 v(x, y)}{\partial y^2} \cos k_x' x \, dx\Bigg\} + \Bigg(\int_{-\infty}^{0^-} + \int_{0^+}^{\infty}\Bigg) \frac{\partial^4 v(x, y)}{\partial y^4} \cos k_x' x \, dx\Bigg] - \omega^2 m \Bigg(\int_{-\infty}^{0^-} + \int_{0}^{\infty}\Bigg) v(x, y) \cos k_x' x \, dx$$

$$- \rho_o \omega^2 \left(\int_{-\infty}^{0^-} + \int_{0^+}^{\infty} \right) \phi(x, y, z = 0) \cos k_x' x \, dx = - EI_b \frac{\partial^4 v(x = 0, y)}{\partial y^4}$$

$$+ \omega^2 M_b \, v(x = 0, y) - i\omega F_o \, \delta(y) + b \rho_o \omega^2 \phi(x, y, z = 0) \, . \tag{2.25}$$

Because the structure, fluid pressure, and excited force are symmetrical about x=0, Equation (2.25) can be expressed in terms of the Fourier transform by multiplying both sides by $\frac{1}{\sqrt{2\pi}}$. Moreover, due to the fact that the dimension b is a comparatively small quantity and that there is no torsion existing along the beam, one can simplify Equation (2.25) as follows

$$D\left[k_x^4 \tilde{v}(k_x, y) - 2k_x^2 \frac{d^2 \tilde{v}(k_x, y)}{dy^2} + \frac{d^4 \tilde{v}(k_x, y)}{dy^4}\right] - \omega^2 m \tilde{v}(k_x, y)$$

$$- \rho_o \omega^2 \tilde{\phi}(k_x, y, z = 0) = \frac{1}{\sqrt{2\pi}} \left[- EI \frac{\partial^4 v(x = 0, y)}{\partial y^4} + \omega^2 M v(x = 0, y) \right.$$

$$\left. - i\omega F_o \, \delta(y) \right] \, , \tag{2.26}$$

where $EI = EI_b - bD$, $M = M_b - bm$, and k_x' is replaced by k_x.

It can be easily verified that Equation (2.26) is the Fourier transform of the following equation:

$$D\left[\frac{\partial^4 v(x, y)}{\partial x^4} + 2\frac{\partial^4 v(x, y)}{\partial x^2 \partial y^2} + \frac{\partial^4 v(x, y)}{\partial y^4}\right] + \delta(x) \, EI \frac{\partial^4 v(x, y)}{\partial y^4}$$

$$- \omega^2 [m + M \delta(x)] \, v(x, y) = - i\omega F_o \, \delta(x) \, \delta(y)$$

$$+ \rho_o \omega^2 \phi(x, y, z = 0) \, . \tag{2.27}$$

Equation (2.27) represents the coupled beam-plate differential equation which will be used to develop the governing differential equation for the acoustic fairing problem in subsequent sections.

2.4 Far-Field Pressure of the Beam-Plate System with Two Additional Spring-Mass Systems

2.4.1 Statement of the Problem. By providing two additional spring-mass systems symmetrically about x=0 as shown in Figure 2.2, the governing differential equation for the whole system will be, of course, different from that derived in Section 2.3. However, the desired differential equation for this simple idealized model can be obtained by modifying the previous equation without resorting to the rederivation of the new coupled plate-beam-sprung masses system. This can be done because the chosen simple model for the sprung masses does not involve complicated couplings with the plate.

The following differential equations represent the coupled motion for this problem:

(beam-plate):

$$D\frac{\partial^4\bar{W}}{\partial x^4} + 2D\frac{\partial^4\bar{W}}{\partial x^2\partial y^2} + D\frac{\partial^4\bar{W}}{\partial y^4} + \delta(x)\ EI\frac{\partial^4\bar{W}}{\partial y^4}$$

$$+ [m + M\,\delta(x)]\frac{\partial^2\bar{W}}{\partial t^2} = F_o\, e^{-i\omega t}\,\delta(x)\,\delta(y)$$

$$+ k_1(\bar{W}_1-\bar{W})\,\delta(x+d) + k_1(\bar{W}_1-\bar{W})\,\delta(x-d) - p(x, y, z = 0). \tag{2.28}$$

(spring-mass):

$$m_1\ddot{\bar{W}}_1 + k_1(\bar{W}_1-\bar{W}) = 0\ , \tag{2.29}$$

where $\bar{W}_1$ represents the motion of the mass M_1, see Figure 2.2, k_1 is

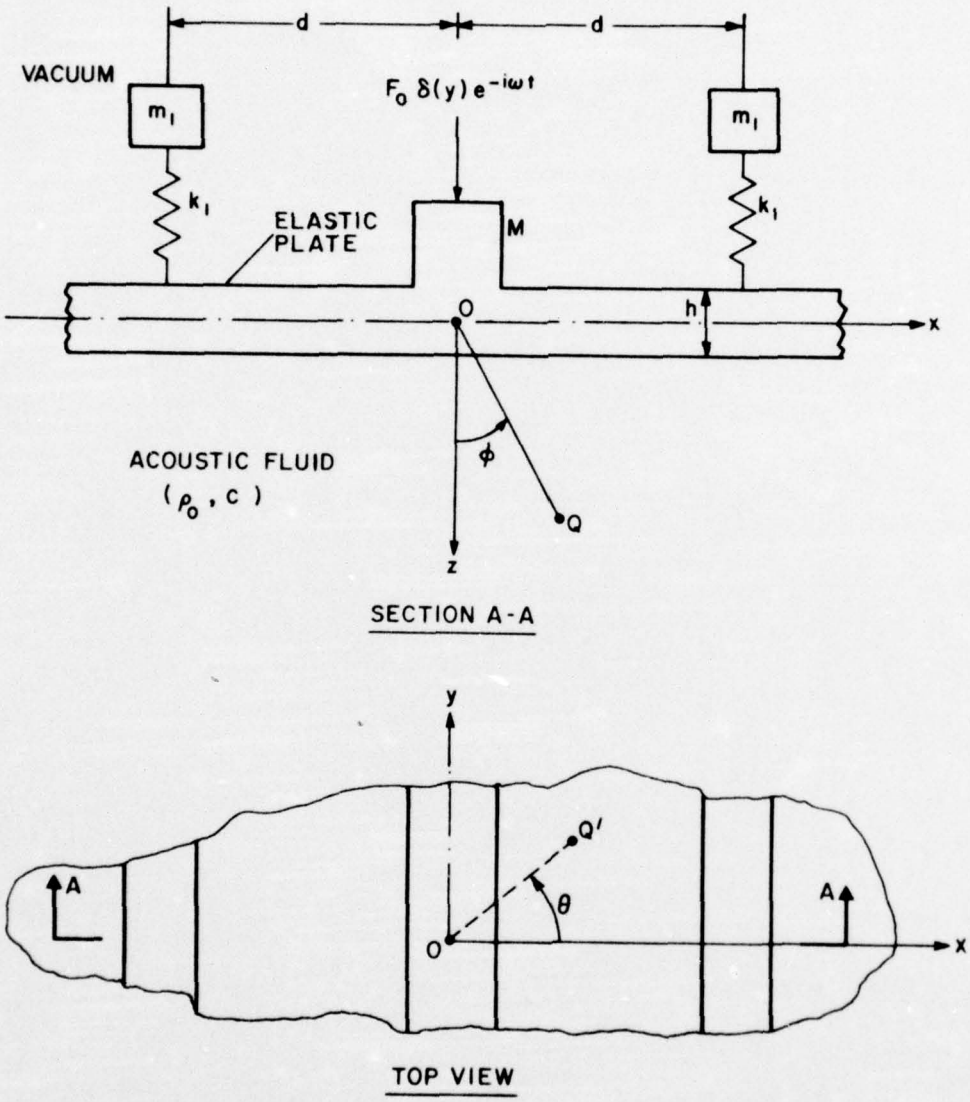

Figure 2.2 Geometry of Beam-Reinforced Plate with Two Additional Spring-Mass Systems

the spring constant and d is half the separation distance between the masses.

Combining Equations (2.28) and (2.29), and differentiating the result with respect to time t, one obtains the following differential equation:

$$D\left[\frac{\partial^4 v}{\partial x^4} + 2\,\frac{\partial^4 v}{\partial x^2\,\partial y^2} + \frac{\partial^4 v}{\partial y^4}\right] + \delta(x)\ EI\ \frac{\partial^4 v}{\partial y^4} - \omega^2[m + M\,\delta(x)]\ v$$

$$= -i\omega\ F_o\ \delta(x)\ \delta(y) + \rho_o\ \omega^2\ \phi(x,\ y,\ z = 0) + \frac{k_1\ \omega^2}{\omega_1^2 - \omega^2}\ v\ \delta(x+d)$$

$$+ \frac{k_1\ \omega^2}{\omega_1^2 - \omega^2}\ v\ \delta(x-d) \quad . \tag{2.30}$$

2.4.2 General Solutions. Applying the Fourier transform on variables x and y of Equation (2.30), one can get

$$D[(-ik_x)^4\ \tilde{v} + 2(-ik_x)^2\ (-ik_y)^2\ \tilde{v} + (-ik_y)^4\ \tilde{v}] + \frac{EI}{\sqrt{2\pi}}\ (-ik_y)^4\ \tilde{v}(x=0,\ k_y)$$

$$- \omega^2\ m\ \tilde{v} - \frac{\omega^2\ M}{\sqrt{2\pi}}\ \tilde{v}(x=0,\ k_y) = -\frac{i\omega\ F_o}{2\pi} + \rho_o\ \omega^2\ \tilde{\phi}$$

$$+ \frac{1}{\sqrt{2\pi}}\left(\frac{k_1\ \omega^2}{\omega_1^2 - \omega^2}\right)\tilde{v}(x = -d,\ k_y)\ e^{ik_x d}$$

$$+ \frac{1}{\sqrt{2\pi}}\left(\frac{k_1\ \omega^2}{\omega_1^2 - \omega^2}\right)\tilde{v}(x = d,\ k_y)\ e^{-ik_x d} \quad . \tag{2.31}$$

In order to solve the complete problem, the velocity potential will prove to be a convenient tool. Starting with the wave equation on the velocity potential for the acoustic medium, given in Equation (2.10),

$$\frac{\partial^2\phi}{\partial x^2} + \frac{\partial^2\phi}{\partial y^2} + \frac{\partial^2\phi}{\partial z^2} + k_o^2\,\phi = 0 \qquad (2.10)$$

and applying the double Fourier transform on the independent variables x and y of Equation (2.10), one obtains:

$$\frac{d^2\tilde{\phi}}{dz^2} + (k_o^2 - k_x^2 - k_y^2)\tilde{\phi} = 0 \quad . \qquad (2.32)$$

The solution of the differential Equation (2.32) for outgoing waves can be written as:

$$\tilde{\phi}(k_x, k_y, z) = A(k_x, k_y)\, e^{iz\sqrt{k_o^2 - k_x^2 - k_y^2}} \quad . \qquad (2.33)$$

For the determination of the coefficient A, one must solve for $\frac{d\tilde{\phi}(k_x, k_y, z = 0)}{dz}$, $\tilde{\phi}(k_x, k_y, z = 0)$, $\tilde{v}(x=0, k_y)$, and $\tilde{v}(x = \pm d, k_y)$, and then substitute these into Equation (2.31). Thus, the transformed potential at the surface of the plate is given by:

$$\tilde{\phi}(k_x, k_y, z = 0) = A(k_x, k_y) \quad . \qquad (2.34)$$

Using the continuity condition of the normal velocity at the plate-fluid interface,

$$v(x, y, z = 0) = - \left.\frac{\partial\phi(x, y, z)}{\partial z}\right|_{z=0} \quad , \qquad (2.35)$$

the following transformed equations results:

$$\tilde{v}(k_x, k_y, z = 0) = - \left.\frac{d\tilde{\phi}(k_x, k_y, z)}{dz}\right|_{z=0}$$

$$= -Ai\sqrt{k_o^2 - k_x^2 - k_y^2}\; e^{iz\sqrt{k_o^2 - k_x^2 - k_y^2}}\Big|_{z=0} = -Ai\sqrt{k_o^2 - k_x^2 - k_y^2}\,, \qquad (2.36)$$

$$\tilde{v}(x, k_y, z = 0) = -\frac{1}{\sqrt{2\pi}} \int_{-\infty}^{\infty} Ai\sqrt{k_o^2-k_s^2-k_y^2}\, e^{ik_s x}\, dk_s \quad , \tag{2.37}$$

$$\tilde{v}(x = 0, k_y, z = 0) = -\frac{i}{\sqrt{2\pi}} \int_{-\infty}^{\infty} A(s, k_y)\sqrt{k_o^2-s^2-k_y^2}\, ds \tag{2.38}$$

and

$$\tilde{v}(x = \pm d, k_y, z = 0) = \frac{-i}{\sqrt{2\pi}} \int_{-\infty}^{\infty} A(s, k_y)\sqrt{k_o^2-k_y^2-s^2}\, e^{\pm isd}\, ds \quad . \tag{2.39}$$

Substituting Equations (2.35) and (2.39) into Equation (2.31), one obtains:

$$\begin{aligned} -DAi\sqrt{k_o^2-k_x^2-k_y^2}(k_x^4+2k_x^2k_y^2+k_y^4) &- \frac{iEIk_y^4}{2\pi} \int_{-\infty}^{\infty} A(s, k_y)\sqrt{k_o^2-s^2-k_y^2}\, ds \\ &+ \omega^2 mAi\sqrt{k_o^2-k_x^2-k_y^2} + \frac{\omega^2 Mi}{2\pi} \int_{-\infty}^{\infty} A(s, k_y)\sqrt{k_o^2-s^2-k_y^2}\, ds \\ &= \frac{-i\omega F_o}{2\pi} + \rho_o \omega^2 A - \frac{1}{2\pi}\left(\frac{k_1\omega^2}{\omega_1^2-\omega^2}\right) e^{ik_x d} \int_{-\infty}^{\infty} A(s,k_y)\, e^{-isd\sqrt{k_o^2-s^2-k_y^2}}\, ds \\ &- \frac{1}{2\pi}\left(\frac{k_1\omega^2}{\omega_1^2-\omega^2}\right) e^{-ik_x d} \int_{-\infty}^{\infty} A(s, k_y)\, e^{isd\sqrt{k_o^2-s^2-k_y^2}}\, ds \quad . \end{aligned} \tag{2.40a}$$

Rearranging Equation (2.40), an integral equation on the coefficient "A" results:

$$\begin{aligned} A(k_x, k_y) = \Bigg[&\frac{i\omega F_o}{2\pi} + \frac{\omega^2 Mi}{2\pi} \int_{-\infty}^{\infty} A(s, k_y)\sqrt{k_o^2-s^2-k_y^2}\, ds \\ &- \frac{i\, EI\, k_y^4}{2\pi} \int_{-\infty}^{\infty} A(s, k_y)\sqrt{k_o^2-s^2-k_y^2}\, ds \\ &+ \frac{i}{2\pi}\left(\frac{k_1\omega^2}{\omega_1^2-\omega^2}\right) e^{ik_x d} \int_{-\infty}^{\infty} A(s, k_y)\, e^{-isd\sqrt{k_o^2-s^2-k_y^2}}\, ds \end{aligned}$$

$$+ \frac{i}{2\pi}\left(\frac{k_1\,\omega^2}{\omega_1^2-\omega^2}\right) e^{-ik_x d} \int_{-\infty}^{\infty} A(s,\, k_y)\; e^{isd\sqrt{k_o^2-s^2-k_y^2}}\, ds \;\Bigg]$$

$$\left\{ \frac{1}{iD\sqrt{k_o^2-k_x^2-k_y^2}\left[(k_x^2+k_y^2)^2 - \frac{\omega^2 m}{D}\right] + \rho_o\,\omega^2} \right\} . \qquad (2.40b)$$

Before solving this integral equation, one can adapt the following notations to expedite the manipulation; namely,

$$f = \frac{i\omega\, F_o}{2\pi}\,, \quad g_1 = \frac{i\omega^2 M}{2\pi}\,, \quad g_2 = \frac{ik_1\,\omega^2}{2\pi(\omega_1^2-\omega^2)}\,, \quad s_y = \frac{i\,EI}{2\pi}\,,$$

$$Q(k_x,\, k_y) = iD\sqrt{k_o^2-k_x^2-k_y^2}\left[(k_x^2+k_y^2)^2 - \frac{\omega^2 m}{D}\right] + \rho_o\,\omega^2 \quad . \qquad (2.41)$$

Now, Equation (2.40b) can be rewritten in the following brief form:

$$A(k_x,\, k_y) = \frac{f + g_1 G_1 - s_y k_y^4 G_1 + g_2 e^{ik_x d} G_2 + g_2 e^{-ik_x d} G_3}{Q(k_x,\, k_y)}\,, \qquad (2.42)$$

where

$$G_1(k_y) = \int_{-\infty}^{\infty} A(s,\, k_y)\; e^{-isd\sqrt{k_1^2-s^2-k_y^2}}\, ds \quad ,$$

$$G_2(k_y) = \int_{-\infty}^{\infty} A(s,\, k_y)\; e^{-isd\sqrt{k_o^2-s^2-k_y^2}}\, ds$$

and

$$G_3(k_y) = \int_{-\infty}^{\infty} A(s,\, k_y)\; e^{isd\sqrt{k_o^2-s^2-k_y^2}}\, ds \quad . \qquad (2.43)$$

It is expected that G_2 is equal to G_3, but for the time being, G_2 and G_3 are to be considered as two unrelated unknowns. Substituting the expression for A in Equation (2.42) into the integrals in Equation (2.43), three independent equations can be set up to solve for G_1, G_2, and G_3 as follows:

$$G_1 = (f + g_1G_1 - s_yk_y^4G_1)\int_{-\infty}^{\infty}\frac{\sqrt{k_o^2-s^2-k_y^2}}{Q(s,\,k_y)}\,ds + g_2G_2\int_{-\infty}^{\infty}\frac{e^{isd\sqrt{k_o^2-s^2-k_y^2}}}{Q(s,\,k_y)}\,ds$$

$$+ g_2G_3\int_{-\infty}^{\infty}\frac{e^{-isd\sqrt{k_o^2-s^2-k_y^2}}}{Q(s,\,k_y)}\,ds = (f + g_1G_1 - s_yk_y^4G_1)I_1 + g_2G_2I_2$$

$$+ g_2G_3I_2' \quad , \tag{2.44}$$

$$G_2 = (f + g_1G_1 - s_yk_y^4G_1)\int_{-\infty}^{\infty}\frac{e^{-isd\sqrt{k_o^2-s^2-k_y^2}}}{Q(s,\,k_y)}\,ds$$

$$+ g_2G_2\int_{-\infty}^{\infty}\frac{e^{-isd}\,e^{isd\sqrt{k_o^2-s^2-k_y^2}}}{Q(s,\,k_y)}\,ds$$

$$+ g_2G_3\int_{-\infty}^{\infty}\frac{e^{-isd}\,e^{-isd\sqrt{k_o^2-s^2-k_y^2}}}{Q(s,\,k_y)}\,ds = (f + g_1G_1 - s_yk_y^4G_1)I_2'$$

$$+ g_2G_2I_1 + g_2G_3I_3' \tag{2.45}$$

and

$$G_3 = (f + g_1G_1 - s_yk_y^4G_1)\int_{-\infty}^{\infty}\frac{e^{isd\sqrt{k_o^2-s^2-k_y^2}}}{Q(s,\,k_y)}\,ds$$

$$+ g_2G_2\int_{-\infty}^{\infty}\frac{e^{isd}\,e^{isd\sqrt{k_o^2-s^2-k_y^2}}}{Q(s,\,k_y)}\,ds + g_2G_3\int_{-\infty}^{\infty}\frac{e^{isd}\,e^{-isd\sqrt{k_o^2-s^2-k_y^2}}}{Q(s,\,k_y)}\,ds$$

$$= (f + g_1G_1 - s_yk_y^4G_1)I_2 + g_2G_2I_3 + g_2G_3I_1 \quad , \tag{2.46}$$

where

$$I_1 = \int_{-\infty}^{\infty}\frac{\sqrt{k_o^2-s^2-k_y^2}}{Q(s,\,k_y)}\,ds \;;$$

$$I_2 = \int_{-\infty}^{\infty}\frac{e^{isd\sqrt{k_o^2-s^2-k_y^2}}}{Q(s,\,k_y)}\,ds \;;\; I_2' = \int_{-\infty}^{\infty}\frac{e^{-isd\sqrt{k_o^2-s^2-k_y^2}}}{Q(s,\,k_y)}\,ds \;;$$

$$I_3 = \int_{-\infty}^{\infty} \frac{e^{2isd\sqrt{k_o^2-s^2-k_y^2}}}{Q(s,\, k_y)}\, ds \; ; \; I_3' = \int_{-\infty}^{\infty} \frac{e^{-2isd\sqrt{k_o^2-s^2-k_y^2}}}{Q(s,\, k_y)}\, ds \; . \tag{2.47}$$

Since $\sqrt{k_o^2-s^2-k_y^2}$ and $Q(s, k_y)$ are even functions with respect to s, one can prove the following relationship:

$$\begin{aligned} I_2 &= I_2' \\ I_3 &= I_3' \quad . \end{aligned} \tag{2.48}$$

Substituting the above relations into Equations (2.44), (2.45), (2.46), one forms the following three independent simultaneous equations:

$$(1 - g_1 I_1 + s_y k_y^4 I_1)G_1 - (g_2 I_2)G_2 - (g_2 I_2)G_3 = fI_1 \quad , \tag{2.49a}$$

$$(-g_1 I_2 + s_y k_y^4 I_2)G_1 + (1 - g_2 I_1)G_2 - (g_2 I_3)G_3 = fI_2 \tag{2.49b}$$

and

$$(-g_1 I_2 + s_y k_y^4 I_2)G_1 - (g_2 I_3)G_2 + (1 - g_2 I_1)G_3 = fI_2 \; . \tag{2.49c}$$

By inspecting Equation (2.49b) and Equation (2.49c), one can easily conclude that

$$G_2 = G_3 \quad . \tag{2.50}$$

The determination of the coefficient "A" in Equation (2.42) can be accomplished readily if one takes advantage of the property of equality in Equation (2.50). Thus, when Equation (2.50) is substituted back to Equation (2.42), the following simpler relation results:

$$A(k_x, k_y) = \frac{f + g_1 G_1 - s_y k_y^4 G_1 + 2g_2 G_3 \cos k_x d}{Q(k_x, k_y)} \; , \tag{2.51}$$

where

$$2g_2G_3 \cos k_x d = g_2G_2 e^{ik_x d} + g_2G_3 e^{-ik_x d} .$$

Following the same procedure stated above, a new set of algebraic equation on G_1 and G_3 are obtained:

$$G_1 = (f + g_1G_1 - s_y k_y^4 G_1) \int_{-\infty}^{\infty} \frac{\sqrt{k_o^2 - s^2 - k_y^2}}{Q(s, k_y)} ds$$

$$+ 2g_2G_3 \int_{-\infty}^{\infty} \frac{\cos k_x d \sqrt{k_o^2 - s^2 - k_y^2}}{Q(s, k_y)} ds = (f + g_1G_1 - s_y k_y^4 G_1) I_1$$

$$+ 2g_2G_3 I_2 \qquad (2.52a)$$

and

$$G_3 = (f + g_1G_1 - s_y k_y^4 G_1) \int_{-\infty}^{\infty} \frac{e^{isd} \sqrt{k_o^2 - s^2 - k_y^2}}{Q(s, k_y)} ds$$

$$+ 2g_2G_3 \int_{-\infty}^{\infty} \frac{e^{isd} \cos sd \sqrt{k_o^2 - s^2 - k_y^2}}{Q(s, k_y)} ds = (f + g_1G_1 - S_y k_y^4 G_1) I_2$$

$$+ 2g_2G_3 I_4 \quad , \qquad (2.52b)$$

where

$$I_4 = \int_{-\infty}^{\infty} \frac{e^{isd} \cos sd \sqrt{k_o^2 - s^2 - k_y^2}}{Q(s, k_y)} ds \quad , \qquad (2.53a)$$

$$I_1 = \int_{-\infty}^{\infty} \frac{\sqrt{k_o^2 - s^2 - k_y^2}}{Q(s, k_y)} ds \qquad (2.53b)$$

and

$$I_2 = \int_{-\infty}^{\infty} \frac{\cos sd \sqrt{k_o^2 - s^2 - k_y^2}}{Q(s, k_y)} ds = \int_{-\infty}^{\infty} \frac{e^{isd} \sqrt{k_o^2 - s^2 - k_y^2}}{Q(s, k_y)} ds \; . \qquad (2.53c)$$

If one sets

$$I_3 = \int_{-\infty}^{\infty} \frac{e^{2isd\sqrt{k_o^2 - s^2 - k_y^2}}}{Q(s, k_y)}\, ds \quad , \tag{2.53d}$$

one can express the integral I_4 in terms of I_1 and I_3 as follows:

$$I_4 = \frac{1}{2}(I_1 + I_3) \quad . \tag{2.53e}$$

Rearranging Equations (2.52a) and (2.52b), one gets

$$(1 - g_1 I_1 + s_y k_y^4 I_1)G_1 - 2g_2 I_2 G_3 = fI_1 \tag{2.53a}$$

and

$$(- g_1 I_2 + s_y k_y^4 I_2)G_1 + (1 - 2g_2 I_4)G_3 = fI_2 \quad . \tag{2.54b}$$

The two unknown functions G_1 and G_3 in the above two simultaneous equations can be easily solved by using Cramer's rule.

The determinant of the coefficients is

$$\Delta = (1 - g_1 I_1 + s_y k_y^4 I_1)(1 - 2g_2 I_4) + 2g_2 I_2(- g_1 I_2 + s_y k_y^4 I_2) \quad . \tag{2.55}$$

Solving Equation (2.54) for the two unknown functions G_1 and G_3, the following expressions are obtained:

$$G_1 = \frac{f}{\Delta}(I_1 - 2g_1 I_1 I_4 + 2g_2 I_2^2) \tag{2.56a}$$

and

$$G_3 = \frac{f}{\Delta}(I_2 - g_1 I_1 I_2 + s_y k_y^4 I_1 I_2 + g_1 I_1 I_2 - s_y k_y^4 I_1 I_2) = \frac{fI_2}{\Delta} \cdot \tag{2.56b}$$

Finally, the coefficient "A" is obtained in the following:

$$A(k_x, k_y) = \frac{f}{Q}[1 + \{g_1(I_1 - 2g_2 I_1 I_4 + 2g_2 I_2^2) - s_y k_y^4 (I_1 - 2g_2 I_1 I_4 + 2g_2 I_2^2) + 2g_2 I_2 \cos k_x d\}/\Delta] = \frac{f}{Q\Delta}(1 - g_2 I_1 - g_2 I_3 + 2g_2 I_2 \cos k_x d). \tag{2.57}$$

The radiated acoustic pressure can be obtained from the fluid velocity potential by the relationship in Equation (2.11), one gets an integral expression as follows:

$$p(x, y, z, t) = -i\omega \rho_o \phi \, e^{-i\omega t}$$

$$= -\frac{i\omega\rho_o f}{2\pi} e^{-i\omega t} \int_{-\infty}^{\infty}\int_{-\infty}^{\infty} \frac{e^{iz\sqrt{k_o^2-k_x^2-k_y^2}} \, e^{i(k_x x+k_y y)}}{iD\sqrt{k_o^2-k_x^2-k_y^2}\,[(k_x^2+k_y^2)^2 - \frac{\omega^2 m}{D}] + \rho_o\omega^2} C_{ms}\, dk_x dk_y$$

$$= \left(\frac{1}{2\pi}\right)^2 \rho_o\omega^2 F_o e^{-i\omega t} \int_{-\infty}^{\infty}\int_{-\infty}^{\infty} \frac{e^{iz\sqrt{k_o^2-k_x^2-k_y^2}} \, e^{i(k_x x+k_y y)}}{iD\sqrt{k_o^2-k_x^2-k_y^2}\,[(k_x^2+k_y^2)^2 - \frac{\omega^2 m}{D}] + \rho_o\omega^2} C_{ms}\, dk_x dk_y \tag{2.58}$$

where

$$C_{ms} = \frac{1}{\Delta}(1 - g_2 I_1 - g_2 I_3 + 2g_2 I_2 \cos k_x d) \quad .$$

2.4.3 Evaluation of Far-Field Pressure by Asymptotic Methods. In order to carry out the integration in Equation (2.58), the following independent variable transformations are made [23]:

$$k_x = k_o \sin\alpha \cos\beta, \; k_y = k_o \sin\alpha \sin\beta, \; k_z = \sqrt{k_o^2-k_x^2-k_y^2} = k_o \cos\alpha$$

$$x = R \sin\phi \cos\theta, \quad y = R \sin\phi \sin\theta, \quad z = R \cos\phi. \tag{2.59}$$

The Jacobian of such a transformation becomes

$$|J| = \begin{vmatrix} \frac{\partial k_x}{\partial\alpha} & \frac{\partial k_x}{\partial\beta} \\ \frac{\partial k_y}{\partial\alpha} & \frac{\partial k_y}{\partial\beta} \end{vmatrix} = k_o^2 \sin\alpha \cos\alpha. \tag{2.60}$$

Therefore,

$$dk_x dk_y = k_o^2 \sin\alpha \cos\alpha \, d\alpha \, d\beta \ . \tag{2.61}$$

The integration with respect to β will be performed between 0 and 2π, while the integration with respect to α cannot be restricted to real values of this angle. The integration limits for the argument α can be determined as follows:

$$\begin{aligned} &\text{(i)} \quad \text{when} \quad k_x = k_y = 0 : \quad k_z = k_o \ , \quad \alpha = 0 \\ &\text{(ii)} \quad \text{when} \quad k_x \to \pm\infty \ \text{and/or} \ \ k_y \to \pm\infty : \quad k_z \to i\infty \ . \end{aligned} \tag{2.62}$$

since $\cos\alpha = k_z/k_o = i\infty$, one has $\alpha = \frac{\pi}{2} - i\infty$.

As a result, the integral in Equation (2.58) transforms to the following integral:

$$p = \left(\frac{1}{2\pi}\right)^2 \rho_o \omega^2 k_o^2 F_o \int_0^{\frac{\pi}{2} - i\infty} e^{ik_o R \cos\phi \cos\alpha} \left\{ \int_0^{2\pi} e^{ik_o R \sin\phi \sin\alpha \cos(\beta-\theta)} V(\alpha, \beta)\, d\beta \right\} \sin\alpha \, d\alpha \ , \tag{2.63}$$

where

$$V(\alpha, \beta) = \frac{\cos\alpha \, C_{ms}(\alpha, \beta)}{Q(\alpha, \beta)} \ . \tag{2.64}$$

Since the exact solution for the radiated pressure integral representation in Equation (2.63) cannot be obtained, an approximate solution is desirable. For the solution of the far-field pressure when $k_o R \gg 1$ and $k_o z \gg 1$, a useful mathematical tool called the method of steepest descent will be used here [24, 25, 26]. The fundamental concept of this asymptotic method is to distort the

original integration path into the complex path of steepest descent (PSD) so that the complex line integral can be reduced to evaluating a single-valued function at the saddle point where it receives the major contribution in the whole distorted path [27]. It should be noted that any singularities crossed in the deformation of the original integration path into the path PSD should be included as discrete pole contributions according to the residue theorem [28]. However, these discrete residue terms, in general, represent the near-field pressure.

To obtain an asymptotic solution by this method, one can let $g(\beta)$ represent the part of the power of the exponential term in Equation (2.63); i.e.,

$$g(\beta) = i[\sin \phi \sin \alpha \cos (\beta-\theta)] \quad . \tag{2.65}$$

The saddle point β_o is the root of the following equation:

$$g'(\beta_o) = - i \sin \phi \sin \alpha \sin (\beta_o-\theta) = 0 \text{ , or } \beta_o = \theta, \pi+\theta \quad . \tag{2.66}$$

If one puts $\beta = \beta_1 + i\beta_2$, then,

$$g(\beta) = \sin \phi \sin \alpha[\sin (\beta_1-\theta) \sinh \beta_2 + i \cos (\beta_1-\theta) \cosh \beta_2] \ .$$

The regions of convergence of the integral in Equation (2.63) are determined by real part of function $g(\beta)$; namely,

$$\mathrm{Re}\{g(\beta)\} = \sin \phi \sin \alpha \sin (\beta_1-\theta) \sinh \beta_2 \quad . \tag{2.67}$$

In the upper half-plane ($\beta_2 > 0$), the regions of convergence are:

$$\sin(\beta_1-\theta) < 0$$

or

$$-\pi + \theta < \beta_1 < \theta \ , \quad \pi + \theta < \beta_1 < 2\pi + \theta, \ \ldots \ .$$

And in the lower half-plane ($\beta_2 < 0$), the regions of convergence are

$$\sin(\beta_1-\theta) > 0$$

or

$$\theta < \beta_1 < \pi + \theta, \ \ldots \ .$$

The steepest descent paths, which are found from

$$\mathrm{Im}\{g(\beta)\} = \text{constant} \tag{2.68}$$

pass through the two saddle points within the region between $\beta = -\frac{\pi}{2}$ and $\beta = \frac{3\pi}{2}$ are then defined by the following equations (see Figure 2.3):

(i) For saddle point at $(\theta, 0)$: $\cos(\beta_1 - \theta)\cosh\ \beta_2 = 1$.

(ii) For saddle point at $(\theta+\pi, 0)$: $\cos(\beta_1-\theta)\cosh\ \beta_2 = -1$.

The asymptotes of steepest descent paths are determined from

$$\cos(\beta_1-\theta) \to 0 \ , \text{ or } \beta_1 = -\frac{3\pi}{2} + \theta \ , -\frac{\pi}{2} + \theta \ , \frac{\pi}{2} + \theta \ , \frac{3\pi}{2} + \theta \ .$$

Thus, it can be seen that the suitable steepest descent paths for the present case can be taken from $(-\frac{\pi}{2} + \theta + i\infty)$ to (θ), then to $(\frac{\pi}{2} + \theta - i\infty)$, and then from $(\frac{\pi}{2} + \theta - i\infty)$ to $(\pi+\theta)$ and then to $(\frac{3\pi}{2} + \theta + i\infty)$. In other words, these steepest descent paths can be shown to be equivalent to the inner integral in Equation (2.63), provided that there are no singularities within the complete close contour described by $(-\frac{\pi}{2} + \theta) \to (\theta) \to (\pi+\theta) \to (\frac{3\pi}{2} + \theta) \to (\frac{3\pi}{2} + \theta + i\infty)$

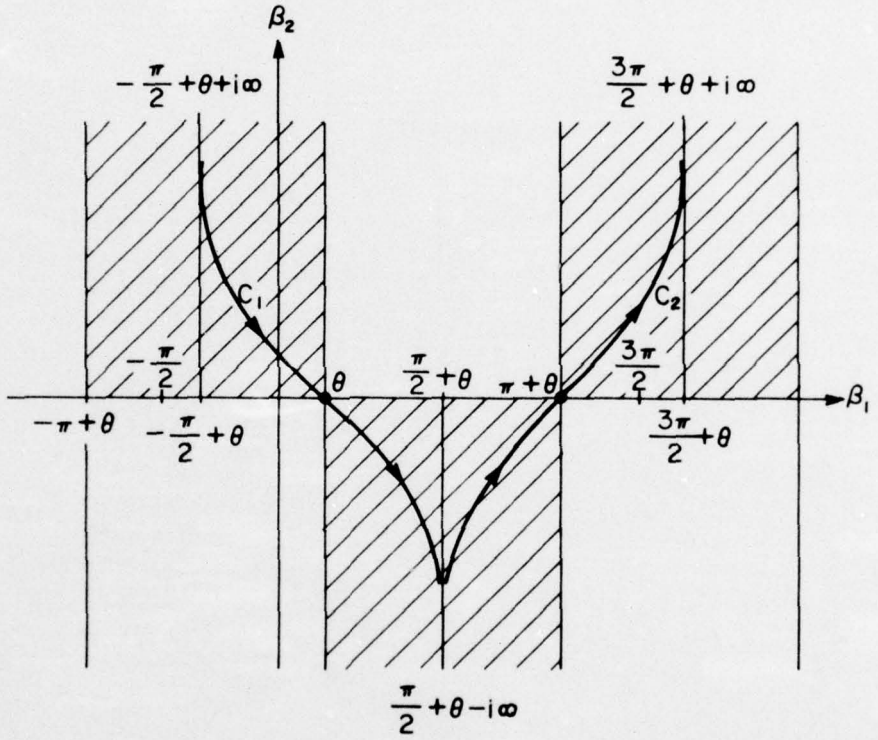

Figure 2.3 Steepest Descent Paths for the Far-Field Pressure Integral

$\rightarrow (-C_2) \rightarrow (-C_1) \rightarrow (-\frac{\pi}{2} + \theta + i\infty) \rightarrow (-\frac{\pi}{2} + \theta)$.

The proof of this statement is simple, since the periodicity of the integrand is 2π; thus,

$$\text{(i)} \quad \int_0^{2\pi} [\ ]\, d\beta = \left\{ \int_0^{2\pi} + \int_{-\frac{\pi}{2}+\theta}^{0} - \int_{-\frac{\pi}{2}+\theta}^{0} \right\} [\ ]\, d\beta = \int_{-\frac{\pi}{2}+\theta}^{\frac{3\pi}{2}+\theta} [\ ]\, d\beta$$

and

$$\text{(ii)} \quad \int_{-\frac{\pi}{2}+\theta+i\infty}^{-\frac{\pi}{2}+\theta} [\ ]\, d\beta = \int_{\frac{3\pi}{2}+\theta+i\infty}^{\frac{3\pi}{2}+\theta} [\ ]\, d\beta ,$$

or

$$\left\{ \int_{-\frac{\pi}{2}+\theta+i\infty}^{-\frac{\pi}{2}+\theta} + \int_{\frac{3\pi}{2}+\theta}^{\frac{3\pi}{2}+\theta+i\infty} \right\} [\ ]\, d\beta = 0 .$$

From the residue theory,

$$\oint [\ ]\, d\beta = \left\{ \int_{-\frac{\pi}{2}+\theta}^{\frac{3\pi}{2}+\theta} + \int_{\frac{3\pi}{2}+\theta}^{\frac{3\pi}{2}+\theta+i\infty} - \int_{C_2} - \int_{C_1} + \int_{-\frac{\pi}{2}+\theta+i\infty}^{-\frac{\pi}{2}+\theta} \right\} [\ ]\, d\beta = 0 .$$

Therefore,

$$\int_0^{2\pi} [\ ]\, d\beta = \int_{-\frac{\pi}{2}+\theta}^{\frac{3\pi}{2}+\theta} [\ ]\, d\beta = \left\{ \int_{C_1} + \int_{C_2} \right\} [\ ]\, d\beta ,$$

where [ ] denotes the integrand in Equation (2.63).

Letting

$$u = g(\beta_o) - g(\beta) ,$$

or

$$u_1 = i \sin\phi \sin\alpha[1 - \cos(\beta-\theta)] \quad , \quad \text{on path } C_1 \qquad (2.69a)$$

$$u_2 = i \sin\phi \sin\alpha[-1 - \cos(\beta-\theta)] \quad , \quad \text{on path } C_2 , \qquad (2.69b)$$

then, the inner integral in Equation (2.63) can be written as follows:

$$\left[\int_{\theta}^{\frac{\pi}{2}+\theta-i\infty} - \int_{\theta}^{-\frac{\pi}{2}+\theta+i\infty}\right]_{\text{on } C_1} e^{ik_oR\{i \sin\phi \sin\alpha - u_1\}} V(\alpha, \beta) \frac{d\beta}{du_1} du_1$$

$$+\left[\int_{\pi+\theta}^{\frac{3\pi}{2}+\theta+i\infty} - \int_{\pi+\theta}^{-\frac{\pi}{2}+\theta+i\infty}\right]_{\text{on } C_2} e^{ik_oR\{-i \sin\phi \sin\alpha - u_2\}} V(\alpha, \beta) \frac{d\beta}{du_2} du_2 \tag{2.70}$$

where C_1 and C_2 are two paths of integration as shown in Figure 2.3.

Before the integral in Equation (2.70) can be simplified any further, the terms $\frac{d\beta}{du_1}$ and $\frac{d\beta}{du_2}$ have to be expressed in terms of u_1 and u_2, respectively. If Equation (2.69a) is differentiated with respect to u_1, one obtains

$$\frac{d\beta}{du_1} = \frac{1}{i \sin\phi \sin\alpha \sin(\beta-\phi)} = \frac{\pm 1}{\sqrt{2i \sin\phi \sin\alpha\, u_1 - u_1^2}} .$$

Since k_oR is assumed to be large, only small values of u_1 will contribute significantly to the integral. Thus, the above expression for $\frac{d\beta}{du_1}$ can be expanded into a Taylor's series in u_1 and by retaining the leading term in the series, an approximate expression for the derivative results:

$$\frac{d\beta}{du_1} \simeq \sqrt{\frac{1}{2 \sin\phi \sin\alpha}}\, u_1^{-1/2}\, e^{-\pi i/4} \quad , \quad \text{or} \sqrt{\frac{1}{2 \sin\phi \sin\alpha}}\, u_1^{-1/2}\, e^{3\pi i/4}.$$

For uniqueness, one requires that the above expression with the factor $e^{-\pi i/4}$ is used for the path from $\beta=\theta$ to $\beta = \frac{\pi}{2} + \theta - i\infty$, while that with the factor $e^{3\pi i/4}$ used for the path from $\beta=\theta$ to $\beta = -\frac{\pi}{2} + \theta + i\infty$.

Similarly,

$$\frac{d\beta}{du_2} \simeq \sqrt{\frac{1}{2 \sin \phi \sin \alpha}}\ u_2^{-1/2}\ e^{\pi i/4}$$

should be used for the integration path from $\pi+\theta$ to $\frac{3\pi}{2} + \theta + i\infty$ and

$$\frac{d\beta}{du_2} \simeq \sqrt{\frac{1}{2 \sin \phi \sin \alpha}}\ u^{-1/2}\ e^{5\pi i/4}$$

used for the path from $\beta = \pi+\theta$ to $\beta = \frac{\pi}{2} + \theta - i\infty$.

Thus,

$$\int_0^{2\pi} e^{ik_oR \sin \phi \sin \alpha \cos(\beta-\theta)}\ V(\alpha, \beta)\ d\beta$$

$$= 2V(\alpha, \theta)\ e^{ik_oR \sin \phi \sin \alpha} \sqrt{\frac{1}{2 \sin \phi \sin \alpha}}\ e^{-i\pi/4} \int_0^{\infty} e^{-k_oRu_1}\ u_1^{-1/2}\ du_1$$

$$+ 2V(\alpha, \pi+\theta)\ e^{-ik_oR \sin \phi \sin \alpha} \sqrt{\frac{1}{2\sin\phi\sin\alpha}}\ e^{\pi i/4} \int_0^{\infty} e^{-k_oRu_2}\ u_2^{-1/2}\ du_2$$

$$= \sqrt{\frac{2\pi}{k_oR \sin \phi}}\ V(\alpha, \theta)\ e^{ik_oR \sin \phi \sin \alpha} \sqrt{\frac{1}{\sin \alpha}}\ e^{-\pi i/4}$$

$$+ \sqrt{\frac{2\pi}{k_oR \sin \phi}}\ V(\alpha, \pi+\theta)\ e^{-ik_oR \sin \phi \sin \alpha} \sqrt{\frac{1}{\sin \alpha}}\ e^{\pi i/4} \quad . \qquad (2.71)$$

Substituting Equation (2.71) into Equation (2.63), an integral representation for the far-field fluid pressure p is obtained:

$$p = \left(\frac{1}{2\pi}\right)^2 \rho_o \omega^2 F_o \sqrt{\frac{2\pi}{k_oR \sin \phi}}\ k_o^2 \int_0^{\frac{\pi}{2} - i\infty} e^{ik_oR \cos \phi \cos \alpha} \left[V(\alpha, \theta) \right.$$

$$\left. e^{ik_oR\sin\phi\sin\alpha} \sqrt{\frac{1}{\sin\alpha}}\ e^{-\pi i/4} + V(\alpha, \pi+\theta)\ e^{-ik_oR\sin\phi\sin\alpha} \sqrt{\frac{1}{\sin\alpha}}\ e^{\pi i/4} \right]$$

$$\sin \alpha\ d\alpha \quad . \qquad (2.72)$$

Noting that $V(\alpha, \theta) = V(\alpha, \pi+\theta)$ and

$$\int_0^{\frac{\pi}{2}-i\infty} e^{ik_o R\cos\phi\cos\alpha}\, V(\alpha, \pi+\theta)\, e^{ik_o R\sin\phi\sin\alpha} \sqrt{\frac{1}{\sin\alpha}}\, e^{\pi i/4} \sin\alpha\, d\alpha$$

$$= \int_{-\frac{\pi}{2}+i\infty}^{0} e^{ik_o R\cos\phi\cos\alpha}\, V(\alpha, \theta)\, e^{ik_o R\sin\phi\sin\alpha} \sqrt{\frac{1}{\sin\alpha}}\, e^{-\pi i/4} \sin\alpha\, d\alpha ,$$

the expression in Equation (2.72) can be rewritten as

$$p = \left(\frac{1}{2\pi}\right)^2 \rho_o \omega^2 k_o^2 F_o \sqrt{\frac{2\pi}{k_o R\sin\phi}} \int_{-\frac{\pi}{2}+i\infty}^{\frac{\pi}{2}-i\infty} e^{ik_o R\cos\phi\cos\alpha}\, V(\alpha, \theta)\, e^{ik_o R\sin\phi\sin\alpha}\, e^{-\pi i/4} \sqrt{\sin\alpha}\, d\alpha$$

$$= \left(\frac{1}{2\pi}\right)^2 F_o \rho_o \omega^2 k_o^2 e^{-\pi i/4} \sqrt{\frac{2\pi}{k_o R\sin\phi}} \int_{-\frac{\pi}{2}+i\infty}^{\frac{\pi}{2}-i\infty} e^{ik_o R\cos(\alpha-\phi)}\, V(\alpha,\theta)\sqrt{\sin\alpha}\, d\alpha. \tag{2.73}$$

The integral in Equation (2.73) can be obtained by following the same procedure and method outlined above. Let

$$s(\alpha) = i\cos(\alpha-\phi) ,$$

then, the saddle point α_o is defined by

$$s'(\alpha_o) = -i\sin(\alpha_o-\phi) = 0 , \quad \text{or} \quad \alpha_o = \phi ,$$

letting

$$u_3 = s(\alpha_o) - s(\alpha) = i - i\cos(\alpha-\phi) .$$

Then

$$\frac{d\alpha}{du_3} = \sqrt{\frac{1}{2}}\, u_3^{-1/2}\, e^{-\pi i/4} , \quad \text{or} \sqrt{\frac{1}{2}}\, u_3^{-1/2}\, e^{3\pi i/4}$$

and

$$p = \left(\frac{1}{2\pi}\right)^2 \rho_o \omega^2 k_o^{\,2} F_o \sqrt{\frac{2\pi}{k_o R \sin\phi}}\, e^{i(k_o R - \pi/4)}\, V(\phi,\theta)\, e^{-\pi i/4}\, \frac{2}{\sqrt{2}}\, \sqrt{\sin\phi}$$

$$\int_0^\infty e^{-k_o R u_3}\, u_3^{-1/2}\, du_3$$

$$= -\frac{ik_o F_o}{2\pi R} \frac{e^{ik_o R}\cos\phi}{1 - \frac{ik_o m \cos\phi}{\rho_o}\left[1 - \frac{\omega^2}{\omega_o^2}\sin^4\phi\right]}\, C_{ms}(\phi,\theta) \quad , \qquad (2.74)$$

where

$$C_{ms}(\phi,\theta) = \left[1 + \mu_1\left(\frac{m_1}{\rho_o h^2}\right)\left(\frac{\omega_1^2}{\omega_1^2-\omega^2}\right)\left\{2I_2^{\,0}\cos(k_o d\cos\theta\sin\phi) - I_1^{\,0} - I_3^{\,0}\right\}\right] \Bigg/$$

$$\left[1 - \mu_1 I_1^{\,0}\left\{\frac{M}{\rho_o h^2} + \left(\frac{m_1}{\rho_o h^2}\right)\left(\frac{\omega_1^2}{\omega_1^2-\omega^2}\right)\right\} - \mu_1 I_3^{\,0}\left(\frac{m_1}{\rho_o h^2}\right)\left(\frac{\omega_1^2}{\omega_1^2-\omega^2}\right)\right.$$

$$+ \mu_1^{\,2}\left(\frac{M}{\rho_o h^2}\right)\left(\frac{m_1}{\rho_o h^2}\right)\left(\frac{\omega_1^2}{\omega_1^2-\omega^2}\right)\left(I_1^{\,0^2} + I_1^{\,0} I_3^{\,0} - 2I_2^{\,o^2}\right)$$

$$+ \mu_3 U_y \sin^4\phi \sin^4\theta \left\{I_1^{\,0} - \mu_1\left(\frac{m_1}{\rho_o h^2}\right)\left(\frac{\omega_1^2}{\omega_1^2-\omega^2}\right)\right.$$

$$\left.\left.\left(I_1^{\,0^2} + I_1^{\,0} I_3^{\,0} - 2I_2^{\,0^2}\right)\right\}\right],$$

$$\mu_1 = \left(\frac{i}{2\pi}\right)\left(\frac{\omega}{\omega_o}\right)^2\left(\frac{c}{c_p}\right)^2 12(1-\nu^2) \quad , \quad c_p = \sqrt{\frac{E}{\rho}} \quad ,$$

$$\mu_3 = 12\left(\frac{\rho}{\rho_o}\right)\left(\frac{\omega}{\omega_o}\right)^2 (1-\nu^2)\,\mu_1 \quad ,$$

$$U_y = q_3\{(1-\nu^2)(q_2^{\,3} + 3q_2^{\,2} + 3q_2) - \nu^2\}/12(1-\nu^2) \quad ,$$

$$I_1^{\,0} = \int_{-\infty}^{\infty} \frac{\sqrt{1 - q^2 - \eta^2}\; d\eta}{ia\sqrt{1-q^2-\eta^2}\,\{b(\eta^2 + q^2)^2 - 1\} + 1} \quad , \quad q = \sin\theta\sin\phi \quad ,$$

$$b = \left(\frac{\omega}{\omega_o}\right)^2 = \Omega^2 \quad ,$$

$$a = \left(\frac{\rho}{\rho_o}\right)\left(\frac{\omega}{\omega_o}\right) c\sqrt{\frac{12\rho(1 - \nu^2)}{E}} \quad ,$$

$$I_2^0 = \int_{-\infty}^{\infty} \frac{e^{ik_o d\eta} \sqrt{1 - q^2 - \eta^2}\, d\eta}{ia\sqrt{1 - q^2 - \eta^2}\, \{b(\eta^2 + q^2)^2 - 1\} + 1}$$

and

$$I_3^0 = \int_{-\infty}^{\infty} \frac{e^{2ik_o d\eta} \sqrt{1 - q^2 - \eta^2}\, d\eta}{ia\sqrt{1 - q^2 - \eta^2}\, \{b(\eta^2 + q^2)^2 - 1\} + 1} \quad .$$

2.4.4 Discussion of the Possibility of Replacing the Original Integration Paths by Paths of Steepest Descent. To deform the original integration paths into paths of steepest descent continuously, certain singularities may be encountered in the complex α and complex β planes, which are enumerated below:

(i) $\sqrt{\sin \alpha}$ has a branch point at $\alpha = 0$. However, this point is of no great significance since the steepest descent path shall not pass through it.

(ii) In the present case, the only singularities present would be poles of the function $V(\alpha, \beta)$ in the β-plane and those of the function $V(\alpha, \phi)$ in the α-plane. If such a pole is crossed in the deformation of original integration paths into steepest descent paths, then the residue at the pole must be added. The contribution of such poles can be shown to give an exponentially decaying solution in the distance R or z and hence they contribute significantly to the near-field pressure, but their contribution to the far-field pressure can be neglected.

2.4.5 Evaluation of Non-Dimensional Integrals Contained in the Far-Field Pressure Solution. To evaluate the non-dimensional integrals I_j^o (j=1,2,3), one can extend the independent variable η to the complex plane and use the method of Cauchy contour integration. The choice of the branch cuts, contour integration paths, etc., are enumerated below.

2.4.5a Choice of Branch Cuts. The existence of branch cuts requires that the integrand be made a single-valued function before Cauchy's theorem is applied [29]. This requirement can be fulfilled by introducing cuts in the complex plane. Letting $\xi = \sqrt{1 - q^2 - \eta^2}$, where η is a complex variable, then the sign of the radical $\xi = \sqrt{1 - q^2 - \eta^2}$ will be determined by the radiation condition $\text{Im}\ \xi > 0$ which guarantees the convergence of the integral along the entire complex path. The branch points are defined by $\xi = 0$, which yields the fixed values $= \pm \sqrt{1 - q^2}$ on the real axis. To allow an effective application of the methods of operational analysis, the complex value of $(1 + i\varepsilon/2)\sqrt{1 - q^2}$ has to be used instead of $\sqrt{1 - q^2}$ in order to avoid difficulties with the path of integration. In another word, at least an infinitesimal amount of material damping should be assumed [27]. Therefore, branch points will be located at $\eta_b = \pm (1 + \frac{i\varepsilon}{2}) \sqrt{1 - q^2}$, where ε is the elastic loss factor. After the branch cuts have been determined, the undamped response can then be obtained by setting $\varepsilon \to 0$.

For the determination of Sommerfeld branch cuts, one can start with the equation

$$\xi^2 = \left(1 + \frac{i\varepsilon}{2}\right)^2 (1 - q^2) - \eta^2$$

$$\xi = \xi_1 + i\xi_2 \quad , \quad \eta = \eta_1 + i\eta_2 \quad ,$$

then

$$(\xi_1 + i\xi_2)^2 = \left(1 + \frac{i\varepsilon}{2}\right)^2 (1 - q^2) - (\eta_1 + i\eta_2)^2$$

$$= \left(1 - \frac{\varepsilon^2}{4}\right)(1 - q^2) - (\eta_1^2 - \eta_2^2) + 2i\left\{\frac{\varepsilon}{2}(1 - q^2) - \eta_1\eta_2\right\} .$$

To satisfy the condition, Im $\xi = 0$, two conditions result; namely,

$$\eta_1\eta_2 = \frac{\varepsilon}{2}(1 - q^2) \tag{2.75a}$$

and

$$(\eta_1^2 - \eta_2^2) < \left(1 - \frac{\varepsilon^2}{4}\right)(1 - q^2) \quad . \tag{2.75b}$$

These two equations restrict the choice of a branch cut as shown in Figure 2.4.

At this point, one must consider the changes of the branch cuts necessitated by the limit $\varepsilon \to 0$ and choose the contour of integration in the upper-half of the complex η plane either for the top Riemann sheet (T) or bottom Riemann sheet (B). The sign of Reξ, in the first and second quadrants of the top and bottom Riemann sheets, can be obtained by the following procedure.

Let

$$\xi = \sqrt{1 - q^2 - \eta^2} = \left(\sqrt{1 - q^2} + \eta\right)^{1/2} \left(\sqrt{1 - q^2} - \eta\right)^{1/2}$$

$$= (r_- r_+)^{1/2} \exp\left\{i\left(\frac{\theta_- + \theta_+ \pm \pi}{2}\right)\right\} = \gamma_o \exp\{i\phi\} , \tag{2.76}$$

where $r_o = (r_- r_+)^{1/2}$ and $\phi = \dfrac{\theta_- + \theta_+ \pm \pi}{2}$ are the amplitude and phase angle of ξ, respectively; (r_-, θ_-) and (r_+, θ_+) the amplitude and phase angle pair for vectors $(\eta + \sqrt{1 - q^2})$ and $(\eta - \sqrt{1 - q^2})$,

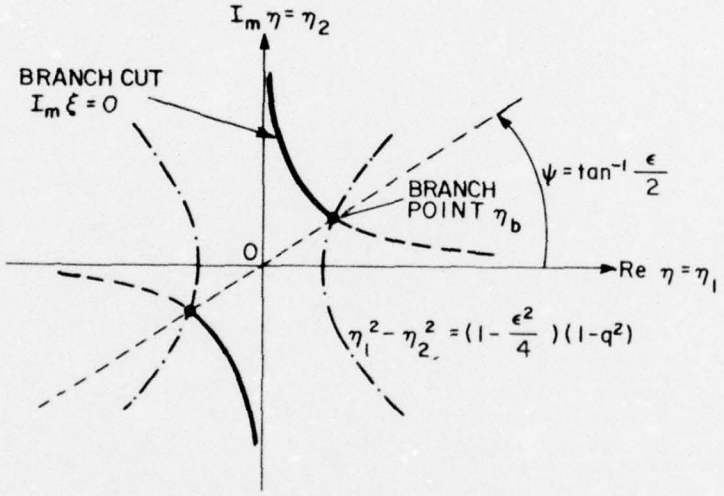

Figure 2.4 Sommerfeld Branch Cuts

respectively. Thus, the multivalued angle function ϕ can be defined as

$$\text{top Riemann sheet:} \quad \phi = \frac{\theta_- + \theta_+ + \pi}{2}$$

$$\text{bottom Riemann sheet:} \quad \phi = \frac{\theta_- + \theta_+ - \pi}{2}$$

where the positive direction of θ_- and θ_+ is measured from the positive real axis of the complex plane η in the counterclockwise sense as shown in Figure 2.5. The variations of the phase angle ϕ are tabulated below:

Table 2.1

Phase of Complex Variable η

	Top Riemann Sheet	Bottom Riemann Sheet
Q_1	$\frac{\pi}{2} \leq \phi \leq \pi$	$-\frac{\pi}{2} \leq \phi \leq 0$
Q_2	$0 \leq \phi \leq \frac{\pi}{2}$	$-\pi \leq \phi \leq -\frac{\pi}{2}$
$\overline{AF}$	$\phi = \frac{\pi}{2}$	$\phi = -\frac{\pi}{2}$
$\overline{FOD}$	$\phi = 0$	$\phi = -\pi$
$\overline{DB}$	$\phi = \frac{\pi}{2}$	$\phi = -\frac{\pi}{2}$

The above table can be briefly described by

$$-n\pi \leq \phi \leq \pi - n\pi \,, \quad n = 0, 1 \quad ,$$

where n = 0 and n = 1 refer to the top and bottom Riemann sheets, respectively.

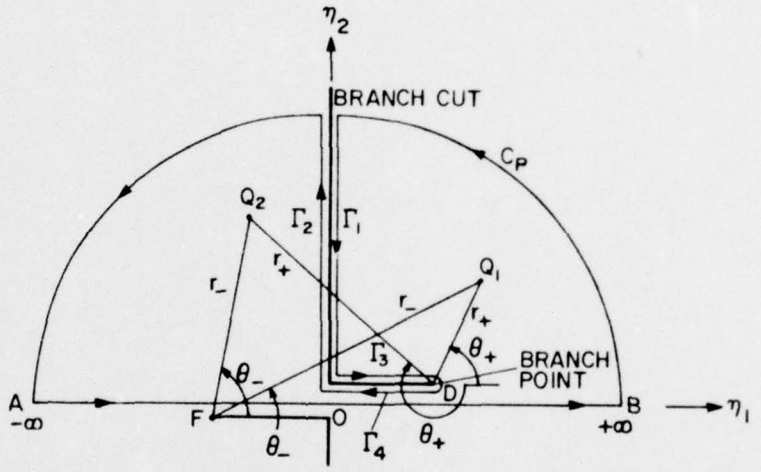

Figure 2.5 Complete Contour of the Pressure Integral

Examining the integrand in I_j^o (j=1,2,3) together with the radiation condition Im $\xi > 0$, which arises from the physical requirement contained in the original pressure integral-representation, it can be shown that the integrand of I_j^o will converge on the top Riemann sheet along the entire closed path in the upper complex half-plane.

2.4.5b Evaluation of Branch Cut Integrals B. In what follows, the procedures followed for the evaluation of branch cut integrals will be shown for the case of the integral I_2^o only. The branch cut integrals of I_1^o and I_3^o require similar procedures with only slight modifications.

The branch cut integral B of I_2^o may be written as

$$B = \underset{i\infty\ (\Gamma_1)}{\int^{0}} + \underset{0\ (\Gamma_3)}{\int^{\sqrt{1-q^2}}} + \underset{\sqrt{1-q^2}\ (\Gamma_4)}{\int_{0}^{0}} + \underset{0\ (\Gamma_2)}{\int_{0}^{i\infty}} \left[\frac{e^{ik_o d\eta} \sqrt{1-q^2-\eta^2}\ d\eta}{ia\{b(\eta^2+q^2)^2 - 1\}\sqrt{1-q^2-\eta^2} + 1} \right].$$

The signs of the radical in the integrand can be properly chosen by the evaluation of phase angle ϕ at the corresponding location on the top Riemann sheet:

$$\Gamma_1 : \sqrt{1-q^2-\eta^2} = -\sqrt{|1-q^2-\eta^2|} = -\sqrt{1-q^2+r^2}$$

$$\Gamma_2 : \sqrt{1-q^2-\eta^2} = \sqrt{|1-q^2-\eta^2|} = \sqrt{1-q^2+r^2}$$

$$\Gamma_3 : \sqrt{1-q^2-\eta^2} = -\sqrt{|1-q^2-\eta^2|} = -\sqrt{1-q^2-r^2}$$

$$\Gamma_4 : \sqrt{1-q^2-\eta^2} = \sqrt{|1-q^2-\eta^2|} = \sqrt{1-q^2-r^2} \quad , \qquad (2.77)$$

where r is a positive real variable representing the radius of the corresponding vector.

Using Equation (2.77), the following simplifications can be made:

$$\Gamma_1 + \Gamma_2 = \int_{\infty}^{0} \frac{e^{-k_o dr\{-\sqrt{1-q^2+r^2}\}}(idr)}{-ia\sqrt{1-q^2+r^2}\{b(q^2-r^2)^2-1\}+1} + \int_{0}^{\infty} \frac{e^{-k_o dr\sqrt{1-q^2+r^2}}(idr)}{ia\sqrt{1-q^2+r^2}\{b(q^2-r^2)^2-1\}+1}$$

$$= 2i\int_{0}^{\infty} \frac{e^{-k_o dr\sqrt{1-q^2+r^2}}\, dr}{1 + a^2\{b(q^2-r^2)^2 - 1\}^2(1-q^2+r^2)}$$

$$\Gamma_3 + \Gamma_4 = \int_{0}^{\sqrt{1-q^2}} \frac{\{-\sqrt{1-q^2-r^2}\}\, e^{ik_o dr}\, dr}{-ia\sqrt{1-q^2-r^2}\, b(q^2+r^2)^2-1\} + 1}$$

$$- \int_{0}^{\sqrt{1-q^2}} \frac{\sqrt{1-q^2-r^2}\, e^{ik_o dr}\, dr}{ia\sqrt{1-q^2-r^2}\{b(q^2+r^2)^2 - 1\} + 1}$$

$$= -2\int_{0}^{\sqrt{1-q^2}} \frac{e^{ik_o dr}\sqrt{1-q^2-r^2}\, dr}{1 + a^2\{b(q^2+r^2)^2 - 1\}^2(1-q^2-r^2)} \quad , \tag{2.78}$$

Thus, the total integral becomes:

$$B = 2i\left[\int_{0}^{1} \frac{e^{-k_o dr}\sqrt{1-q^2+r^2}\, dr}{1+a^2\{b(q^2-r^2)^2-1\}(1-q^2+r^2)}\right.$$

$$\left. + \int_{0}^{1} \frac{e^{-k_o d/r}\, r^7\sqrt{1+(1-q^2)r^2}\, dr}{r^{10}+a^2\{b(q^2r^2-1)^2-r^4\}^2\{1+(1-q^2)r^2\}}\right]$$

$$- 2\left[\int_{0}^{\sqrt{1-q^2}} \frac{e^{ik_o dr}\sqrt{1-q^2-r^2}\, dr}{1+a^2\{b(q^2+r^2)^2-1\}^2(1-q^2-r^2)}\right] \quad , \tag{2.78}$$

where the integral of $(\Gamma_1 + \Gamma_2)$ is first divided into two subintegrals (from 0 to 1 and from 1 to ∞), and then the subintegral from 1 to ∞

is again retransformed to an integral from 0 to 1 for numerical evaluation.

2.4.5c Evaluation of the Pole Contributions. The positions of the poles are determined by the zeros of the denominator of the integrand in the integral I_j^o (j=1,2,3), i.e.,

$$ia\{b(\eta^2 + q^2)^2 - 1\}\sqrt{1 - q^2 - \eta^2} + 1 = 0 \quad . \qquad (2.79a)$$

If one lets

$$\sqrt{1 - q^2 - \eta^2} = is \quad ,$$

Equation (2.79a) becomes

$$s^5 + 2s^3 + s(1 - \frac{1}{\Omega^2}) - \frac{1}{\ell} = 0 \quad , \qquad (2.79b)$$

where

$$\ell = \frac{Dk_o^5}{\rho_o \omega^2} = \Omega^3 \left(\frac{c\rho}{\rho_o}\right)\sqrt{\frac{12\rho(1 - \nu^2)}{E}} \quad .$$

Once the roots of Equation (2.79b) are found for different frequencies, the variable will be obtained in terms of the variable s by the following relationship:

$$\eta = \sqrt{1 - q^2 + s^2} \quad . \qquad (2.80)$$

From Equations (2.80) and (2.79a), it becomes obvious that there exists ten poles in the integrands of I_j^o (j=1,2,3). However, only those roots on the top Riemann sheet are needed for the use in the Residue theorem. The roots that fall in the top Riemann sheet can be found from the mappings between variable s and ξ imposed by the radiation condition Im $\xi > 0$. Since

$$\xi = \sqrt{1 - q^2 - \eta^2} = is \quad ,$$

or

$$\xi_1 + i\xi_2 = i(s_R + is_I) = - s_I + is_R \quad ,$$

the condition Im $\xi > 0$ is seen to correspond to the condition Re $s > 0$. Numerical computation shows that the typical five roots of Equation (2.79b) are

1 positive real root: (s_{R1})

4 complex roots: $(s_{R2} + is_{I2})$, $(s_{R2} - is_{I2})$

$(-s_{R3} + is_{I3})$, $(-s_{R3} - is_{I3})$,

where s_{Rj} (j=1,2,3) and s_{Ij} (j=2,3) are positive real numbers.

Thus, the desired roots in η can be found first by employing the condition Re $s > 0$ to pick out the three roots in s which consist of one positive real root (s_{R1}) and two complex roots $(+s_{R2} + is_{I2})$, $(+s_{R2} - is_{I2})$ and then substituting these into Equation (2.80) to obtain six roots in η on the top Riemann sheet. Out of these six roots, only the three roots which include one positive real root and the two complex roots lying in the upper half plane of the complex variable η are the desired ones. The reason for excluding the negative real pole is that if a slight amount of damping is assumed, this negative real root will be shifted off the real axis into the lower half complex plane η and outside the domain of the closed contour integration.

2.4.5d Computation of Residues R_j. In general, the residue of $A(\eta)/B(\eta)$ at a simple pole $\eta = \eta_j$ can be found by the formula:

$$R_j = \left. \frac{A(\eta)}{\frac{\partial}{\partial \eta} B(\eta)} \right|_{\eta = \eta_j} .$$

If the expressions $A(\eta)$ and $B(\eta)$ contain multi-valued functions, such as a square root, the signs of the radical have to be carefully evaluated. Thus, if one takes the integral $I_2^{\,o}$, for example, the residues of this integral are:

$$R_j = \left. \frac{e^{ik_o d\eta \sqrt{1-q^2-\eta^2}}}{\frac{\partial}{\partial\eta}\{ia\sqrt{1-q^2-\eta^2}[b(\eta^2+q^2)^2-1]+1\}} \right|_{\eta=\eta_j}$$

$$= \left. \frac{e^{ik_o d\eta \sqrt{1-q^2-\eta^2}}}{ia\{4b\eta(\eta^2+q^2)\sqrt{1-q^2-\eta^2} - \eta[b(\eta^2+q^2)^2-1](1-q^2-\eta^2)^{-1/2}\}} \right|_{\eta=\eta_j}$$

$$= \frac{e^{ik_o d\eta_j (1-q^2-\eta_j^2)}}{ia\eta_j\{b(\eta_j^2+q^2)(-5\eta_j^2-5q^2+4)+1\}}, \quad j=1,2,3$$

It is noted that the numerator and denominator of the residue expression is simplified by multiplying both by the same branch of $\sqrt{1-q^2-\eta^2}$, resulting in a final residue expression which is free from the multivalued radicals.

2.4.5e Final Solutions of the Integrals $I_j^{\,o}$ (j=1,2,3). Using the methods of evaluating branch cut integrals and residues developed in previous sections, the integrals $I_j^{\,o}$ (j=1,2,3) can be evaluated according to the theory of contour integration as follows:

$$I_j^{\,o} = -\left\{\int_{\Gamma_1} + \int_{\Gamma_4} + \int_{\Gamma_3} + \int_{\Gamma_4}\right\}_j [\text{Integrand}]_j + 2\pi i\left\{\sum_{n=1}^{3} \text{Residue}\right\}_j$$

or

$$I_1^{\,o} = -2i\int_0^{\infty} \frac{\sqrt{1-q^2+r^2}\,dr}{1+a^2\{b(q^2-r^2)^2-1\}^2(1-q^2+r^2)} + 2\int_0^{\sqrt{1-q^2}} \frac{\sqrt{1-q^2-r^2}\,dr}{1+a^2\{b(q^2+r^2)^2-1\}^2(1-q^2-r^2)}$$

$$+ 2\pi i \sum_{n=1}^{3} \frac{(1-q^2-\eta_n^2)}{ia\eta_n\{b(\eta_n^2+q^2)(-5\eta_n^2-5q^2+4)-1\}} ,$$

$$I_2^o = -2i \int_0^{\infty} \frac{e^{-k_o dr\sqrt{1-q^2+r^2}}\, dr}{1+a^2\{b(q^2-r^2)^2-1\}^2 (1-q^2+r^2)} + 2\int_0^{\sqrt{1-q^2}} \frac{e^{ik_o dr\sqrt{1-q^2-r^2}}\, dr}{1+a^2\{b(q^2+r^2)^2-1\}^2 (1-q^2-r^2)}$$

$$+ 2\pi i \sum_{n=1}^{3} \frac{e^{ik_o d\eta_n (1-q^2-\eta_n^2)}}{ia\eta_n\{b(\eta_n^2+q^2)(-5\eta_n^2-5q^2+4)-1\}} ,$$

$$I_3^o = -2i \int_0^{\infty} \frac{e^{-2k_o dr\sqrt{1-q^2+r^2}}\, dr}{1+a^2\{b(q^2-r^2)^2-1\}^2 (1-q^2+r^2)} + 2\int_0^{\sqrt{1-q^2}} \frac{e^{2ik_o dr\sqrt{1-q^2-r^2}}\, dr}{1+a^2\{b(q^2+r^2)^2-1\}^2 (1-q^2-r^2)}$$

$$+ 2\pi i \sum_{n=1}^{3} \frac{e^{2ik_o d\eta_n} (1-q^2-\eta_n^2)}{ia\eta_n\{b(\eta_n^2+q^2)(-5\eta_n^2-5q^2+4)-1\}} .$$

2.4.6 Approximate Expressions for the Integrals I_j^o (j=1,2,3). Although a digital computer can be used for the numerical computation of the integrals I_j^o (j=1,2,3), which consist of branch cut integrals and residue terms, the resulting numerical values, when substituted back into the radiated pressure in Equation (2.74), do not completely allow one to interpret the trend in the variation of radiated far-field pressure. Thus, in order to gain more insight into the behavior of the integrals, it seems plausible to obtain the approximate expression for the integrals I_j^o. These asymptotic expressions allow a better understanding of the fundamental characteristics which govern the physical phenomena of the radiated far-field pressure distribution.

2.4.6a Approximate Expressions of the Integral $I_1^{\,o}$. To begin with, one can express $I_1^{\,o}$ in terms of branch cut integrals and residue contribution as developed in previous sections, i.e.,

$$I_1^{\,o} = \int_{-\infty}^{\infty} \frac{\sqrt{1-q^2-\eta^2}\; d\eta}{ia\sqrt{1-q^2-\eta^2}\; b(\eta^2+q^2)^2 - 1\}+ 1} = A - i(B+C)$$

$$+ \sum_{n=1}^{3} \frac{1-q^2-\eta_n^{\,2}}{ia\eta_n\{b(\eta_n^{\,2}+q^2)(-5\eta_n^{\,2}-5q^2+4)+1\}} \quad ,$$

where

$$q = \sin\theta \sin\phi, \quad a = \frac{\rho c}{\rho_o}\sqrt{\frac{12\rho(1-\nu^2)}{E}}\left(\frac{\omega}{\omega_o}\right) = a_o\Omega, \quad b = \left(\frac{\omega}{\omega_o}\right)^2 = \Omega^2 \quad ,$$

$$A = \int_0^{\sqrt{1-q^2}} \frac{2\sqrt{1-q^2-r^2}\; dr}{1+a^2\{b(r^2+q^2)^2-1\}^2(1-q^2-r^2)} \quad ,$$

$$B = \int_0^{\sqrt{1-q^2}} \frac{2\sqrt{1-q^2+r^2}\; dr}{1+a^2\{b(q^2-r^2)^2-1\}^2(1-q^2+r^2)}$$

and

$$C = \int_0^{1/\sqrt{1-q^2}} \frac{2r^7\sqrt{1+(1-q^2)r^2}\; dr}{r^{10}+a^2\{b(q^2r^2-1)^2-r^4\}^2\{1+(1-q^2)r^2\}}$$

$$= 2(1-q^2)\int_0^1 \frac{r^7\sqrt{1+r^2}\; dr}{r^{10}+a^2(1-q^2)\{b[q^2r^2-(1-q^2)]^2-r^4\}^2(1+r^2)} \quad .$$

(1) Low frequency approximation ($\Omega << 1$):

$$A \simeq 2\int_0^{\sqrt{1-q^2}} \sqrt{1-q^2-r^2}\; dr = (1-q^2)\frac{\pi}{2} \quad ,$$

$$B \simeq 2\int_0^{\sqrt{1-q^2}} \sqrt{1-q^2+r^2}\; dr = (1-q^2)\{\sqrt{2} + \log_e(1+\sqrt{2})\} \quad ,$$

and

$$C = (1-q^2)\int_0^1 \frac{r^3\sqrt{1+r}\,dr}{r^5+a^2(1-q^2)\{b[q^2r-(1-q^2)]^2-r^2\}^2(1+r)}$$

$$\simeq (1-q^2)\left\{\int_0^{(1-q^2)\Omega} \frac{r^3\,dr}{r^5+a^2b^2(1-q^2)^5} + \int_{(1-q^2)\Omega}^1 \frac{dr}{r^2}\right\}$$

$$= (1-q^2)\left\{\int_0^{\mu^{1/5}} \frac{r^3dr}{r^5+\mu} + \int_{\mu^{1/5}}^{(1-q^2)\Omega} \frac{r^3dr}{r^5+\mu}\right\} + \frac{1}{\Omega}$$

$$= (1-q^2)\left[\frac{r^4}{4\mu} - \frac{r^9}{9\mu^2} + \frac{r^{14}}{14\mu^3} - \cdots\right]_0^{\mu^{1/5}}$$

$$+\left[-\frac{1}{r} + \frac{\mu}{6r^6} - \frac{\mu^2}{11r^{11}} + \cdots\right]_{\mu^{1/5}}^{(1-q^2)\Omega} + \frac{1}{\Omega}$$

$$\simeq \frac{3145}{2772}(a_o^{-2/5})(\Omega^{-6/5}) = 1.135(a_o^{-2/5})(\Omega)^{-6/5} \quad .$$

[Note that $u = a^2b^2(1-q^2)^5$]

Poles: $\eta_1 \simeq a_o^{-1/5}\,\Omega^{-3/5}$

$\eta_2 \simeq a_o^{-1/5}\,\Omega^{-3/5}\,e^{2\pi i/5}$

$\eta_3 \simeq a_o^{-1/5}\,\Omega^{-3/5}\,e^{3\pi i/5}$

Summing up the various contributions evaluated above, one obtains:

$$I_1^{\,o} \simeq (1-q^2)\,\frac{\pi}{2} - i\{(1-q^2)[\sqrt{2} + \log_e(1+\sqrt{2})] + 1.135a_o^{-2/5}\,\Omega^{-6/5}\} + \sum_{n=1}^{3} \text{Res.}$$

(2) High frequency approximation ($\Omega > 1$):

(i) When $q^2 < \frac{1}{\Omega} = \sigma$:

$$A = 2(1-q^2)\int_0^1 \frac{\sqrt{1-r^2}\,dr}{1+a^2b^2(1-q^2)(1-r^2)[\{(1-q^2)r^2+q^2\}^2-\sigma^2]^2}$$

$$= (1-q^2)\int_0^1 \sqrt{\frac{1-r}{r}}\,\frac{dr}{1+a^2b^2(1-q^2)(1-r)[\{(1-q^2)r+q^2\}^2-\sigma^2]^2}$$

$$\simeq \frac{1-q^2}{2}\sqrt{\frac{1-\sigma}{\sigma-q^2}}\int_{-\infty}^{\infty}\frac{dr}{1+a^2b^2(1-\sigma)[\{(1-q^2)r\}^2-\sigma^2]^2}$$

$$= \frac{1-q^2}{2}\sqrt{\frac{1-\sigma}{\sigma-q^2}}\,2\pi i\,\frac{\sigma^6/a_o^2}{4(1-q^2)(1-\sigma)}\,\frac{\sqrt{1-\sigma}}{i\sigma^3/a_o}\,\frac{2\Omega}{1+\tau^2}$$

$$= \frac{\pi\sigma^2}{2a_o\sqrt{\sigma-q^2}} = \frac{\pi\Omega^{-2}}{2a_o\sqrt{1/\Omega-q^2}}\,, \quad \left(\text{Note that } \tau = \frac{1}{2a_o\sqrt{1-\sigma}}\right)$$

$$D = B+C = 2(1-q^2)\int_0^\infty \frac{\sqrt{1+r^2}\,dr}{1+a^2b^2(1-q^2)(1+r^2)[\{(1-q^2)r^2-q^2\}^2-\sigma^2]^2}$$

$$= (1-q^2)\int_0^\infty \sqrt{\frac{1+r}{r}}\,\frac{dr}{1+a^2b^2(1-q^2)(1+r)[(1-q^2)^2r^2-\sigma^2]^2}$$

$$= \frac{1-q^2}{2}\sqrt{\frac{1+\sigma}{q^2+\sigma}}\int_{-\infty}^{\infty}\frac{dr}{1+a^2b^2(1+\sigma)[(1-q^2)^2r^2-\sigma^2]^2}$$

$$= \frac{\pi\sigma^2}{2a_o\sqrt{\sigma+q^2}}$$

Poles: $\eta_1 \simeq \sqrt{1-q^2}$

$$\eta_2 \simeq \frac{\sigma^2}{4a_o\sqrt{1+\sigma}\,\sqrt{\sigma+q^2}} + i\sqrt{\sigma+q^2} \simeq i\sqrt{\sigma+q^2}$$

$$\eta_3 \simeq \frac{-\sigma^2}{4a_o\sqrt{1+\sigma}\,\sqrt{\sigma+q^2}} + i\sqrt{\sigma+q^2} \simeq i\sqrt{\sigma+q^2}$$

$$\sum_{n=1}^{3}\text{Res.} \simeq \frac{i\pi\sigma^2}{a_o\sqrt{\sigma+q^2}}$$

Summing the various contributions obtained above, $I_1^{\,o}$ becomes:

$$I_1^{\,o} = \frac{\pi\sigma^2}{2a_o\sqrt{\sigma-q^2}} + \frac{i\pi\sigma^2}{2a_o\sqrt{\sigma+q^2}} \quad .$$

(ii) When $q^2 = 1/\Omega = \sigma$,

$$A = 2(1-q^2)\int_0^1 \frac{\sqrt{1-r^2}\,dr}{1+a^2b^2(1-q^2)(1-r^2)[\{(1-q^2)r^2+q^2\}^2-\sigma^2]^2}$$

$$\simeq 2(1-q^2)\int_0^1 \frac{dr}{1+4a^2b^2q^4(1-q^2)^3r^4}$$

$$\simeq (1-q^2)\int_{-\infty}^{\infty} \frac{dr}{1+4a^2b^2q^4(1-q^2)^3r^4}$$

$$= \frac{\pi\Omega^{-1}}{2a_o^{1/2}}\,(1-1/\Omega)^{1/4}\left\{1 - \frac{1}{4ab\sigma(1-\sigma)^{3/2}}\right\}$$

$$= \frac{\pi\sigma(1-\sigma)^{1/4}}{2a_o^{1/2}}\left\{1 - \frac{1}{4ab\sigma(1-\sigma)^{3/2}}\right\}$$

$$D = \frac{\pi\sigma(1-\sigma)^{1/4}}{2a_o^{1/2}}\left\{1 + \frac{1}{4ab\sigma(1-\sigma)^{3/2}}\right\} + \frac{\pi\sigma^{3/2}}{2\sqrt{2}\,a_o} \quad .$$

Note that there are two critical points $\left(r_1 \simeq \frac{\sigma+q^2}{1-q^2}, r_2 \simeq \frac{q^2-\sigma}{1-q^2}\right)$ existing in the integral D.

$$\sum_{n=1}^{3} \text{Res.} \simeq \frac{i\pi\sigma^{3/2}}{\sqrt{2}\,a_o} \quad .$$

Summing up, the integral $I_1^{\,o}$ becomes:

$$I_1^{\,o} = \frac{\pi\sigma(1-\sigma)^{1/4}}{2a_o^{1/2}}\left\{1 - \frac{1}{4ab\sigma(1-\sigma)^{3/2}}\right\} - i\left[\frac{\pi\sigma(1-\sigma)^{1/4}}{2a_o^{1/2}}\left\{1 + \frac{1}{4ab\sigma(1-\sigma)^{3/2}}\right\} - \frac{\pi\sigma^{3/2}}{2\sqrt{2}\,a_o}\right] .$$

(iii) When $q^2 > 1/\Omega = \sigma$:

$$A = \frac{2(1-q^2)}{1+a^2b^2(1-q^2)(q^4-\sigma^2)^2} \int_0^1 \sqrt{1-r^2}\, dr$$

$$= \frac{\pi\sigma^6}{2a_o^2(q^4-\sigma^2)^2}$$

$$D \simeq \frac{\pi}{2a_o}\left(\frac{\sigma^2}{\sqrt{\sigma+q^2}} + \frac{\sigma^2}{\sqrt{q^2-\sigma}}\right)$$

$$\sum_{n=1}^{3} \text{Res.} \simeq \frac{i\pi\sigma^2}{a_o\sqrt{\sigma+q^2}} .$$

Therefore,

$$I_1^o \simeq \frac{\pi\sigma^6}{2a_o^2(q^4-\sigma^2)^2} - \frac{i\pi}{2a_o}\left(\frac{\sigma^2}{\sqrt{q^2-\sigma}} - \frac{\sigma^2}{\sqrt{q^2+\sigma}}\right).$$

2.4.6b Approximate Expressions for the Integral I_2^o. Integral I_2^o can be expressed in the following form:

$$I_2^o = \int_{-\infty}^{\infty} \frac{e^{ik_o d\eta}\sqrt{1-q^2-\eta^2}\, d\eta}{iab\sqrt{1-q^2-\eta^2}[(\eta^2+q^2)^2-\sigma^2]+1} = A - iD$$

$$+ \sum_{n=1}^{3} \frac{e^{ik_o d\eta_n}(1-q^2-\eta_n^2)}{ia\eta_n\{b(\eta_n^2+q^2)(-5\eta_n^2-5q^2+4)+1\}} .$$

(1) Low frequency approximation ($\Omega << 1$):

(i) When $1/2 < k_o d < 1$:

$$A = \int_0^{\sqrt{1-q^2}} \frac{2e^{ik_o dr}\sqrt{1-q^2-r^2}\, dr}{1+a^2b^2(1-q^2-r^2)\{(r^2+q^2)^2-\sigma^2\}^2}$$

$$= 2\int_0^{\sqrt{1-q^2}} e^{ik_o dr}\sqrt{1-q^2-r^2}\,dr \simeq 2\int_0^{\sqrt{1-q^2}} \left\{1 - \frac{(k_o dr)^2}{2} + ik_o dr\right\} \sqrt{1-q^2-r^2}\,dr$$

$$= \frac{(1-q^2)\pi}{2} - (k_o d)^2(1-q^2)^2\,\frac{\pi}{16} + \frac{2k_o di}{3}(1-q^2)^{3/2} \quad ,$$

$$D \simeq 2(1-q^2)\int_0^{\infty} \frac{e^{-k_o d\sqrt{1-q^2}\,r}\sqrt{1+r^2}\,dr}{1+a^2b^2(1-q^2)(1+r^2)[\{(1-q^2)r^2-q^2\}-\sigma^2]^2}$$

$$\simeq 2(1-q^2)\left\{\int_0^1 e^{-k_o dr\sqrt{1-q^2}}\left(1+\frac{r^2}{2}\right)dr + \int_1^{\infty} e^{-k_o dr\sqrt{1-q^2}}\,r\,dr\right\}$$

$$\simeq \sqrt{1-q^2}\left(\frac{2-e^{-k_o d\sqrt{1-q^2}}}{k_o d}\right) + \frac{2}{\sqrt{1-q^2}}\left(\frac{1-e^{-k_o d\sqrt{1-q^2}}}{k_o{}^3 d^3}\right).$$

Poles: $\eta_1 \simeq a_o^{-1/5}\,\Omega^{-3/5}$

$\eta_2 \simeq a_o^{-1/5}\,\Omega^{-3/5}\,e^{2\pi i/5}$

$\eta_3 \simeq a_o^{-1/5}\,\Omega^{-3/5}\,e^{3\pi i/5}$.

Thus, the integral $I_2^{\,o}$ has the following approximation:

$$I_2^{\,o} \simeq \frac{(1-q^2)\pi}{2} - \frac{\pi(k_o d)^2(1-q^2)^2}{16} + \frac{2k_o di(1-q^2)^{3/2}}{3}$$

$$- i\left[\sqrt{1-q^2}\left(\frac{2-e^{-k_o d\sqrt{1-q^2}}}{k_o d}\right) + \frac{2}{\sqrt{1-q^2}}\left(\frac{1-e^{-k_o d\sqrt{1-q^2}}}{k_o{}^3 d^3}\right)\right] + \sum_{n=1}^{3} \text{Res.}$$

(ii) When $k_o d > 1$:

$$A \simeq 2\int_0^{\sqrt{1-q^2}} e^{ik_o dr}\sqrt{1-q^2-r^2}\,dr$$

$$\simeq 2(1-q^2)\int_0^1 e^{ik_o dr\sqrt{1-q^2}}\left(1-\frac{r^2}{2}\right)\,dr$$

$$= 2(1-q^2)\left[\frac{e^{ik_o dr\sqrt{1-q^2}}}{ik_o d\sqrt{1-q^2}} - \frac{r^2 e^{ik_o dr\sqrt{1-q^2}}}{2ik_o d\sqrt{1-q^2}} + \frac{e^{ik_o dr\sqrt{1-q^2}}}{(ik_o d\sqrt{1-q^2})^3}\left\{ik_o dr\sqrt{1-q^2}-1\right\}\right]_o^1$$

$$= \frac{2i\{k_o^2 d^2(1-q^2)-1\}}{k_o^3 d^3\sqrt{1-q^2}} + \frac{2e^{ik_o d\sqrt{1-q^2}}}{k_o^3 d^3\sqrt{1-q^2}}\left\{-k_o d\sqrt{1-q^2}-i-\frac{ik_o^2 d^2(1-q^2)}{2}\right\},$$

$$D \simeq \frac{2\sqrt{1-q^2}}{k_o d} \qquad \text{[obtained from case (i)]}.$$

Poles: $\eta_1 \simeq a_o^{-1/5}\,\Omega^{-3/5}$ (dominate)

$\eta_2 \simeq a_o^{-1/5}\,\Omega^{-3/5}\,e^{2\pi i/5}$

$\eta_3 \simeq a_o^{-1/5}\,\Omega^{-3/5}\,e^{3\pi i/5}$.

It is not difficult to understand that the branch cut integrals "A" and "D" may be negligible compared with the residue contribution due to the real pole; thus,

$$I_2^o \simeq \sum_{n=1}^{3} \text{Res.}$$

(2) High frequency approximation ($\Omega > 1$):

(i) When $q^2 < 1/\Omega = \sigma$:

$$A = \int_0^{\sqrt{1-q^2}} \frac{2e^{ik_o dr\sqrt{1-q^2-r^2}}\,dr}{1+a^2b^2(1-q^2-r^2)[(r^2+q^2)^2-\sigma^2]^2}$$

$$= 2(1-q^2)\int_0^1 \frac{e^{ik_o dr\sqrt{1-q^2}}\sqrt{1-r^2}\,dr}{1+a^2b^2(1-q^2)(1-r^2)[\{(1-q^2)r^2+q^2\}^2-\sigma^2]^2}$$

$$\simeq \frac{\pi\sigma^2}{2a_o\sqrt{\sigma-q^2}}\,e^{ik_o d\sqrt{\sigma-q^2}}$$

and

$$D = 2(1-q^2)\int_0^{\infty} \frac{e^{-k_o dr\sqrt{1-q^2}}\sqrt{1+r^2}\,dr}{1+a^2b^2(1-q^2)(1+r^2)[\{(1-q^2)r^2-q^2\}^2-\sigma^2]^2}$$

$$\simeq \frac{\pi\sigma^2}{2a_o\sqrt{\sigma+q^2}}\, e^{-k_o d\sqrt{\sigma+q^2}}$$

The expression for "D" is expected to be a good approximation under the conditions of high frequency ($\Omega >> 1$) and not very large $k_o d$. In another word, the approximate result is good for when

$e^{-k_o dr\sqrt{1-q^2}}$ is a slowly varying function.

$$\sum_{n=1}^{3} \text{Res.} \simeq \frac{i\pi\sigma^2}{2a_o\sqrt{\sigma+q^2}}\, e^{-k_o d\sqrt{\sigma+q^2}} .$$

Thus, the approximate expression for I_2^o can be obtained as follows:

$$I_2^o = \frac{\pi\sigma^2}{2a_o\sqrt{\sigma-q^2}}\, e^{ik_o d\sqrt{\sigma-q^2}} + \frac{i\pi\sigma^2}{2a_o\sqrt{\sigma+q^2}}\, e^{-k_o d\sqrt{\sigma+q^2}} .$$

(ii) When $q^2 = 1/\Omega = \sigma$:

(a) $k_o d\sqrt{1-q^2} < 1$:

$$A \simeq 2(1-q^2)\int_0^1 \frac{(1-\frac{r^2}{2})\, e^{ik_o dr\sqrt{1-q^2}}\, dr}{1+4a^2b^2q^4(1-q^2)^3 r^4} .$$

Since

$$e^{ik_o dr\sqrt{1-q^2}} \simeq 1 - \frac{k_o^2 d^2(1-q^2)r^2}{2} + ik_o dr\sqrt{1-q^2} ,$$

$$A \simeq \frac{\pi\sigma(1-\sigma)^{1/4}}{2a_o^{1/2}}\left\{1 - \frac{1}{4ab\sigma(1-\sigma)^{3/2}}\right\} - \left\{\frac{\pi\sigma^3 k_o^2 d^2}{8a_o^{3/2}(1-\sigma)^{1/4}}\right\} + \frac{i\pi k_o d\sigma^2}{4a_o} .$$

Similarly, since

$$e^{-k_o dr\sqrt{1-q^2}} \simeq 1-k_o dr\sqrt{1-q^2} ,$$

$$D = 2(1-q^2)\int_0^\infty \frac{e^{-k_o dr\sqrt{1-q^2}}\sqrt{1+r^2}\,dr}{1+a^2b^2(1-q^2)(1+r^2)[\{(1-q^2)r^2-q^2\}^2-\sigma^2]^2}$$

$$\simeq (1-q^2)\int_{-\infty}^{\infty} \frac{(1-k_o dr\sqrt{1-q^2})\,dr}{1+4a^2b^2q^4(1-q^2)^3r^4}$$

$$\simeq \frac{\pi\sigma(1-\sigma)^{1/4}}{2a_o^{1/2}} - \frac{\pi k_o d\sigma^2}{4a_o} + \frac{\pi\sigma^{3/2}e^{-k_o d\sqrt{2\sigma}}}{2\sqrt{2}\,a_o}$$

$$\sum_{n=1}^{3} \text{Res.} \simeq \frac{i\pi\sigma^{3/2}}{\sqrt{2}\,a_o} e^{-k_o d\sqrt{2\sigma}}$$

Thus, the integral $I_2^{\,o}$ can be represented by:

$$I_2^{\,o} = \frac{\pi\sigma(1-\sigma)^{1/4}}{2a_o^{1/2}}\left\{1 - \frac{1}{4ab\sigma(1-\sigma)^{3/2}}\right\} - \frac{\pi\sigma^3 k_o^2 d^2}{8a_o^{3/2}(1-\sigma)^{1/4}}$$

$$- i\left\{\frac{\pi\sigma(1-\sigma)^{1/4}}{2a_o^{1/2}} - \frac{\pi\sigma^2 k_o d}{2a_o} - \frac{\pi\sigma^{3/2}}{2\sqrt{2a_o}} e^{-k_o d\sqrt{2\sigma}}\right\}$$

(b) $k_o d\sqrt{1-q^2} > 1$:

$$A \simeq 2(1-q^2)\int_0^1 \frac{(1-\frac{r^2}{2})\,e^{ik_o dr\sqrt{1-q^2}}\,dr}{1+4a^2b^2q^4(1-q^2)^3r^4}$$

$$\simeq (1-q^2)\int_{-\infty}^{\infty} \frac{\cos(k_o dr\sqrt{1-q^2})\,dr}{1+4a^2b^2q^4(1-q^2)^3r^4} + 2(1-q^2)\int_0^1 \frac{\sin(k_o dr\sqrt{1-q^2})\,dr}{1+4a^2b^2q^4(1-q^2)^3r^4}$$

$$\simeq \frac{\pi\sigma(1-\sigma)^{1/4}}{\sqrt{2}\,a_o^{1/2}} e^{-\sin\frac{\pi\sigma k_o d/4}{\sqrt{2}\,a_o^{1/2}(1-\sigma)^{1/4}}} \sin\left(\cos\frac{\pi\sigma k_o d/4}{\sqrt{2}a_o^{1/2}(1-\sigma)^{1/4}} + \frac{\pi}{4}\right)$$

$$+ \frac{\sigma^2 k_o d}{\pi} \tan^{-1}\left\{\frac{\pi^2 a(1-\sigma)^{1/2}}{2(k_o d\sigma)^2}\right\}$$

and

$$D \simeq \frac{2(1-\sigma)^{1/2}}{k_o d}$$

$$\sum_{n=1}^{3} \text{Res.} \simeq \frac{i\pi\sigma^{3/2}}{\sqrt{2}a_o} e^{-k_o d\sqrt{2\sigma}}$$

$$I_2{}^o \simeq \frac{\pi\sigma(1-\sigma)^{1/4}}{\sqrt{2}a_o{}^{1/2}} e^{-\sin\frac{\pi\sigma k_o d/4}{\sqrt{2}a_o{}^{1/2}(1-\sigma)^{1/4}}} \sin\left(\cos\frac{\pi\sigma k_o d/4}{\sqrt{2}a_o{}^{1/2}(1-\sigma)^{1/4}} + \frac{\pi}{4}\right)$$

$$+ \frac{\sigma^2 k_o d}{\pi} \tan^{-1}\left\{\frac{\pi^2 a(1-\sigma)^{1/2}}{2(k_o d\sigma)^2}\right\} - \frac{2i(1-\sigma)^{1/2}}{k_o d} + \frac{i\pi\sigma^{3/2}}{\sqrt{2}a_o} e^{-k_o d\sqrt{2\sigma}} .$$

(iii) When $q^2 > 1/\Omega = \sigma$:

(a) $k_o d\sqrt{1-q^2} < 1$:

$$A \simeq \frac{2(1-q^2)}{1+a^2b^2(1-q^2)(q^4-\sigma^2)^2} \int_0^1 e^{ik_o dr\sqrt{1-q^2}} \sqrt{1-r^2}\, dr$$

$$\simeq \frac{\pi\sigma^6}{2a_o{}^2(q^4-\sigma^2)^2} + i\left\{\frac{2k_o d\sqrt{1-q^2}(\sigma^6)}{3a_o{}^2(q^4-\sigma^2)^2}\right\}$$

$$D \simeq \frac{\pi}{2a_o}\left\{\frac{\sigma^2}{\sqrt{\sigma+q^2}} e^{-k_o d\sqrt{\sigma+q^2}} + \frac{\sigma^2}{\sqrt{q^2-\sigma}} e^{-k_o d\sqrt{q^2-\sigma}}\right\} .$$

The expression for "D" is expected to be a good approximation for high frequency ($\Omega >> 1$) and not very large values of $k_o d$.

$$\sum_{n=1}^{3} \text{Res.} \simeq \frac{i\pi\sigma^2}{a_o\sqrt{\sigma+q^2}} e^{-k_o d\sqrt{\sigma+q^2}} .$$

Thus, an approximation for $I_2^{\,o}$ can be written as:

$$I_2^{\,o} \simeq \frac{\pi\sigma^6}{2a_o^{\,2}(q^4-\sigma^2)^2} + i\left\{\frac{2k_o d\sigma^6(1-q^2)^{1/2}}{3a_o^{\,2}(q^4-\sigma^2)^2}\right\} + \frac{i\pi}{2a_o}$$
$$\left\{\frac{\sigma^2}{\sqrt{\sigma+q^2}}\, e^{-k_o d\sqrt{\sigma+q^2}} - \frac{\sigma^2}{\sqrt{q^2-\sigma}}\, e^{-k_o d\sqrt{q^2-\sigma}}\right\}$$

(b) $k_o d\sqrt{1-q^2} > 1$:

$$A \simeq \frac{2(1-q^2)}{1+a^2b^2(1-q^2)(q^4-\sigma^2)^2}\int_0^1 e^{ik_o dr\sqrt{1-q^2}}\sqrt{1-r^2}\, dr$$

$$\simeq \frac{2(1-q^2)}{a_o^{\,2}(1-q^2)^{1/2}(q^4-\sigma)^2(k_o d)^3}\left[i\{k_o^{\,2}d^2(1-q^2)-1\} + e^{ik_o d\sqrt{1-q^2}}\right.$$
$$\left.\left\{-k_o d\sqrt{1-q^2} - i - \frac{ik_o^{\,2}d^2(1-q^2)}{2}\right\}\right]$$

and

$$D \simeq \frac{\pi}{2a_o}\left\{\frac{\sigma^2}{\sqrt{\sigma+q^2}}\, e^{-k_o d\sqrt{\sigma+q^2}} + \frac{\sigma^2}{\sqrt{q^2-\sigma}}\, e^{-k_o d\sqrt{q^2-\sigma}}\right\}.$$

The expression for "D" is valid for high frequency ($\Omega >> 1$) and not very large values of $k_o d$.

$$\sum_{n=1}^{3} \text{Res.} \simeq \frac{i\pi\sigma^2}{a_o\sqrt{\sigma+q^2}}\, e^{-k_o d\sqrt{\sigma+q^2}}$$

and

$$I_2^{\,o} \simeq \frac{4\sigma^6}{a_o^{\,2}(1-q^2)^{1/2}(q^4-\sigma^2)^2(k_o d)^3}\left[i\left\{k_o^{\,2}d^2(1-q^2)-1\right\} + e^{ik_o d\sqrt{1-q^2}}\right.$$

$$\left\{ - k_o d\sqrt{1-q^2} - i - \frac{ik_o^2 d^2 (1-q^2)}{2} \right\} \Bigg] + \frac{i\pi}{2a_o}$$

$$\left\{ \frac{\sigma^2 e^{-k_o d\sqrt{\sigma+q^2}}}{\sqrt{\sigma+q^2}} - \frac{\sigma^2 e^{-k_o d\sqrt{q^2-\sigma}}}{\sqrt{q^2-\sigma}} \right\} .$$

2.4.6c Approximate Expressions for the Integral I_3^o. The solutions of the integral I_3^o can be obtained by replacing $(k_o d)$ by $(2k_o d)$ in the solutions I_2^o.

2.5 Evaluation of the Radiated Acoustic Power

2.5.1 Acoustic Power Generated by Far-Field Pressure (N_{ff}). The radiated acoustic power can be evaluated by integrating the square of the radiated far-field pressure over a large spherical surface, as follows:

$$N_{ff} = \frac{1}{2} \int_{\phi=0}^{\pi/2} \int_{\theta=0}^{2\pi} pvR^2 \sin\phi \, d\phi \, d\theta$$

$$= \frac{R^2}{2\rho_o c} \int_{\phi=0}^{\pi/2} \int_{\theta=0}^{2\pi} |p(R, \phi, \theta)|^2 \sin\phi \, d\phi \, d\theta$$

$$= \frac{2R^2}{\rho_o c} \int_{\phi=0}^{\pi/2} \int_{\theta=0}^{\pi/2} |p(R, \phi, \theta)|^2 \sin\phi \, d\phi \, d\theta ,$$

where

$$p(R, \phi, \theta) = \frac{-ik_o F_o \, e^{ik_o R \cos\phi / 2\pi R}}{1 - \frac{ik_o m}{\rho_o} \cos\phi \left(1 - \frac{\omega^2}{\omega_o^2} \sin^4\phi \right)} \; C_{ms}(\theta, \phi)$$

and

$$C_{ms}(\theta,\phi) = \left[1+\mu_1\left(\frac{m_1}{\rho_o h^2}\right)\left(\frac{\omega_1^2}{\omega_1^2-\omega^2}\right)\left\{2I_2^{\,o}\cos(k_o d\cos\theta\cos\phi) - I_1^{\,o} - I_3^{\,o}\right\}\right]\Bigg/$$

$$\left[1 - \mu_1 I_1^{\,o}\left\{\frac{M}{\rho_o h^2} + \left(\frac{m_1}{\rho_o h^2}\right)\left(\frac{\omega_1^2}{\omega_1^2-\omega^2}\right)\right\} - \mu_1 I_3^{\,o}\left(\frac{m_1}{\rho_o h^2}\right)\left(\frac{\omega_1^2}{\omega_1^2-\omega^2}\right)\right.$$

$$+ \mu_1^2\left(\frac{M}{\rho_o h^2}\right)\left(\frac{m_1}{\rho_o h^2}\right)\left(\frac{\omega_1^2}{\omega_1^2-\omega^2}\right)\left(I_1^{\,o2} + I_1^{\,o}I_3^{\,o} - 2I_2^{\,o2}\right)$$

$$+ \mu_3 U_y \sin^4\phi \sin^4\theta\left\{I_1^{\,o} - \mu_1\left(\frac{m_1}{\rho_o h^2}\right)\left(\frac{\omega_1^2}{\omega_1^2-\omega^2}\right)\right.$$

$$\left.\left.\left(I_1^{\,o2} + I_1^{\,o}I_3^{\,o} - 2I_2^{\,o2}\right)\right\}\right] .$$

For the complete definition of "C_{ms}," one can refer to Equation (2.74). Since

$$|p(R,\phi,\theta)| = \frac{F_o k_o \cos\theta/2\pi R}{\sqrt{1+\left(\frac{k_o m}{\rho_o}\right)^2\cos^2\phi\left(1-\frac{\omega^2}{\omega_o^2}\sin^4\phi\right)^2}}\,|C_{ms}| ,$$

the radiated acoustic power can be written in the following integral form:

$$N_{ff} = \frac{F_o^{\,2}k_o^{\,2}}{2\pi^2\rho_o c}\int_0^{\pi/2}\int_0^{\pi/2}\frac{\cos^2\phi\sin\phi\,|C_{ms}|^2\,d\phi\,d\theta}{1+\left(\frac{k_o m}{\rho_o}\right)^2\cos^2\phi\left(1-\frac{\omega^2}{\omega_o^2}\sin^4\phi\right)^2} \qquad (2.81)$$

2.5.2 Acoustic Power Generated at the Surface of the Plate (N_{sp}). The Fourier transform of the velocity distribution over the surface of the infinite plate under discussion can easily be obtained by substituting Equation (2.57) into Equation

(2.36), i.e.,

$$\tilde{v}(k_x, k_y, z=0) = \frac{(i\omega F_o/2\pi)\sqrt{k_o^2-k_x^2-k_y^2}\ (-i)\ C_{ms}}{iD\sqrt{k_o^2-k_x^2-k_y^2}\{(k_x^2+k_y^2)^2 - \frac{\omega^2 m}{D}\} + \rho_o\omega^2}$$

$$= \frac{(-i\omega F_o/2\pi D)\ C_{ms}}{\{(k_x^2+k_y^2)^2 - k_n^4\} + \frac{-i\omega\rho_o c}{D\sqrt{1-(k_x^2+k_y^2)/k_o^2}}}$$

$$= \frac{(-i\omega F_o/2\pi D)\ C_{ms}}{\{(k_x^2+k_y^2)^2 - k_B^4\} - i\tau} \quad ,$$

where

$$\tau = \frac{\omega\rho_o c/D}{\sqrt{1-(k_x^2+k_y^2)/k_o^2}} = \frac{\rho_o c k_B^4}{\omega m\sqrt{1-(k_x^2+k_y^2)/k_o^2}}$$

$$k_B^4 = \frac{\omega^2 m}{D} \quad .$$

Using the Fourier transform of the velocity distribution given above, the acoustic power can be expressed in terms of this transformed velocity. Starting with the definition for acoustic power,

$$N_{sp} = \frac{1}{2}\ \mathrm{Re}\left\{\int_{-\infty}^{\infty}\int_{-\infty}^{\infty} p\ v^*\ dx\ dy\right\},$$

where v* is the complex conjugate value of v, one can express the pressure and the velocity by the Fourier transform inversion of their Fourier transforms, i.e.,

$$N_{sp} = \frac{1}{2}\,\mathrm{Re}\int_{-\infty}^{\infty}\int_{-\infty}^{\infty}\left\{\left[\frac{1}{2\pi}\int_{-\infty}^{\infty}\int_{-\infty}^{\infty}\tilde{p}\,e^{i(k_x x + k_y y)}\,dk_x\,dk_y\right]\left[\frac{1}{2\pi}\int_{-\infty}^{\infty}\int_{-\infty}^{\infty}\tilde{v}^*\,e^{-i(k_x' x + k_y' y)}\,dk_x'\,dk_y'\right]\right\}dx\,dy$$

$$= \frac{1}{2}\,\mathrm{Re}\left\{\int_{-\infty}^{\infty}\int_{-\infty}^{\infty}\int_{-\infty}^{\infty}\int_{-\infty}^{\infty}\left[\frac{1}{(2\pi)^2}\int_{-\infty}^{\infty}\int_{-\infty}^{\infty}e^{ix(k_x - k_x')}\,e^{iy(k_y - k_y')}\,dx\,dy\right]\tilde{p}\,\tilde{v}^*\,dk_x\,dk_y\,dk_x'\,dk_y'\right\}.$$

The bracketed inner integrals have the properties of a two-dimensional Dirac's delta function $\delta(k_x - k_x')\,\delta(k_y - k_y')$ which can be derived from the following Fourier transform pair:

$$\tilde{\delta}(x, y) = \frac{1}{2\pi}\int_{-\infty}^{\infty}\int_{-\infty}^{\infty}\delta(k_x)\,\delta(k_y)\,e^{-i(k_x x + k_y y)}\,dk_x\,dk_y = \frac{1}{2\pi}$$

and

$$\delta(k_x, k_y) = \delta(k_x)\,\delta(k_y) = \frac{1}{2\pi}\int_{-\infty}^{\infty}\int_{-\infty}^{\infty}\tilde{\delta}(x, y)\,e^{i(k_x x + k_y y)}\,dx\,dy$$

$$= \left(\frac{1}{2\pi}\right)^2\int_{-\infty}^{\infty}\int_{-\infty}^{\infty}e^{i(k_x x + k_y y)}\,dx\,dy\,.$$

Thus, the expression for the radiated power can also be written as:

$$N_{sp} = \frac{\rho_o c}{2}\,\mathrm{Re}\left\{\int_{-\infty}^{\infty}\int_{-\infty}^{\infty}\frac{|\tilde{v}(k_x, k_y, z=0)|^2}{\sqrt{1 - (k_x^2 + k_y^2)/k_o^2}}\,dk_x\,dk_y\right\}, \qquad (2.82)$$

where the relation $\tilde{p}(k_x, k_y, z=0) = \dfrac{\rho_o c k_o \tilde{v}(k_x, k_y, z=0)}{\sqrt{k_o^2 - k_x^2 - k_y^2}}$ has been substituted to arrive at the above result.

The expression for the radiated power, given in Equation (2.82) can be simplified under the transformations of independent coordinates

$$k_x = k_r \cos\theta' \ , \ k_y = k_r \sin\theta' \ , \ dk_x\, dk_y = k_r\, dk_r\, d\theta' \ .$$

Hence, Equation (2.82) becomes

$$N_{sp} = \frac{\rho_o c \omega^2 F_o^2}{8\pi^2 D^2} \int_0^{2\pi} \int_0^{k_o} \frac{k_r |C_{ms}(k_r, \theta')|^2 \, dk_r \, d\theta'}{\{(k_r^4 - k_B^4)^2 + \tau^2\}\sqrt{1 - k_r^2/k_o^2}} \ .$$

The limit of integration on k_r is extended only to $k_r = k_o$, because for $k_r > k_o$, the real part of the integrand vanishes.

One can further simplify the expression for acoustic power by substituting $\sin\phi' = \dfrac{k_r}{k_o}$, $dk_r = k_o \cos\phi'\, d\phi'$ and noting that the response of the entire structure is symmetrical about the x and y axes, i.e., the integrand will remain unchanged when (θ') is replaced by $(-\theta')$ or by $(\pi-\theta')$.

Thus, Equation (2.82) becomes

$$N_{sp} = 2\rho_o c \left(\frac{\omega^2 F_o^2}{4\pi^2 D^2}\right) \int_0^{\pi/2} \int_0^{\pi/2} \frac{k_o \sin\phi' (k_o \cos\phi' \, d\phi') \, d\theta' \, |C_{ms}|^2}{\{(k_o^4 \sin^4\phi' - k_B^4)^2 + \tau^2\}\sqrt{1 - \sin^2\phi'}}$$

$$= 2\rho_o c \left(\frac{\omega^2 F_o^2}{4\rho^2 D^2}\right) \int_0^{\pi/2} \int_0^{\pi/2} \frac{k_o^2 \sin\phi' \, |C_{ms}|^2 \, d\phi' \, d\theta'}{(k_o^4 \sin^4\phi' - K_b^4)^2 + \tau^2}$$

$$= \frac{2\rho_o c k_o^2}{k_B^8}\left(\frac{\omega^2 F_o^2}{4\pi^2 D^2}\right)\left(\frac{k_o m}{\rho_o}\right)^2 \int_0^{\pi/2}\int_0^{\pi/2} \frac{\cos^2\phi' \sin\phi' |C_{ms}|^2 \, d\phi' \, d\theta'}{1 + \left(\frac{k_o m}{\rho_o}\right)^2 \frac{\cos^2\phi' k_B^8 (1 - k_o^4 \sin^4\phi'/k_B^4)}{k_B^8}}$$

$$= \frac{F_o^2 k_o^2}{2\pi^2 \rho_o c} \int_0^{\pi/2}\int_0^{\pi/2} \frac{\cos^2\phi' \sin\phi' \, |C_{ms}|^2 \, d\phi' \, d\theta}{1 + \left(\frac{k_o m}{\rho_o}\right)^2 \cos^2\phi' \left(1 - \frac{\omega^2}{\omega_o^2} \sin^4\phi'\right)^2} \quad .$$

It should be noted that the expression for the radiated acoustic power given in Equation (2.83) is exactly equal to that given in Equation (2.81). This equivalence provides an analytic verification for the asymptotic solutions obtained for the far-field acoustic pressure.

CHAPTER III

NUMERICAL RESULTS

3.1 Numerical Results for a Beam-Reinforced Plate

3.1.1 Input Data. For an aluminum infinite plate in water, numerical results were obtained for the following physical constants:

$$E = 10 \times 10^{6} \text{ psi} \; ; \quad \nu = 0.33,$$

ρ (density of plate) $= 2.56 \times 10^{-4}$ lb-sec^2/in^4,

ρ_o (density of fluid medium) $= 0.948 \times 10^{4}$ lb-sec^2/in^4

and

$$c = 5.64 \times 10^{4} \text{ in/sec} \; ; \quad R = 1 \text{ yd.} = 36 \text{ in.}$$

3.1.2 Far-Field Pressure Spectrum and Directivity Function. The solution for the far-field pressure for the point excited beam-reinforced plate, as shown in Figure 2.1, can be derived directly from Equation (2.74) by letting $m_1 \to 0$ and $k_1 \to 0$ (or $\omega_1 \to 0$). The reduced expression becomes:

$$\bar{p} = \left[\frac{-ik_o F_o}{2\pi R} \frac{e^{ik_o R} \cos\phi}{1 - \frac{ik_o m \cos\phi}{\rho_o} (1 - \Omega^2 \sin^4\phi)} \right] \times \bar{C}_{ms}(\phi, \theta) \; , \tag{3.1}$$

where

$$\bar{C}_{ms}(\phi, \theta) = \frac{1}{I + I_1^{\,o}(\mu_3 U_y \sin^4\phi \sin^4\theta - \mu_1 \gamma)} \; ;$$

$$\Omega = \frac{\omega}{\omega_o} \; ; \quad \omega_o = c^2\sqrt{m/D} \; ;$$

$$\gamma = \frac{M}{\rho_o h^2} \quad ; \; m = \rho_o h \text{ (mass of plate per unit surface area);}$$

$$\mu_1 = \left(\frac{i}{2\pi}\right)\left(\frac{\omega}{\omega_o}\right)^2\left(\frac{c}{c_p}\right) 12(1-\nu^2) \quad ;$$

$$\mu_3 = 12\left(\frac{\rho}{\rho_o}\right)\left(\frac{\omega}{\omega_o}\right)^2 (1-\nu^2)\, \mu_1 \quad ;$$

$$U_y = q_3\{(1-\nu^2)(q_2^3 + 3q_2^2 + 3q_2) - \nu^2\}/12(1-\nu^2) \quad ;$$

$$I_1^{\,o} = \int_{-\infty}^{\infty} \frac{\sqrt{1-q^2-\eta^2}\; d\eta}{ia\sqrt{1-q^2-\eta^2}\,\{b(\eta^2+q^2)^2 - 1\} + 1} \quad ; \; q = \sin\theta \sin\phi;$$

$$a = \left(\frac{\rho}{\rho_o}\right)\left(\frac{\omega}{\omega_o}\right) c\sqrt{\frac{12\rho(1-\nu)^2}{E}} \quad ; \quad b = \Omega^2 \quad .$$

The expression within the bracket in Equation (3.1) represents the radiated far-field acoustic pressure of an infinite isotropic plate due to a point force excitation. The nondimensional coefficient C_{ms} stands for a pressure amplitude modification factor when the plate is reinforced by a line mass, a stiffness member or beam-like discontinuity. The excitation is delivered by a point force located at the discontinuity. This coefficient is a function of the mass and/or the stiffness of the attached reinforcement, the excitation frequency, the plate material properties, the sound velocity as well as the location of an observation point. The dimensionless variables μ_1 and μ_3 both depend on the excitation frequency and the material constants of fluid and plate. It is worth mentioning that μ_1 is a function of the excitation frequency to the second power and is related to the mass effect of the attached reinforcement, while μ_3 is a function of excitation frequency to the fourth power and is associated

with the stiffness of the attached reinforcement. The dimensionless variable U_y when multiplied by the fourth power of the thickness of the plate represents the effective moment of inertia of the attachment. The nondimensional integral I_1^o indicates the strong coupling between a beam-reinforced plate and an adjacent fluid. The integral I_1^o strongly depends on the excitation frequency as well as the location of an observation point. The coincidence frequency ω_o is the frequency at which the flexural wavelength in the plate, as predicted by the classical plate, equals the acoustic wavelength. It should be noted that the thickness of the plate h appears explicitly in the coincidence frequency in ω_o only; hence, the following computations were made such that h does not appear explicitly in the expression for the far-field pressure.

With Equation (3.1) in hand, the following numerical computations were made:

(i) Computations were performed for the prediction of the far-field spectrum at zero azimuthal angle ($\phi = 0°$) per 1 pound force at 1 yard in dB relative to 1 μbar-in versus normalized frequencies (Ω) at five different mass ratios, i.e., $\gamma = 0, 1, 2.7, 5, 10$.

$$20 \log_{10}\left[\frac{\bar{p}(R, \theta, \phi=0°)}{\omega_o/c}\right] = 20 \log_{10}\left[\frac{F_o \Omega}{2\pi R} \times \frac{6.89 \times 10^4 \bar{C}_{ms}(\theta, \phi=0)}{\sqrt{1 + \frac{\Omega^2 c^2 \rho^3 12(1-\nu^2)}{\rho_o^2 E}}}\right]. \quad (3.2)$$

The pressure spectra are plotted for the cases of γ=0,1,10 shown in Figure 3.1. The curves for γ= 2.7 and 5.0 are not shown,

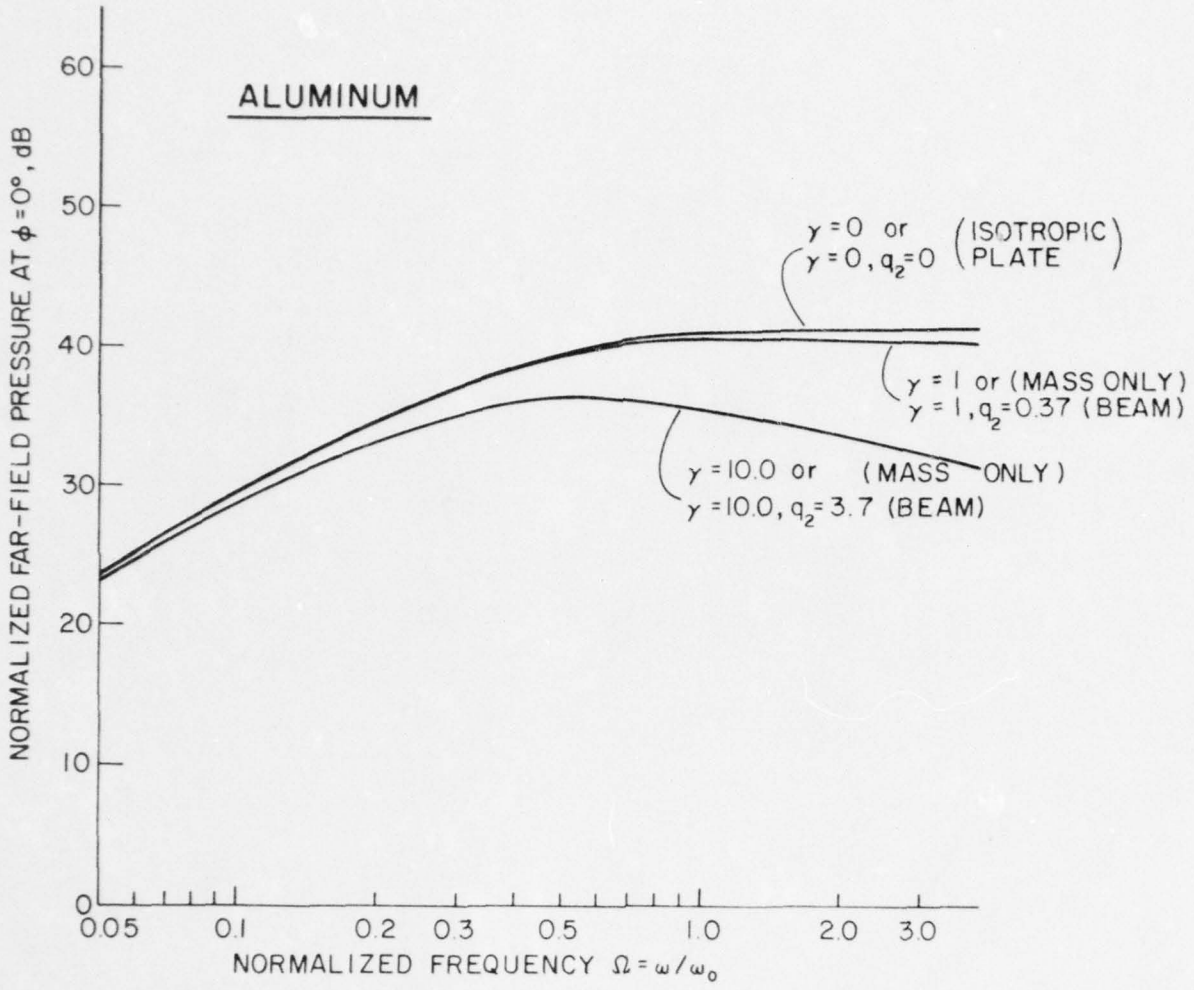

Figure 3.1 Normalized Far-Field Pressure Spectrum at ϕ = 0° of Beam-Reinforced Plate

although they fall between the curves $\gamma = 1$ and $\gamma = 10$. It should be noted that the stiffness of the attachment does not have any influence on the pressure spectrum at this particular point of observation.

(ii) The directivity function for the radiated far-field pressure from a point-excited beam-reinforced plate was computed relative to the far-field pressure at zero-azimuthal angle for a point-excited isotropic plate versus the azimuthal angle ϕ at different rotational angles ($\theta = 0°$, $90°$ and/or $45°$) and different excitation frequencies.

$$\overline{RT} = \left| \frac{p(R, \theta, \phi)}{p_o(R, \theta, \phi=0)} \right| = \frac{\sqrt{1 + \frac{\Omega^2 c^2 \rho^3}{\rho_o^2} \frac{12(1-\nu^2)}{E}} \times \cos\phi}{\sqrt{1 + \frac{\Omega^6 c^2 \rho^3}{\rho_o} \frac{12(1-\nu^2)}{E} \left[\sin^4\phi - \frac{1}{\Omega}\right]^2}} \times \left| \overline{C_{ms}} \right| \tag{3.3}$$

Directivity computations were made at the frequencies $\Omega = 0.01$, 0.1, 0.5, 1.0, 1.5, 2.0, 2.5 for the following three types of the reinforcement; namely,

(1) Mass reinforcement: $\gamma = 0$, 1.0, 2.7, 5.0, 10.0

(2) Stiffness reinforcement: Since the stiffness of the reinforcement can be characterized by the ratio of the depth of the attached rectangular beam ($q_2 h$) to that of the plate (h) while assuming the width of the beam is equal to the depth of the plate, five different values of stiffness are considered, i.e.,

$$q_2 = 0\left(\frac{I_b'}{I_p} = 0\right), \quad 0.37\left(\frac{I_b'}{I_p} = 0.05\right), \quad 1.0\left(\frac{I_b'}{I_p} = 0.89\right),$$

$$3.7\left(\frac{I_b'}{I_p} = 45\right), \text{ where } I_p = bD = hD,$$

$I_b' = \frac{b(q_2 h)^3}{12} = \frac{q_2^3 h^4}{12}$ (Moment of inertia of the attached beam about its own neutral axis).

(3) Beam-like reinforcement: $\{\gamma = 0, q_2 = 0\}$, $\{\gamma = 1.0, q_2 = 0.37\}$, $\{\gamma = 2.7, q_2 = 1.0\}$, $\{\gamma = 5.0, q_2 = 1.85\}$ $\{\gamma = 10.0, q_2 = 3.7\}$.

Plots of the directivity function were made for $\Omega = 0.5$, 1.5, and 2.5 only. The case of $\Omega = 0.5$ has been chosen for a representative excitation frequency which is below the coincidence frequency, since the results for very low frequencies such as $\Omega = 0.01$ and 0.1 do not, in general, show pronounced variation for moderately sized reinforcements. The case of $\Omega = 1.5$ shows the results slightly above the coincidence frequency, which not only represents the phenomenon around the coincidence frequency but also shows more definite and noticeable variation than the case of $\Omega = 1.0$. The frequency at $\Omega = 2.5$ is representative of frequency of excitation much higher than the coincidence frequency.

It was noted earlier that the pressure spectrum computation at $\phi = 0°$ was not influenced by the stiffness of the attachment. Similarly, the pressure spectrum at the particular rotational angle $\phi = 0°$ is unaffected by the stiffness; hence, a reinforcing beam acts just like that of its mass only for the directivity plot at $\phi = 0°$.

There are seven figures plotted for Section (ii):

(1) Below the coincidence frequency at $\Omega = 0.5$: Figure 3.2 was made at two fixed rotational angles ($\theta = 0°$ and 90°) for various types of reinforcements.

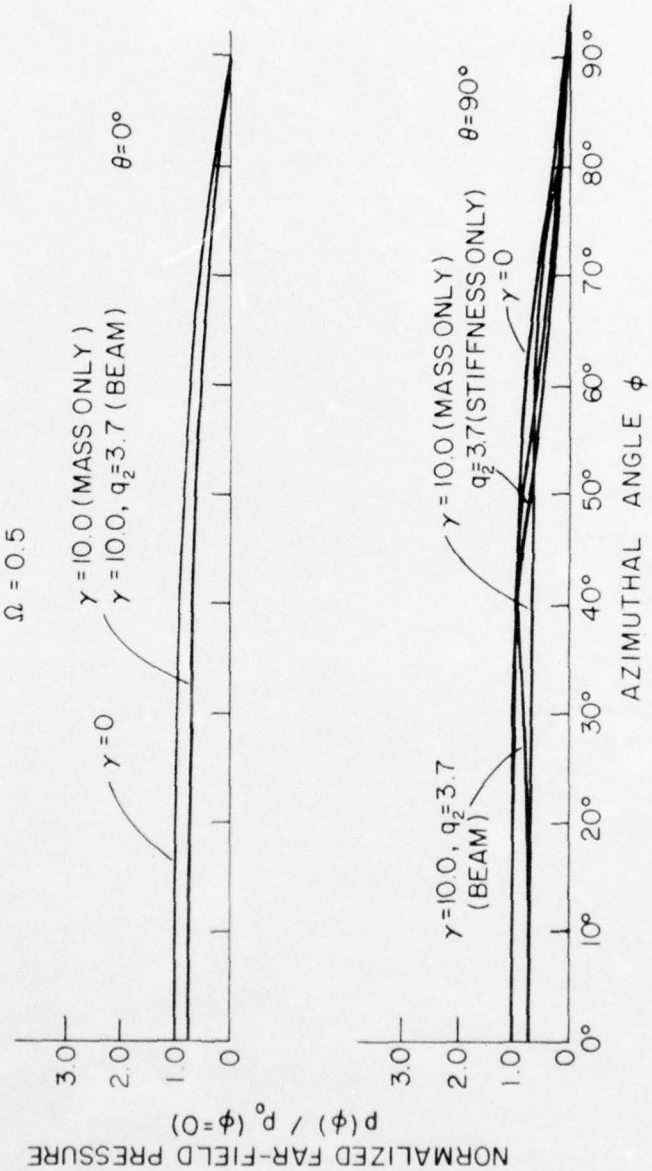

Figure 3.2 Directivity Function of Far-Field Pressure of Beam-Reinforced Plate (Ω = 0.5)

(2) Above the coincidence frequency at $\Omega = 1.5$: Three figures were plotted according to three types of reinforcement. Figure 3.3 was made at three fixed rotational angles ($\theta = 0°, 45°, 90°$) for the different attached mass ratios $\gamma = 0, 1, 5, 10$, to show the effect of mass reinforcement on the acoustic pressure; Figure 3.4 was made at two rotational angles ($\theta = 45°, 90°$) for various depths of the attachment ($q_2 = 0, 0.37, 1.85, 3.7$) to show the stiffness effect on the acoustic pressure, and Figure 3.5 was made at three fixed rotational angles ($\theta = 0°, 45°, 90°$) for various beam sizes to show both the influence of the mass and the stiffness on the radiated acoustic pressure.

(3) Above the coincidence frequency at $\Omega = 2.5$: Three figures, i.e., Figure 3.6, 3.7, and 3.8 were plotted in the same manner as Figures 3.3, 3.4, and 3.5, respectively.

3.1.3 Power Spectrum. The radiated acoustic power (N) from a point-excited beam-reinforced plate was computed relative to the driving power (N_o) of an infinite isotropic plate excited by a point force at the origin, versus the nondimensional frequencies (Ω). The driving power (N_o) can be shown to be

$$N_o = \frac{F_o^2}{16\sqrt{mD}}$$

and therefore,

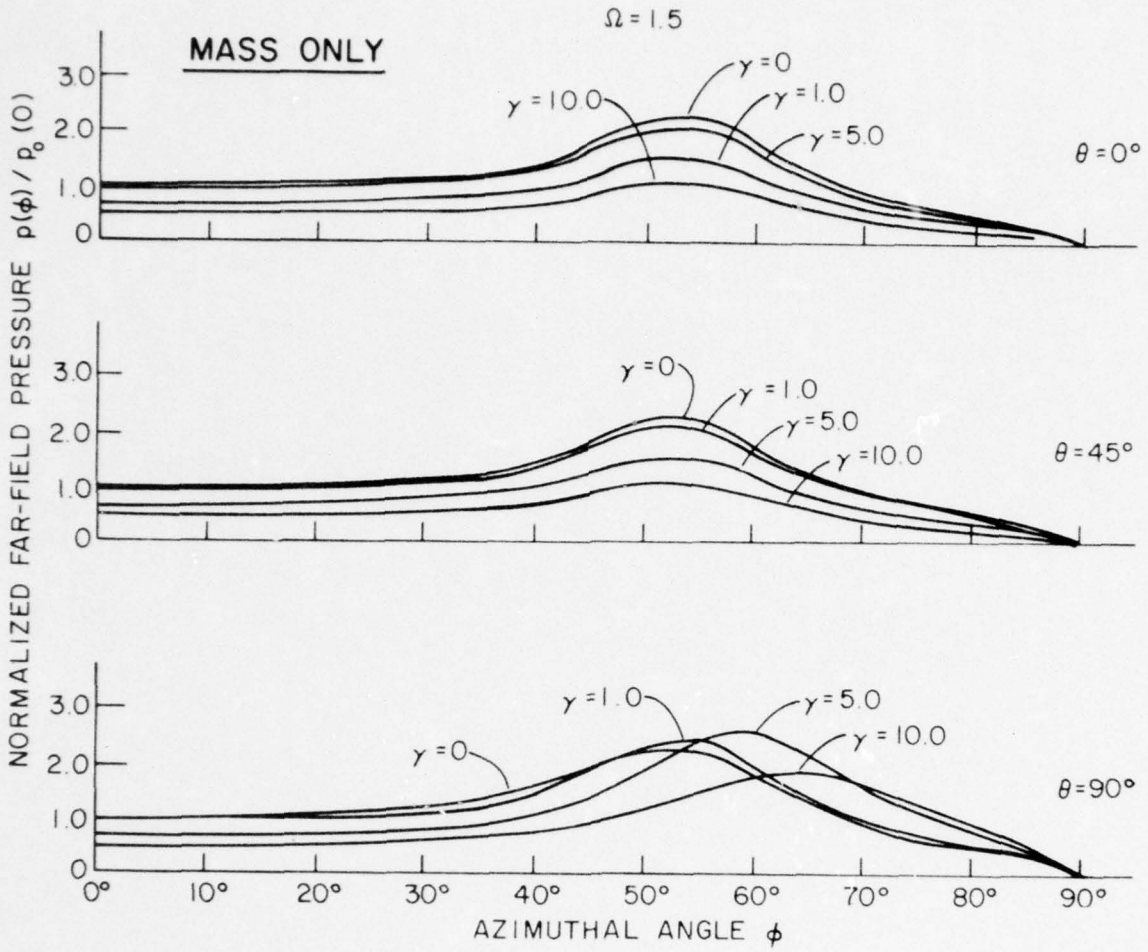

Figure 3.3 Directivity Function of Far-Field Pressure of Beam-Reinforced Plate (Mass Only, Ω = 1.5)

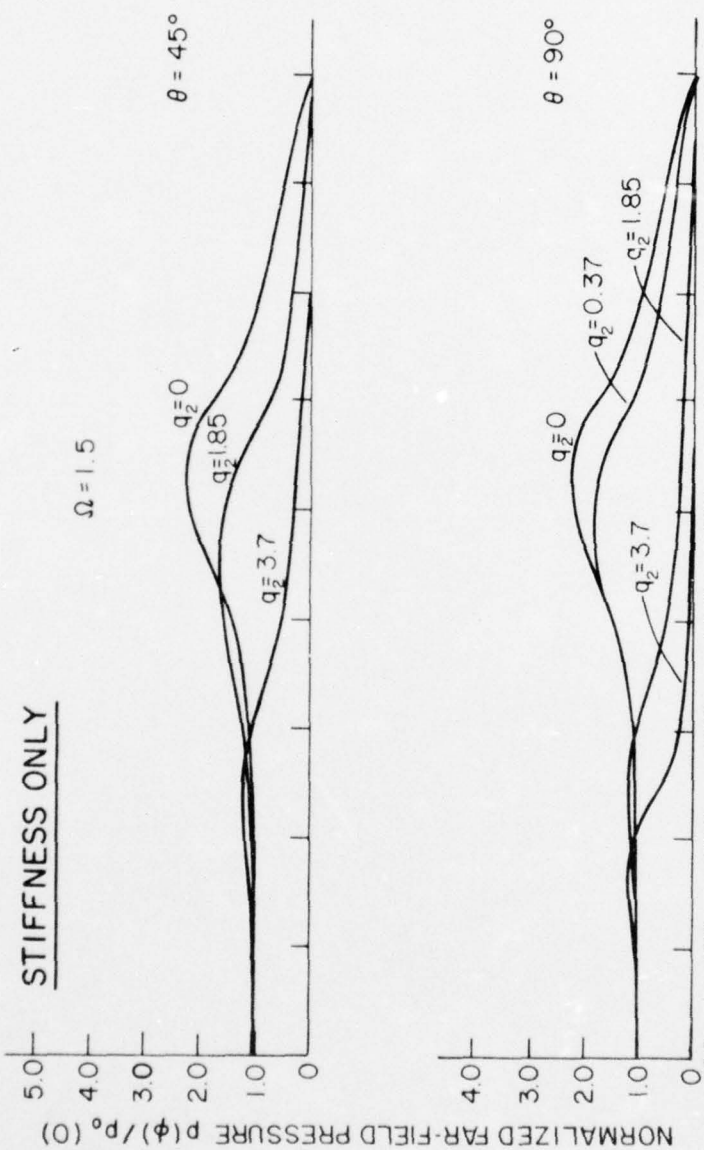

Figure 3.4 Directivity Function of Far-Field Pressure of Beam-Reinforced Plate (Stiffness Only, $\Omega = 1.5$)

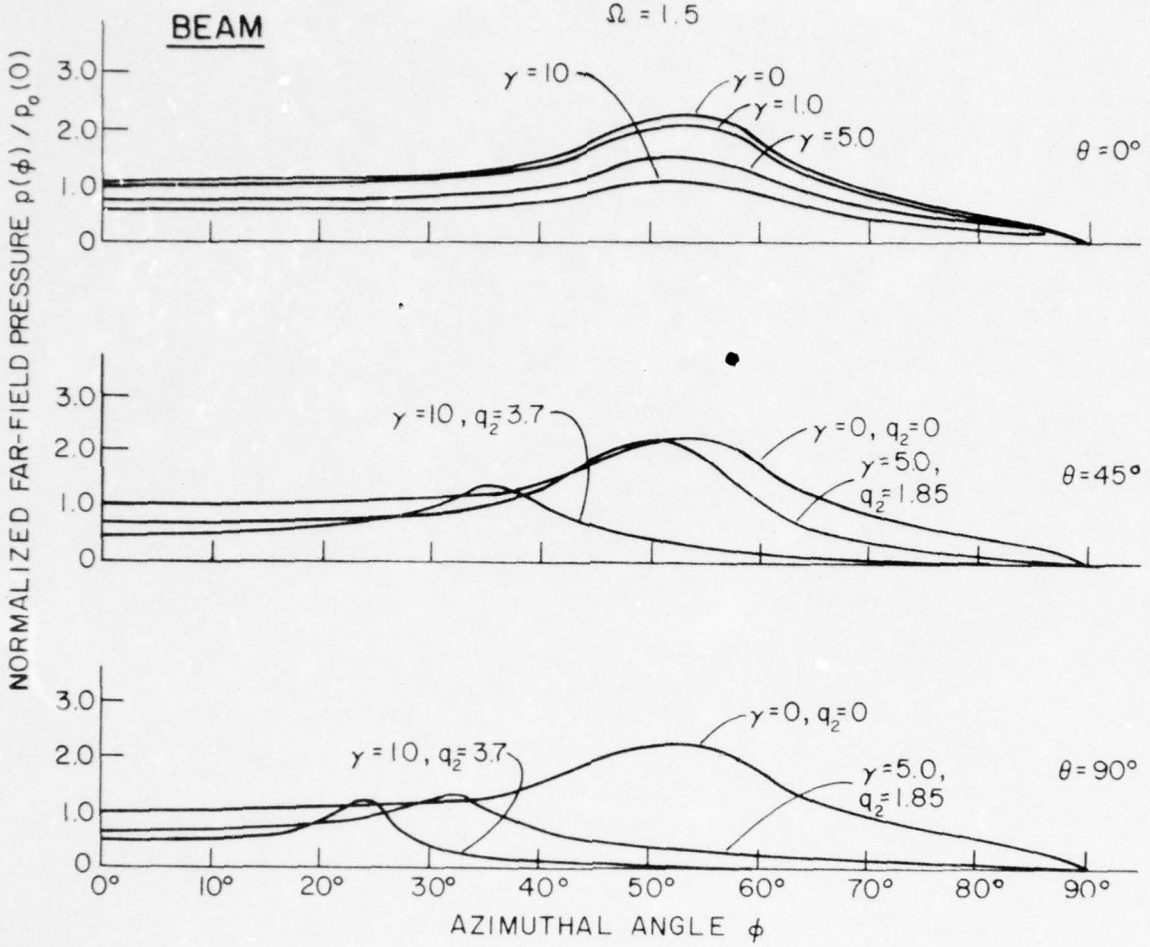

Figure 3.5 Directivity Function of Far-Field Pressure of Beam-Reinforced Plate (Beam, $\Omega = 1.5$)

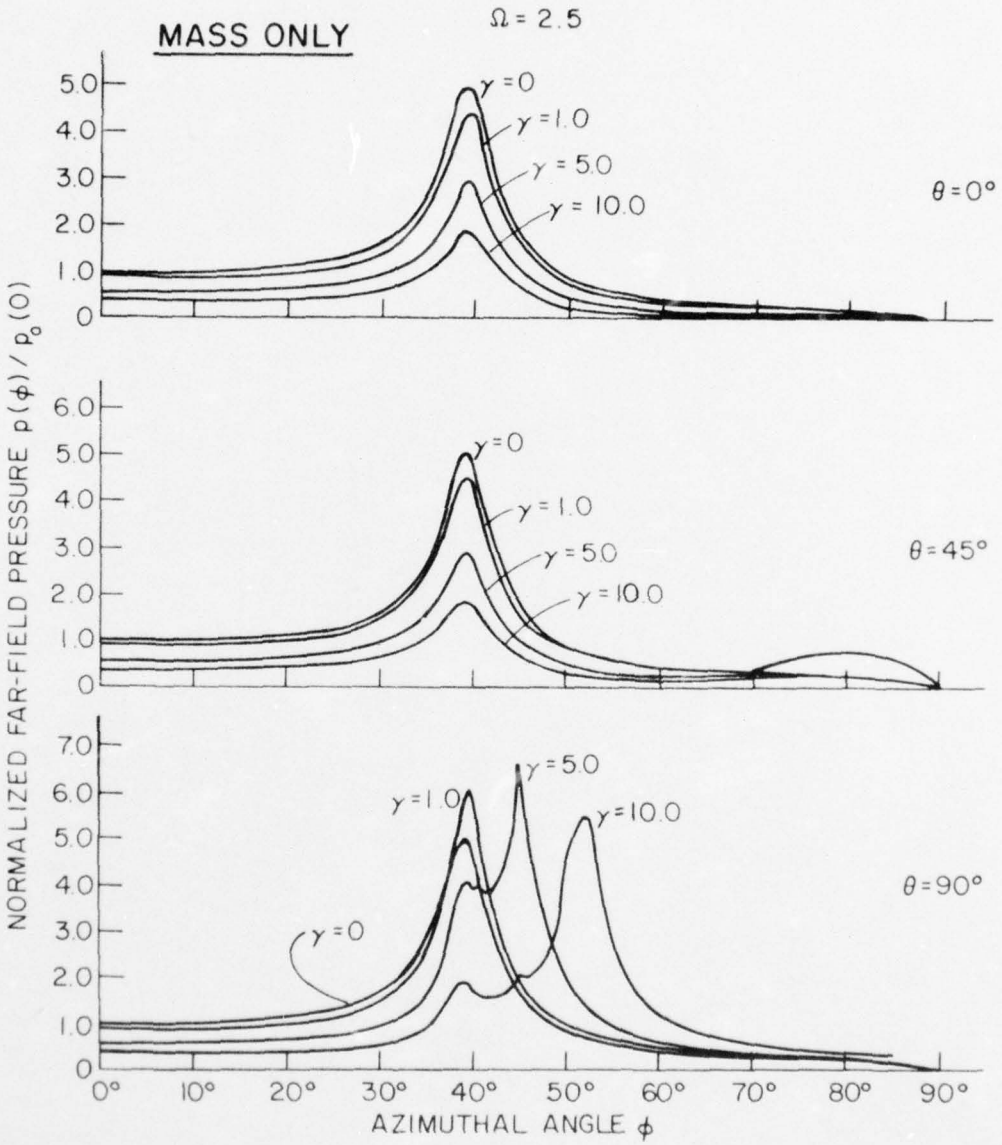

Figure 3.6 Directivity Function of Far-Field Pressure of Beam-Reinforced Plate (Mass Only, $\Omega = 2.5$)

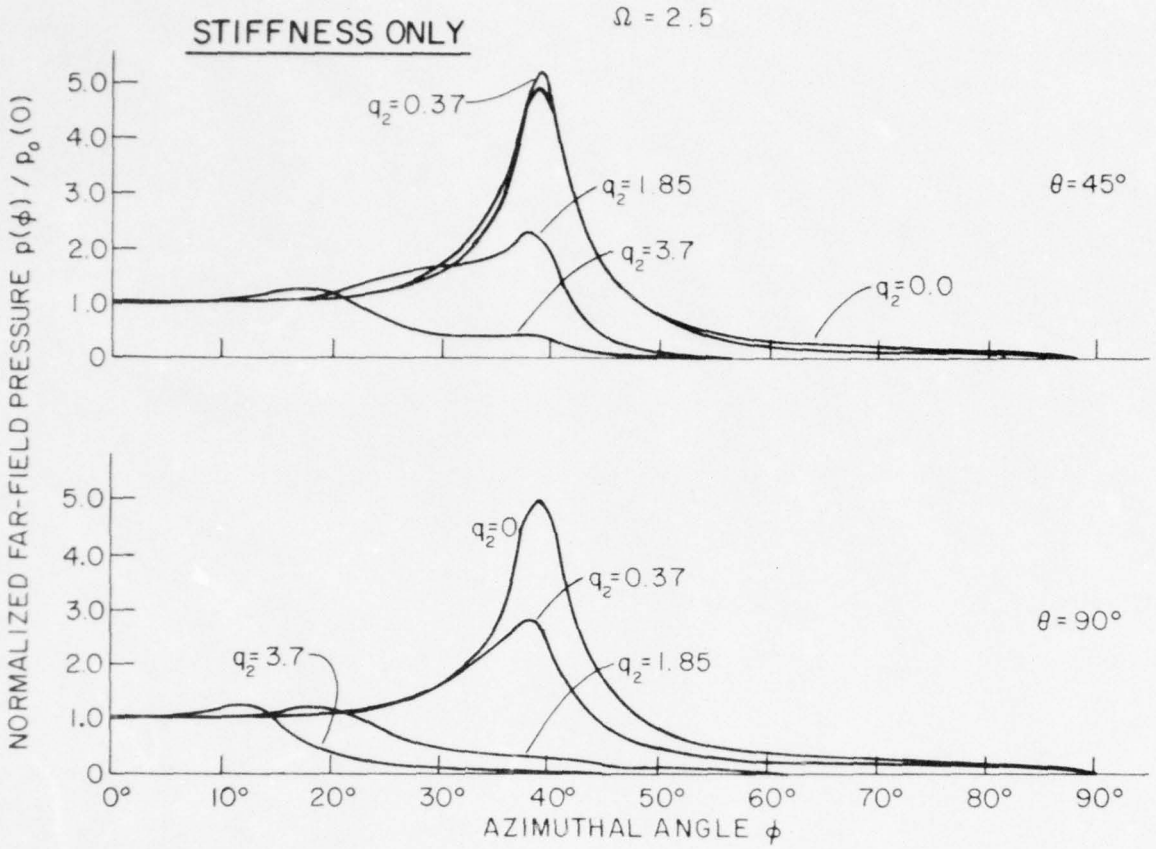

Figure 3.7 Directivity Function of Far-Field Pressure of Beam-Reinforced Plate (Stiffness Only, $\Omega = 2.5$)

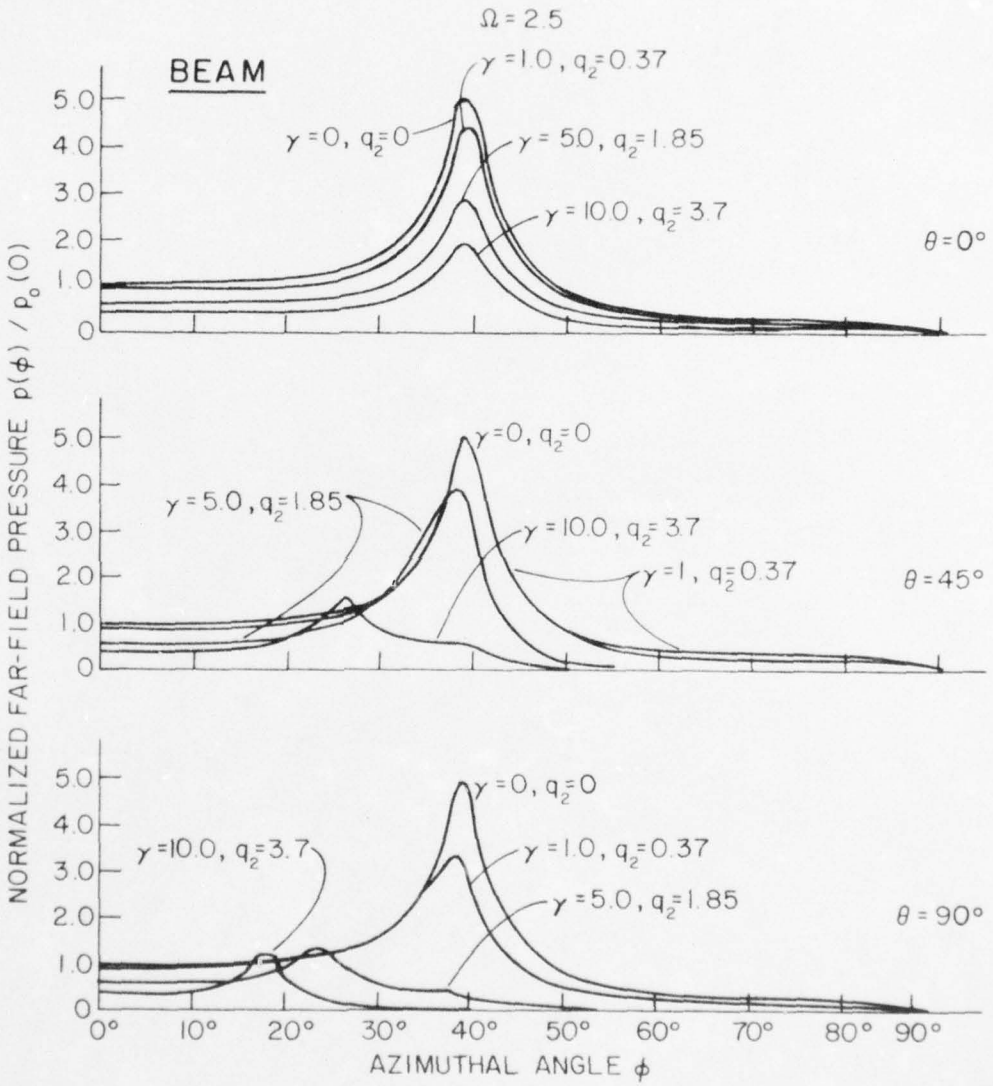

Figure 3.8 Directivity Function of Far-Field Pressure of Beam-Reinforced Plate (Beam, Ω = 2.5)

$$\frac{N}{N_o} = g\Omega^2 \int_0^{\pi/2} \int_0^{\pi/2} \frac{\cos^2\phi \sin\phi |\bar{C}_{ms}|^2 d\theta\, d\phi}{\sqrt{1 + \left\{\frac{\Omega^6 c^2 \rho^3}{\rho_o^2} \frac{12(1-\nu)^2}{E}\right\} \cos^2\phi \{\sin^4\phi - \frac{1}{\Omega^2}\}^2}} , \tag{3.4}$$

where

$$g = \frac{8\rho c}{\pi^2 \rho_o} \sqrt{\frac{12\rho(1-\nu^2)}{E}} .$$

Figure 3.9 presents the power spectrum of a plate with an attached line mass for five mass ratios γ = 0, 1.0, 2.7, 5.0, 10.0. Figure 3.10 presents the power spectrum of a plate with an attached line stiffness for five various depths of attachment q_2 = 0, 0.37, 1.0, 1.85, 3.7. Figure 3.11 presents the power spectrum of a beam-reinforced plate for various beam sizes.

3.2 Numerical Results for Beam-Reinforced Plate with Two Additional Spring-Mass Systems

3.2.1 Input Data. For an aluminum infinite plate in contact with water, numerical results are presented by using the same physical constants given in Section 3.1.1.

3.2.2 Far-Field Pressure Spectrum and Directivity Function. The far-field pressure in the present problem (see Figure 3.3) is shown in Equation (2.74), i.e.,

$$p = \left[\frac{-ik_o F_o}{2\pi R} \frac{e^{ik_o R \cos\phi}}{1 - \frac{ik_o m \cos\phi}{\rho_o}(1 - \Omega^2 \sin^4\phi)}\right] C_{ms}(\phi, \theta) , \tag{2.74}$$

where

AD-A040 669 PENNSYLVANIA STATE UNIV UNIVERSITY PARK APPLIED RESE--ETC F/G 13/13
ACOUSTIC FAIRING - AN APPLICATION TO BEAM REINFORCED PLATES.(U)
AUG 73 G F LIN N00017-73-C-1418
UNCLASSIFIED TM-73-196 NL

2 OF 2
AD
A040669

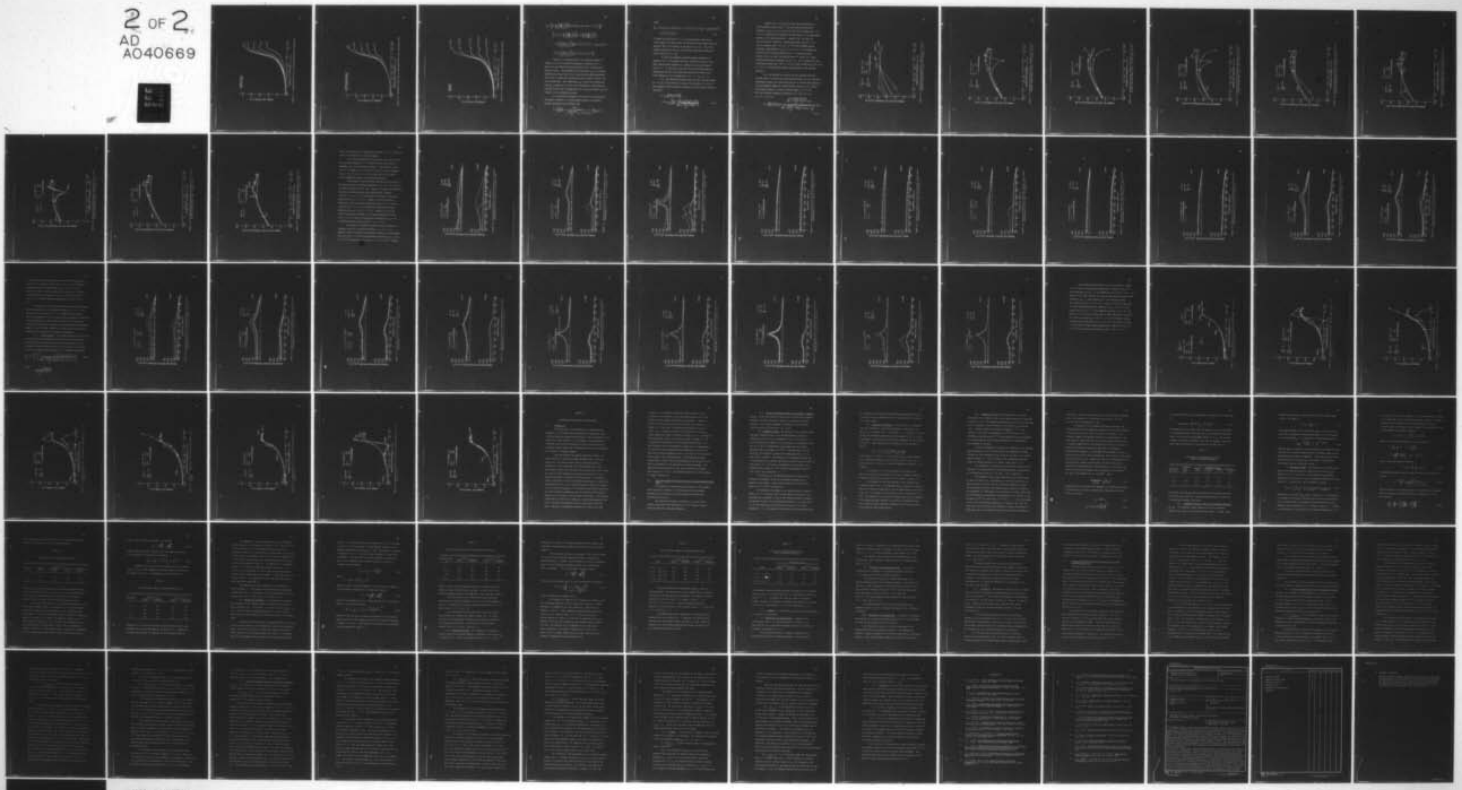

END

DATE
FILMED
7-77

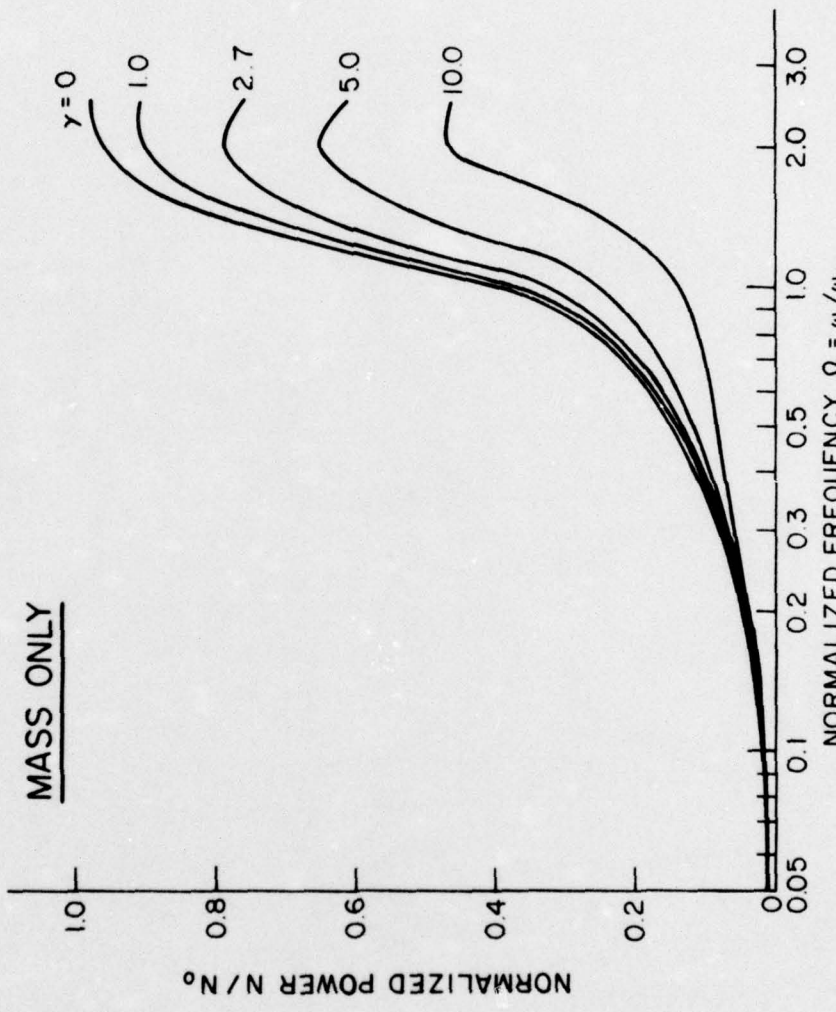

Figure 3.9 Normalized Power N/N_o of Beam-Reinforced Plate (Mass Only)

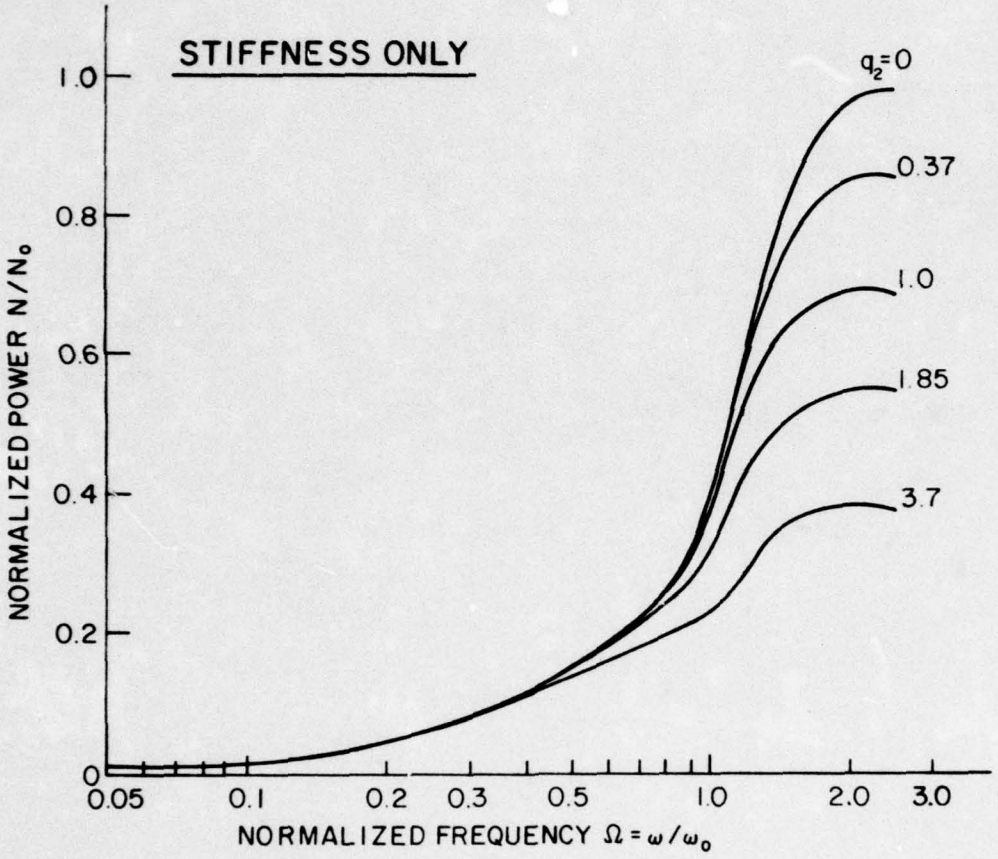

Figure 3.10 Normalized Power N/N_o of Beam-Reinforced Plate (Stiffness Only)

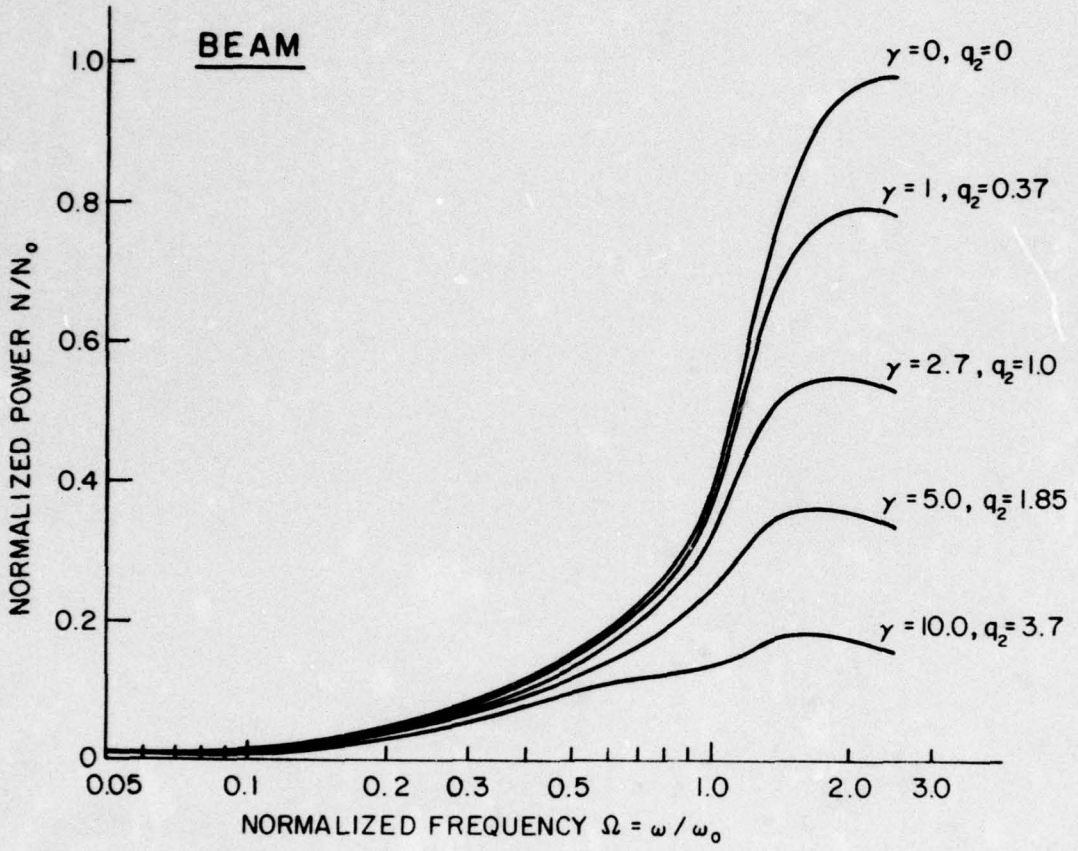

Figure 3.11 Normalized Power N/N_o of Beam-Reinforced Plate (Beam)

$$C_{ms} = \left[1+\mu_1\left(\frac{m_1}{\rho_o h^2}\right)\left(\frac{\omega_1^2}{\omega_1^2-\omega^2}\right)\{2I_2^o\cos(k_o d\cos\theta\sin\phi) - I_1^o - I_3^o\}\right]\Big/$$

$$\left[1-\mu_1 I_1^o\{\gamma+\left(\frac{m_1}{\rho_o h^2}\right)\left(\frac{\omega_1^2}{\omega_1^2-\omega^2}\right)\}-\mu_1 I_3^o\left(\frac{m_1}{\rho_o h^2}\right)\left(\frac{\omega_1^2}{\omega_1^2-\omega^2}\right)\right.$$

$$+\mu_1^2\gamma\left(\frac{m_1}{\rho_o h^2}\right)\left(\frac{\omega_1^2}{\omega_1^2-\omega^2}\right)(I_1^{o2}+I_1^o I_3^o-2I_2^{o2}) + \mu_3 U_y\sin^4\phi\sin^4\theta$$

$$\left.\{I_1^o-\mu_1\left(\frac{m_1}{\rho_o h^2}\right)\left(\frac{\omega_1^2}{\omega_1^2-\omega^2}\right)(I_1^{o2}+I_1^o I_3^o-2I_2^{o2})\}\right] .$$

Similar to the expression for the radiated pressure in Equation (3.1), the bracketed expression in Equation (2.74) is seen to be the radiated far-field pressure from a point-excited isotropic plate. The nondimensional coefficient C_{ms} is a pressure amplitude correction factor for a point-excited beam-reinforcement plate with two additional spring-mass systems equally located from the attached beam. This coefficient C_{ms} is much more complicated than $\bar{C}_{ms}$ in Equation (3.1) due to the couplings of some additional relevant factors such as sprung mass (m_1), spring stiffness (k_1) and location of the spring-mass systems.

If the excitation frequency of the point force approaches the natural frequency of the spring-mass system, the radiated pressure approached the following limit

$$\bar{\bar{p}} = \left[\frac{-ik_o F_o}{2\pi R}\,\frac{e^{ik_o R}\cos\phi}{1-\frac{ik_o m\cos\phi}{\rho_o}(1-\Omega^2\sin^4\phi)}\right]\bar{\bar{C}}_{ms}(\phi,\theta) ,$$

where

$$\bar{C}_{ms} = [2I_2^{o}\cos(k_o d\cos\theta\sin\phi) - I_1^{o} - I_3^{o}]/[-I_1^{o} - I_3^{o} + \{\mu_1\gamma - \mu_3 U_y \sin^4\theta\sin^4\phi\}$$
$$\{I_1^{o\,2} + I_1^{o} I_3^{o} - 2I_2^{o\,2}\}] \quad . \tag{3.5}$$

It should be noted that as $\omega \to \omega_1$, each spring-mass acts like a simple support; in other words, the transverse displacement under the spring is zero, but rotation of the plate is not zero. Thus, the radiated pressure is due to a point excited beam-reinforced plate, simply supported at $x = \pm d$.

By using the radiated far-field pressure expression in Equation (2.74), the pressure spectrum, directivity function, and power spectrum were computed in a similar way as was discussed in Section 3.1. It should be noted that all the following numerical computations done for this particular problem were based on the fixed dimension of the attached beam, i.e., ($\gamma = 2.7$, $q_2 = 1$).

(i) The far-field pressure spectra at zero azimuthal angle ($\phi = 0°$) per 1 pound force at 1 yard in dB relative to 1 μ bar-in were computed versus normalized frequencies (Ω) for several different conditions:

$$20\log_{10}\left[\frac{p(R,\theta,\phi=0)}{\omega_o/c}\right]$$
$$= 20\log_{10}\left[\frac{F_o\Omega}{2\pi R}\,\frac{6.89\times 10^4 |C_{ms}(\theta,\phi=0)|}{\sqrt{1+\frac{\Omega^2 c^2 \rho^3}{\rho_o^2}\,\frac{12(1-\nu)^2}{E}}}\right] . \tag{3.6}$$

Figures 3.12, 3.13, and 3.14 show the pressure spectra of fixed sprung mass ($m_1/\rho_o h^2 = 5.0$) and spring characteristic frequency ($\omega_1/\omega_o = 0.1$, or 1.0, or 2.5) with the variables $k_o d = \pi/5$, π, 3π, to illustrate the influence of the location of the spring-mass systems on the radiated pressure. Figures 3.15, 3.16 and 3.17 show the pressure spectra of a fixed spring mass ($m_1/\rho_o h^2 = 5.0$) and its distance ($k_o d = \pi/5$, or π, or 3π) with variables spring stiffness, represented by $\omega_1/\omega_o = 0.1$, 1.0, 2.5, to illustrate the influence of the spring stiffness k_1 on the radiated pressure. Figures 3.18, 3.19, and 3.20 show the pressure spectra of a fixed spring characteristic frequency ($\omega_1/\omega_o = 1.0$) and the distance of the spring-mass system ($k_o d = \pi/5$, or π, or 3π) with variables $m_1/\rho_o h^2 = 1.0$, 2.7, 5.0, to illustrate the effect of spring mass on the radiated pressure.

(ii) The directivity function for the radiated far-field pressure from a point-excited beam-reinforced plate with two additional spring-mass systems were calculated relative to the far-field pressure at zero-azimuthal angle for a point-excited isotropic plate, versus the azimuthal angle ϕ at three rotational angles ($\theta = 0°$, 45°, 90°) and different excitation frequencies ($\Omega = 0.01$, 0.1, 0.5, 1.0, 1.5, 2.0, 2.5):

$$RT = \left|\frac{p(R, \theta, \phi)}{p_o(R, \theta, \phi=0)}\right| = \frac{\sqrt{1 + \frac{\Omega^2 c^2 \rho^3}{\rho_o^2} \frac{12(1-\nu^2)}{E}} \cos\phi}{\sqrt{1 + \frac{\Omega^6 c^2 \rho^3}{\rho_o^2} \frac{12(1-\nu^2)}{E} \left(\sin^4\phi - \frac{1}{\Omega^2}\right)^2}} |C_{ms}| . \qquad (3.7)$$

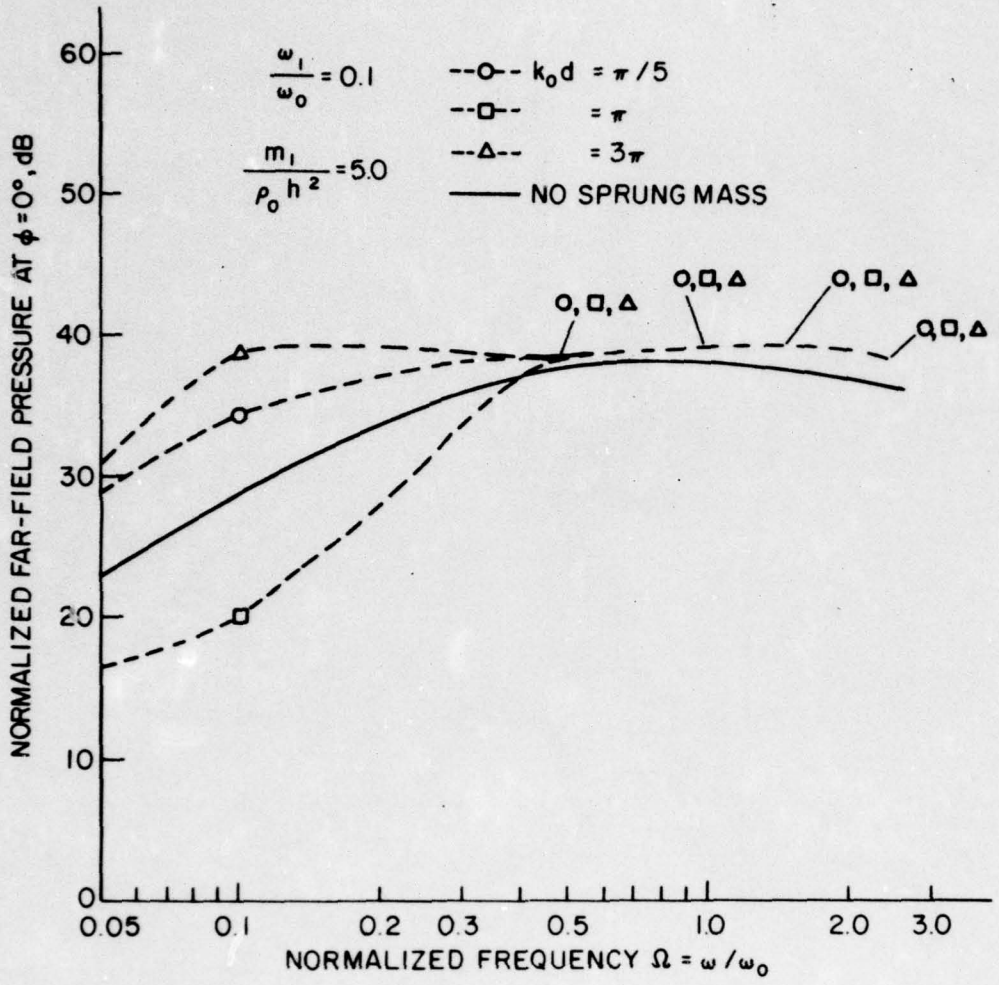

Figure 3.12 Normalized Far-Field Pressure Spectrum at $\phi = 0°$ of an Acoustic Fairing Model ($\omega_1/\omega_0 = 0.1$, $m_1/\rho_0 h^2 = 5.0$)

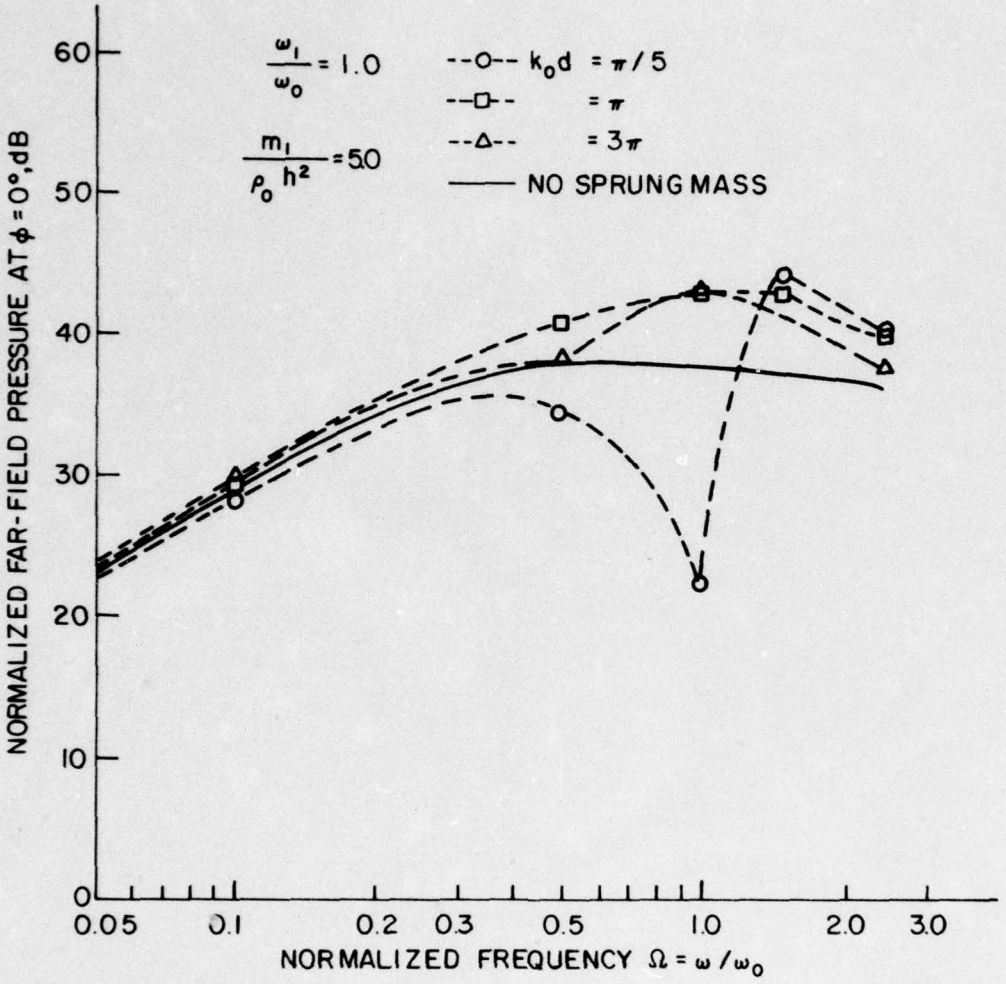

Figure 3.13 Normalized Far-Field Pressure Spectrum at $\phi = 0°$ of an Acoustic Fairing Model ($\omega_1/\omega_o = 1.0$, $m_1/\rho_o h^2 = 5.0$)

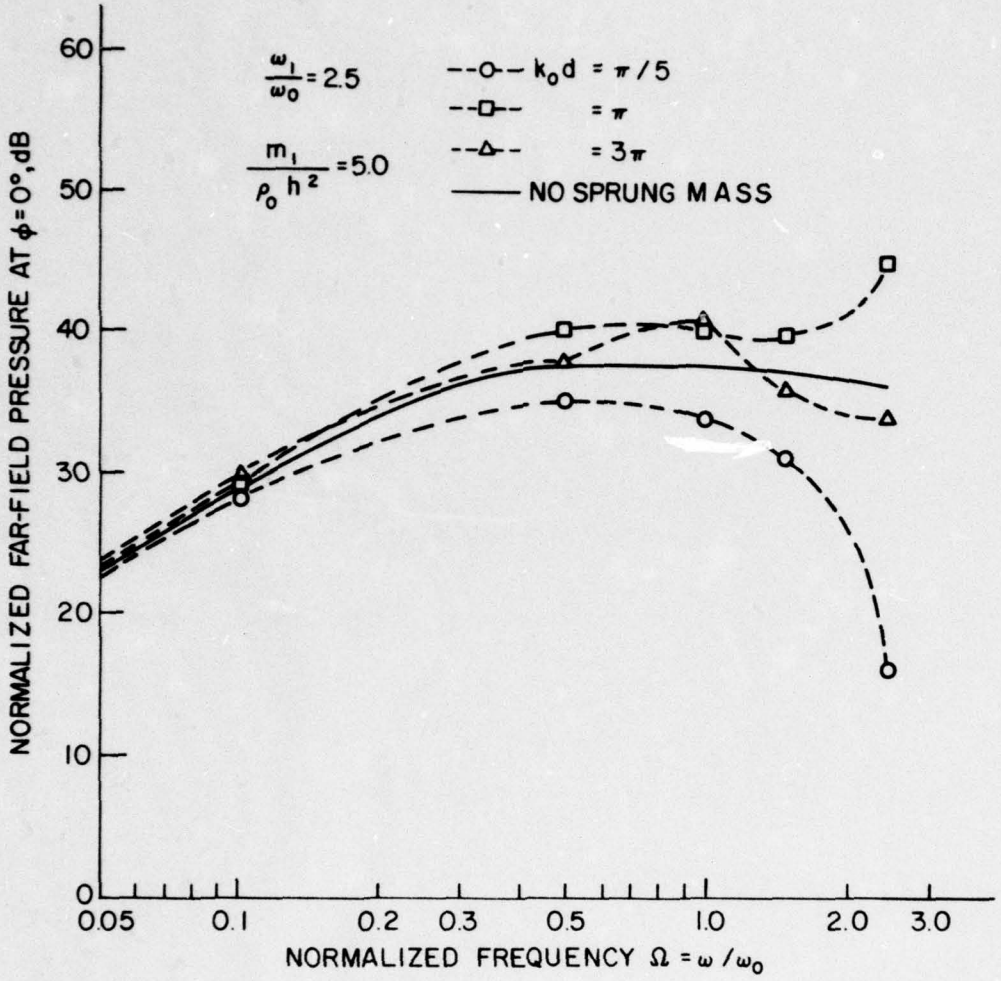

Figure 3.14 Normalized Far-Field Pressure Spectrum at ϕ = 0° of an Acoustic Fairing Model (ω_1/ω_o = 2.5, $m_1/\rho_o h^2$ = 5.0)

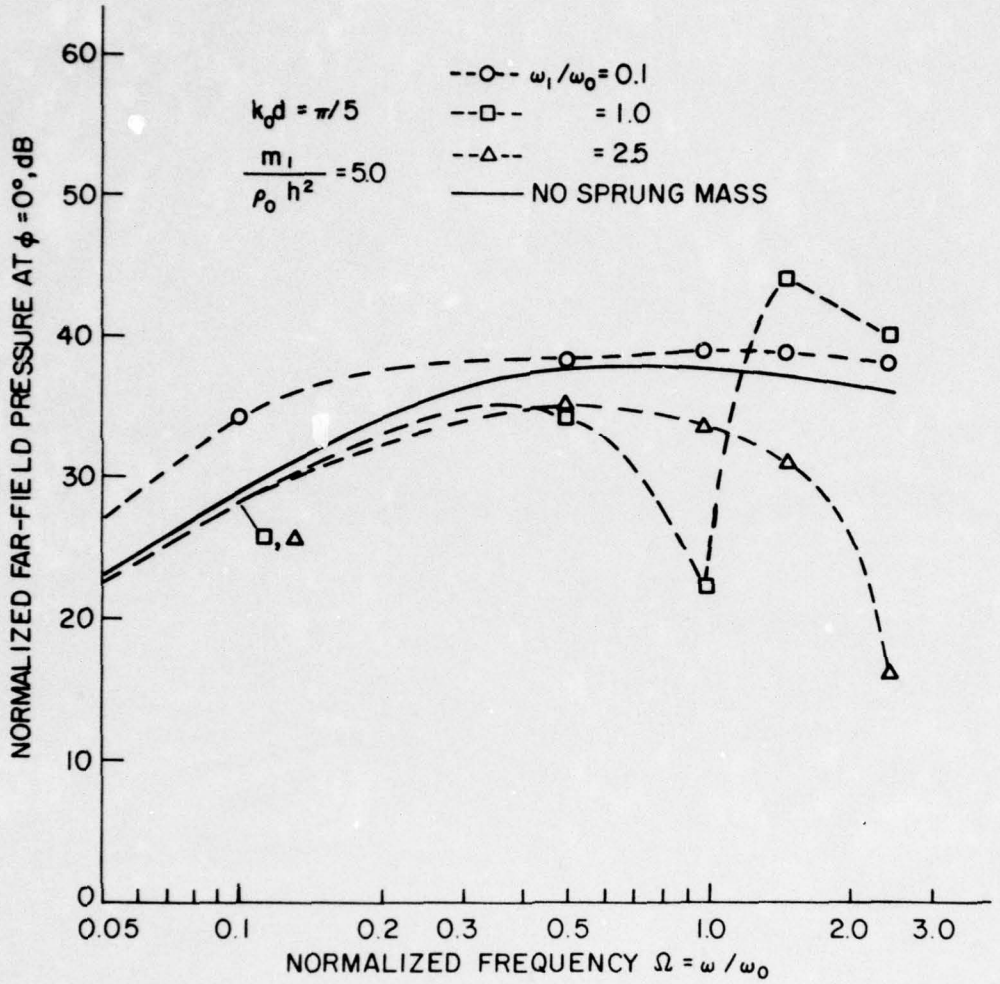

Figure 3.15 Normalized Far-Field Pressure Spectrum at ϕ = 0° of an Acoustic Fairing Model ($k_o d = \pi/5$, $m_1/\rho_o h^2 = 5.0$)

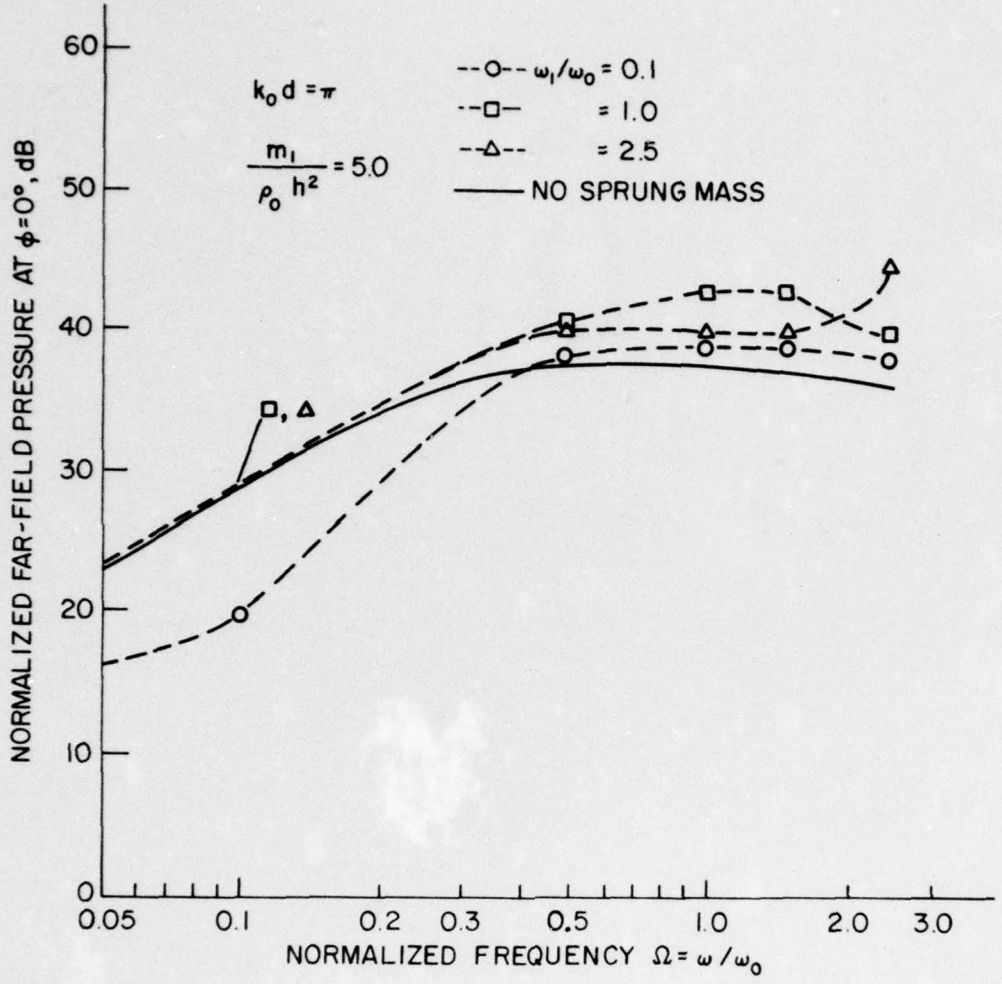

Figure 3.16 Normalized Far-Field Pressure Spectrum at $\phi = 0°$ of an Acoustic Fairing Model ($k_o d = \pi$, $m_1/\rho_o h^2 = 5.0$)

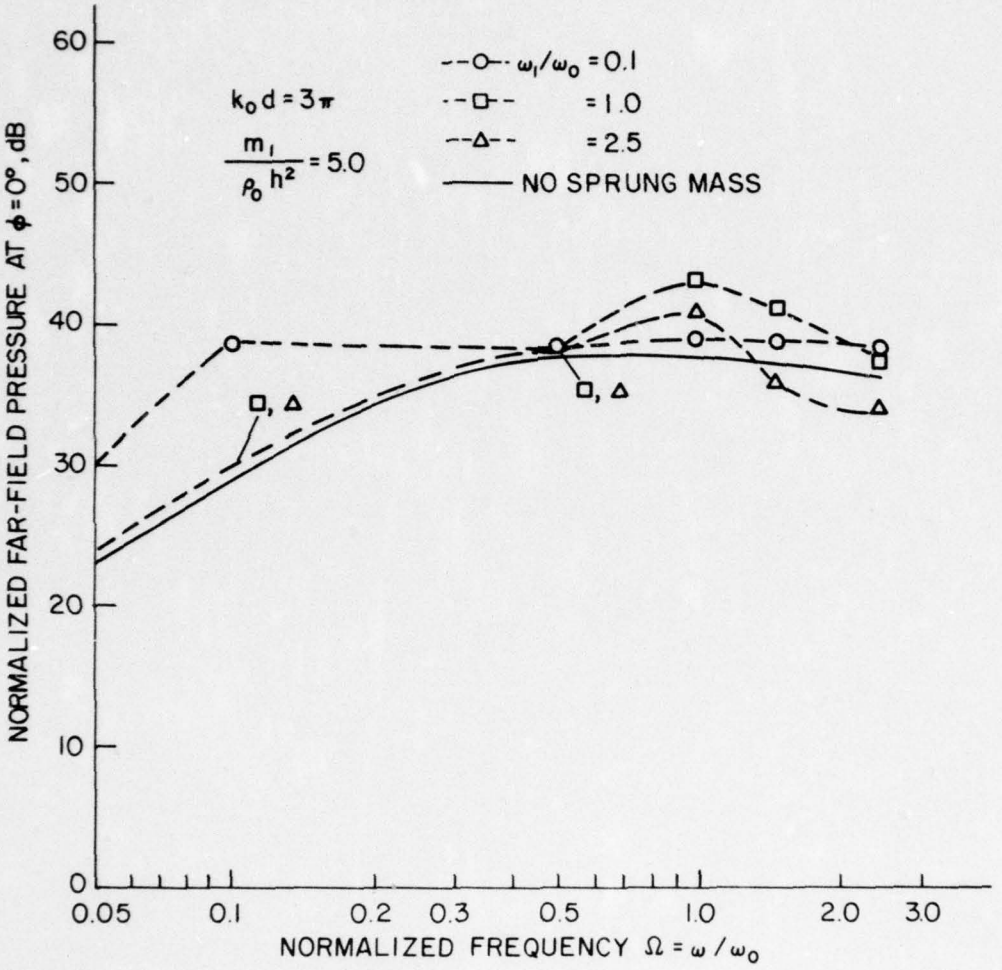

Figure 3.17 Normalized Far-Field Pressure Spectrum at $\phi = 0°$ of an Acoustic Fairing Model ($k_o d = 3\pi$, $m_1/\rho_o h^2 = 5.0$)

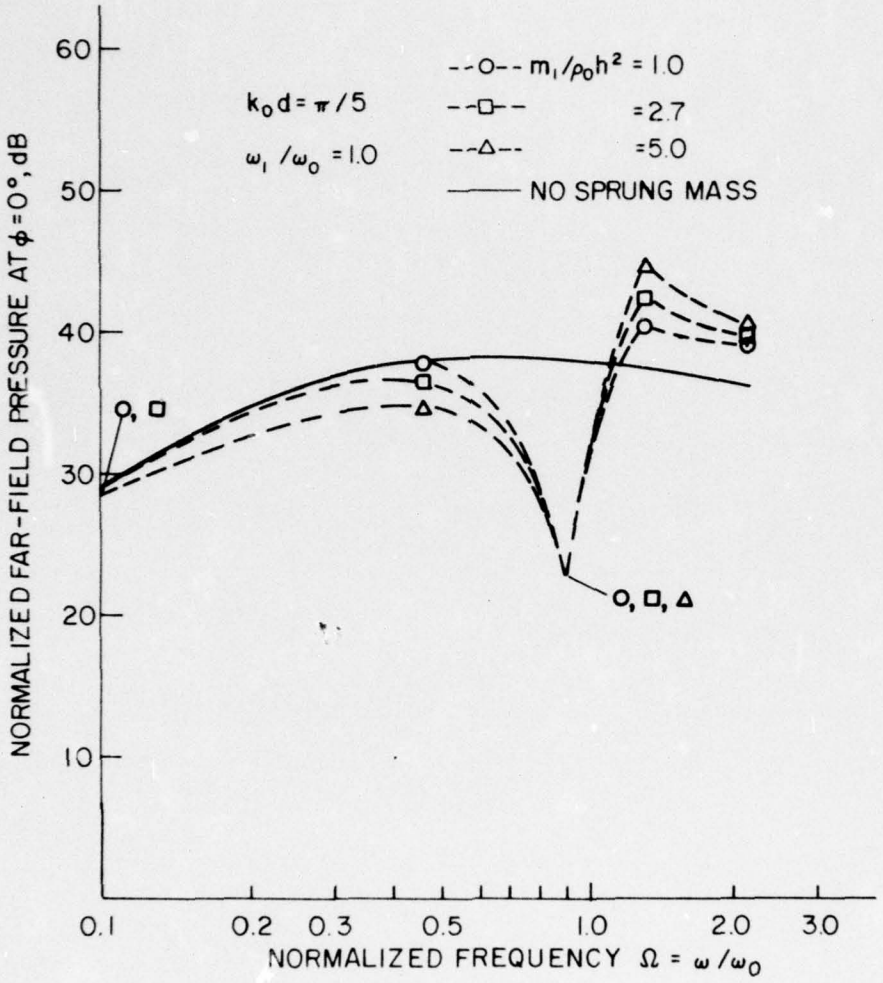

Figure 3.18 Normalized Far-Field Pressure Spectrum at ϕ = 0° of an Acoustic Fairing Model ($k_o d = \pi/5$, ω_1/ω_o = 1.0)

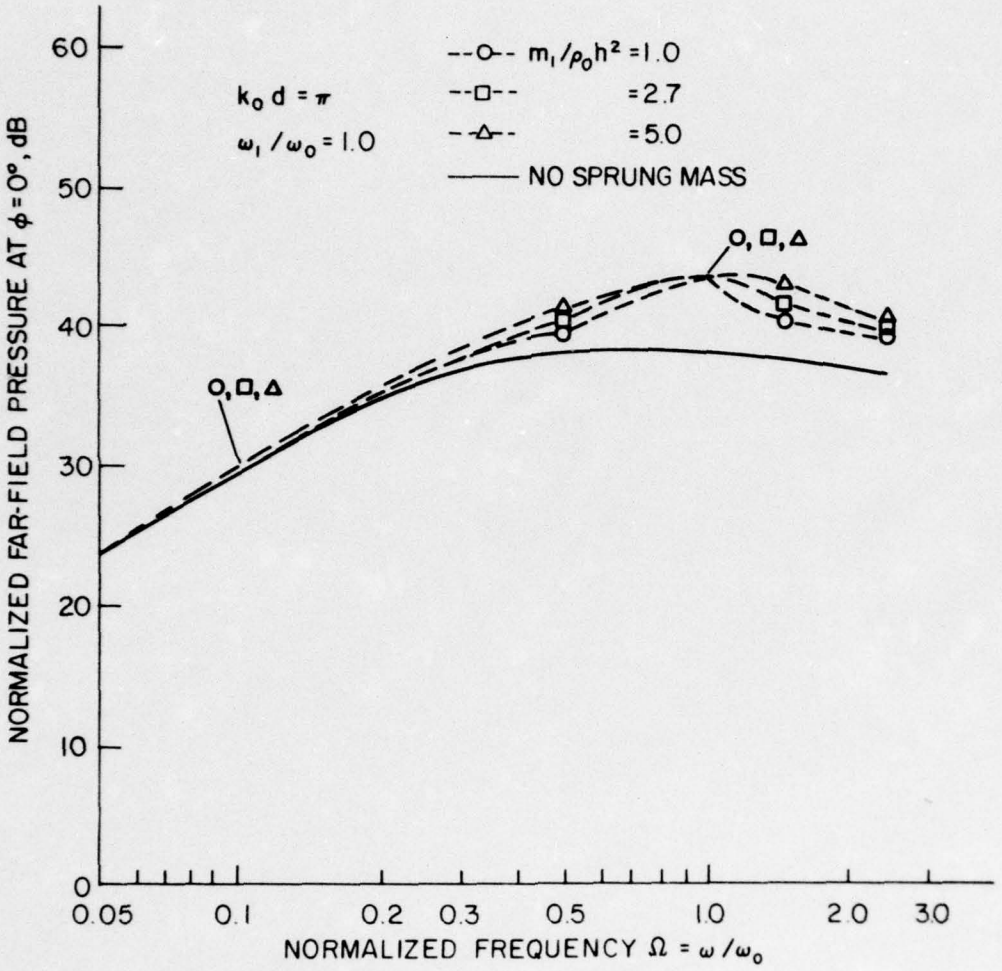

Figure 3.19 Normalized Far-Field Pressure Spectrum at ϕ = 0° of an Acoustic Fairing Model ($k_o d = \pi$, ω_1/ω_o = 1.0)

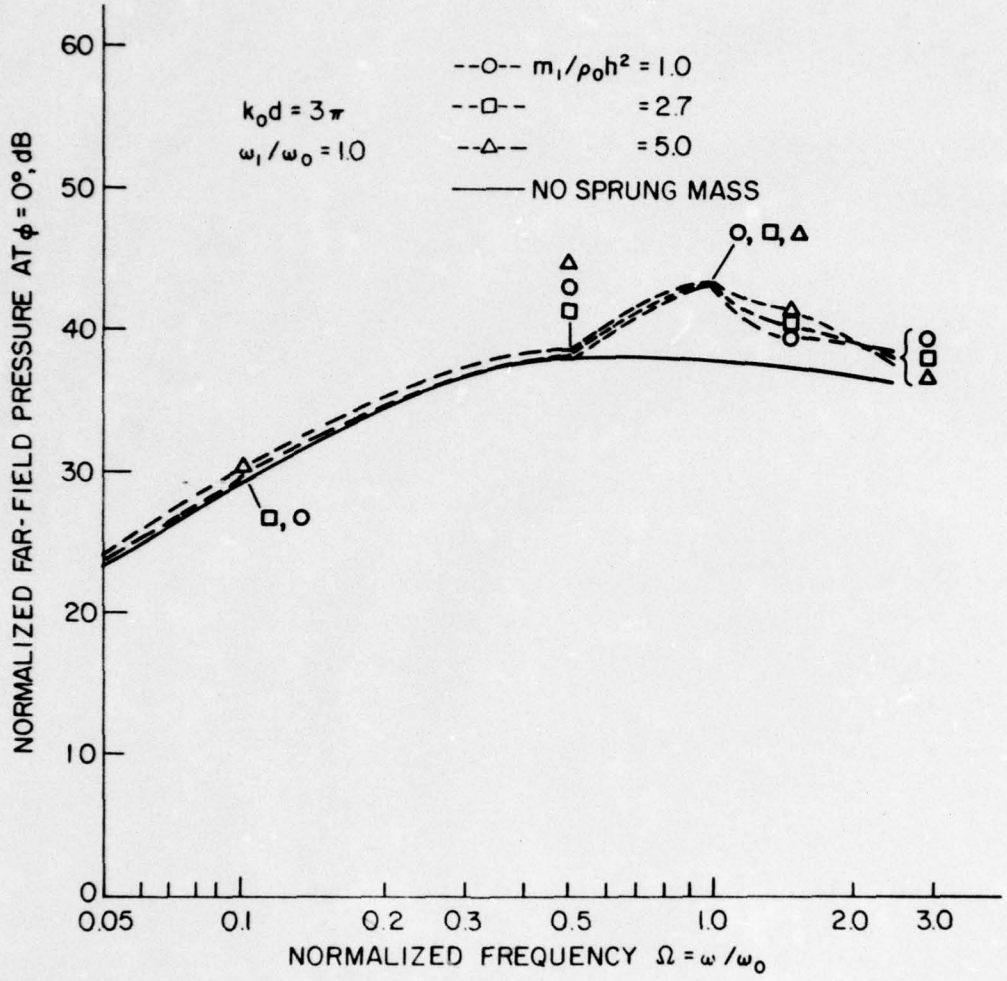

Figure 3.20 Normalized Far-Field Pressure Spectrum at $\phi = 0°$ of an Acoustic Fairing Model ($k_o d = 3\pi$, $\omega_1/\omega_o = 1.0$)

Plots of the directivity function were made for Ω = 0.5, 1.5 and 2.5 only and are presented in nineteen figures.

The most interesting directivity plots are those for which the excitation frequency (ω) coincides with the characteristic frequency (ω_1) of the spring-mass system. Three figures of this case, i.e., Figures 3.21, 3.22, and 3.23 are plotted at frequency ($\omega_1/\omega_o = \omega/\omega_o$ = 0.5, or 1.5 or 2.5) to show the location effect of the spring-mass system on the resulting pressure.

Five figures of the directivity function were plotted for a frequency below the coincidence frequency, i.e., at Ω = 0.5, which are shown in Figures 3.24 to 3.28. Figure 3.24 shows the directivity function at fixed sprung mass and characteristic frequency ($m_1/\rho_o h^2$ = 2.7, ω_1/ω_o = 1) for different locations of the spring-mass system ($k_o d$ = 0, $\pi/5$, π). Figure 3.25 and 3.26 show the directivity function at fixed spring mass ($m_1/\rho_o h^2$ = 2.7) and its location ($k_o d = \pi/5$ or 3π) for different spring characteristic frequencies (ω_1/ω_o = 0, 0.1, 1.0, 2.5). Figure 3.27 and 3.28 show the directivity function at the fixed spring-maws location ($k_o d = \pi/5$ or 3π) and its characteristic frequency (ω_1/ω_o = 1.0) at different sprung masses ($m_1/\rho_o h^2$ = 0, 2.7, 5.0).

Six figures of directivity functions were plotted for a frequency above the coincidence frequency, i.e., at Ω = 1.5. Figures 3.29 and 3.30 show the directivity function at fixed sprung mass ($m_1/\rho_o h^2$ = 2.7) and its characteristic frequency (ω_1/ω_o = 1.0, or 2.5) for different locations ($k_o d$ = 0, $\pi/5$, π, or 3π). Figures

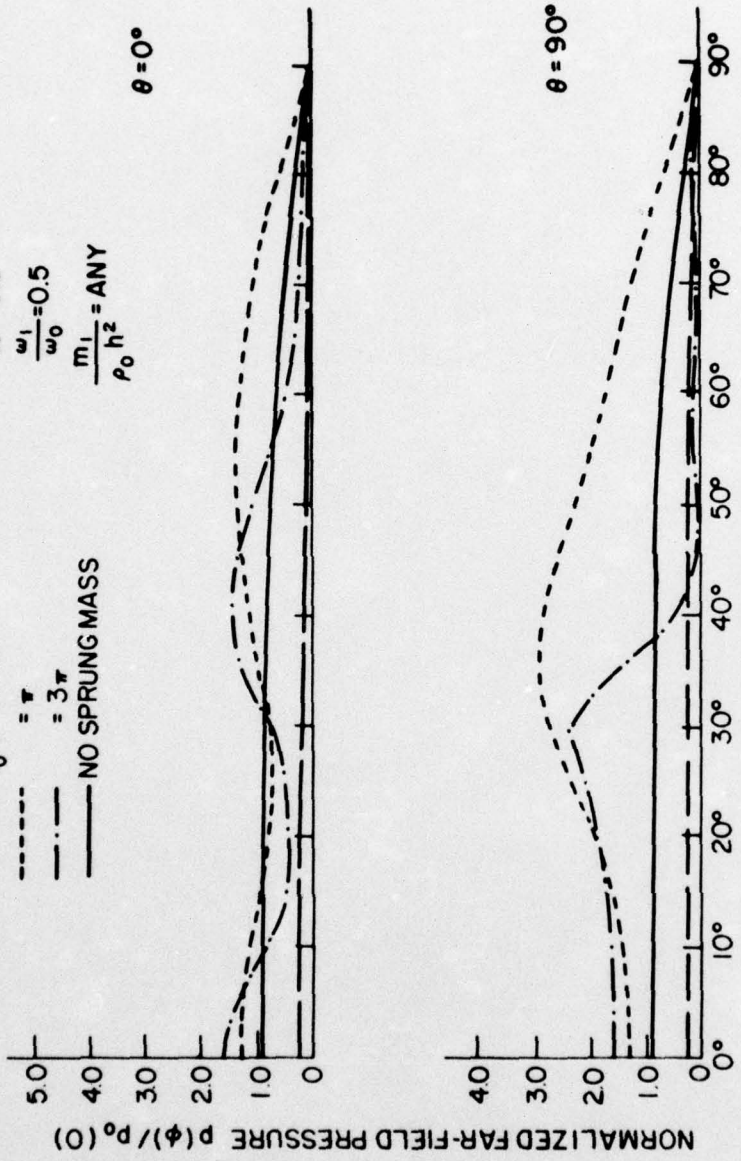

Figure 3.21 Directivity Function of Far-Field Pressure of an Acoustic Fairing Model (Ω = 0.5, ω_1/ω_o = 0.5, $m_1/\rho_o h^2$ = any)

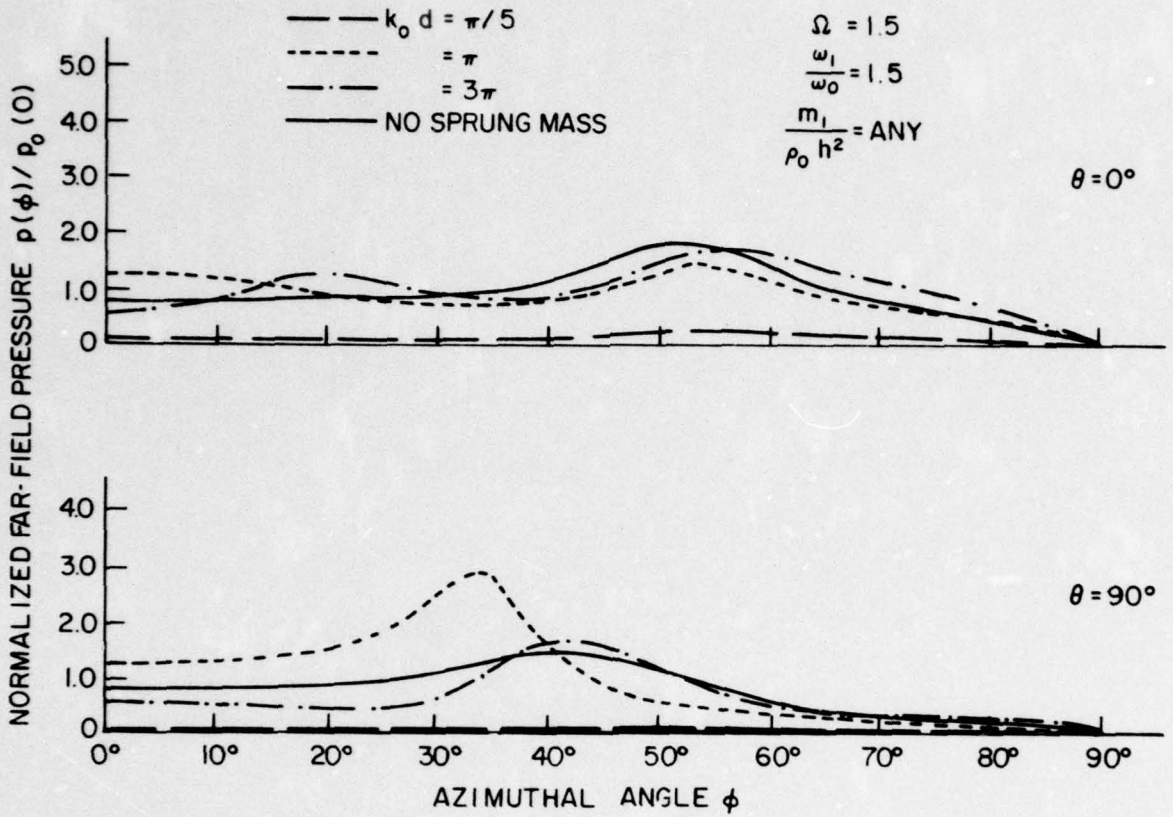

Figure 3.22 Directivity Function of Far-Field Pressure of an Acoustic Fairing Model1 (Ω = 1.5, ω_1/ω_o = 1.5, $m_1/\rho_o h^2$ = any)

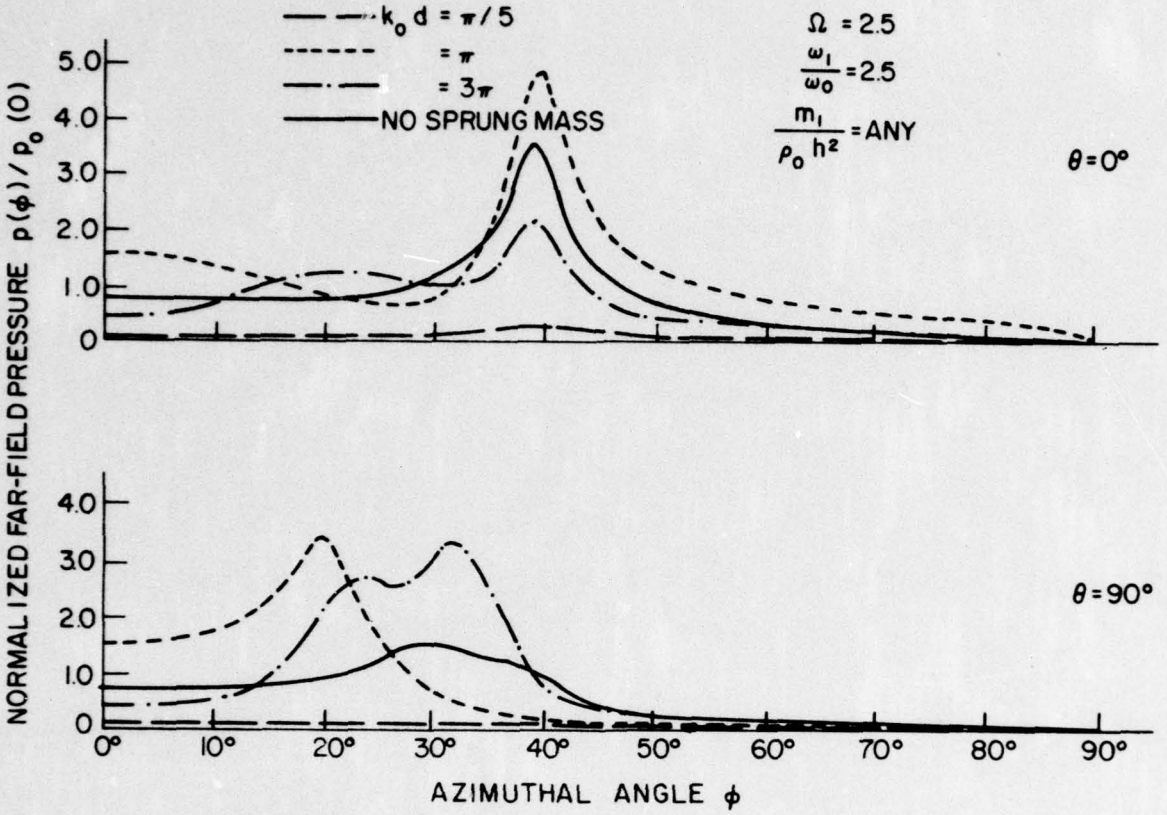

Figure 3.23 Directivity Function of Far-Field Pressure of an Acoustic Fairing Model (Ω = 2.5, ω_1/ω_o = 2.5, $m_1/\rho_o h^2$ = any)

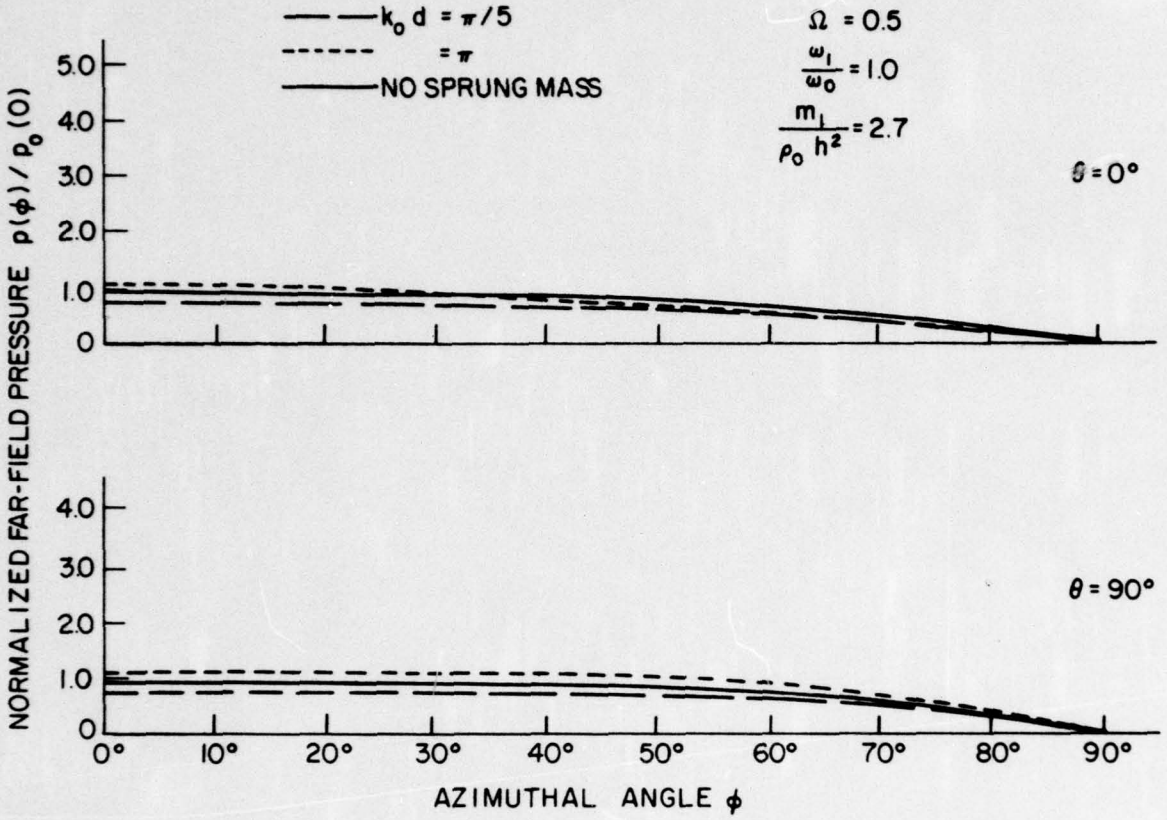

Figure 3.24 Directivity Function of Far-Field Pressure of an Acoustic Fairing Model ($\Omega = 0.5$, $\omega_1/\omega_o = 1.0$, $m_1/\rho_o h^2 = 2.7$)

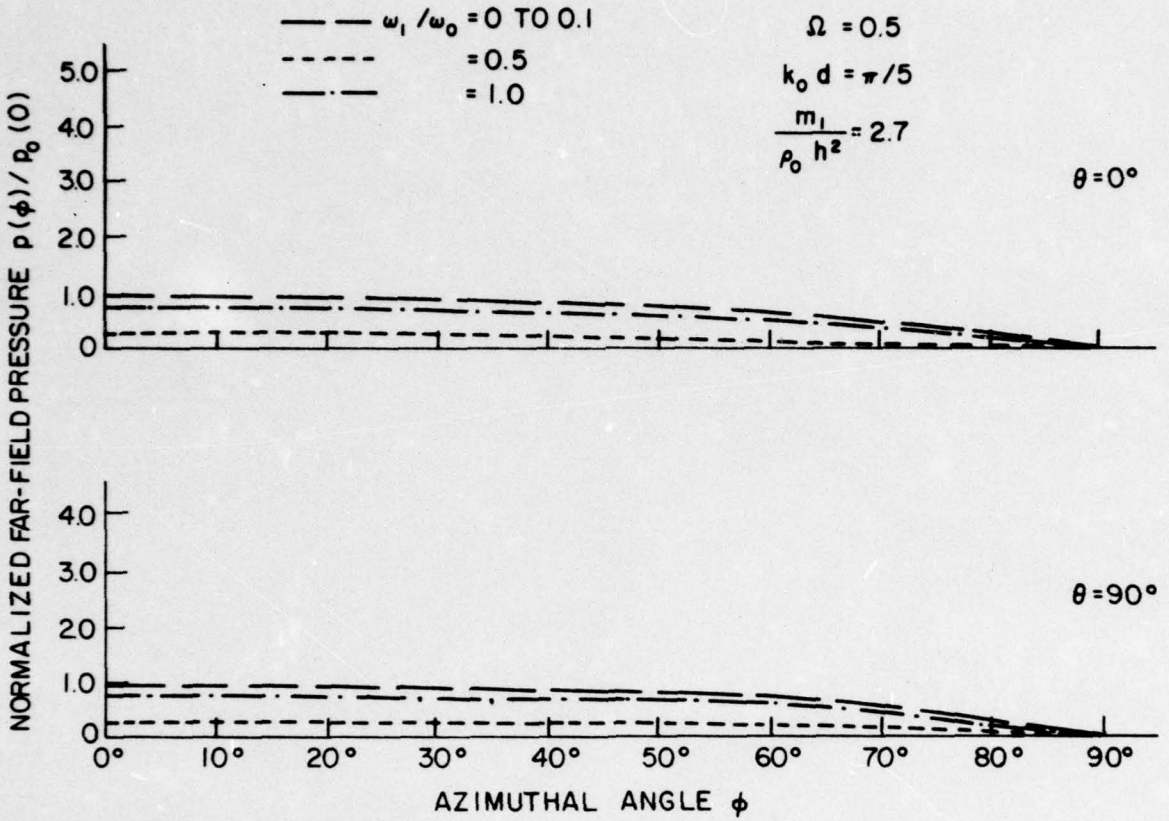

Figure 3.25 Directivity Function of Far-Field Pressure of an Acoustic Fairing Model ($\Omega = 0.5$, $k_o d = \pi/5$, $m_1/\rho_o h^2 = 2.7$)

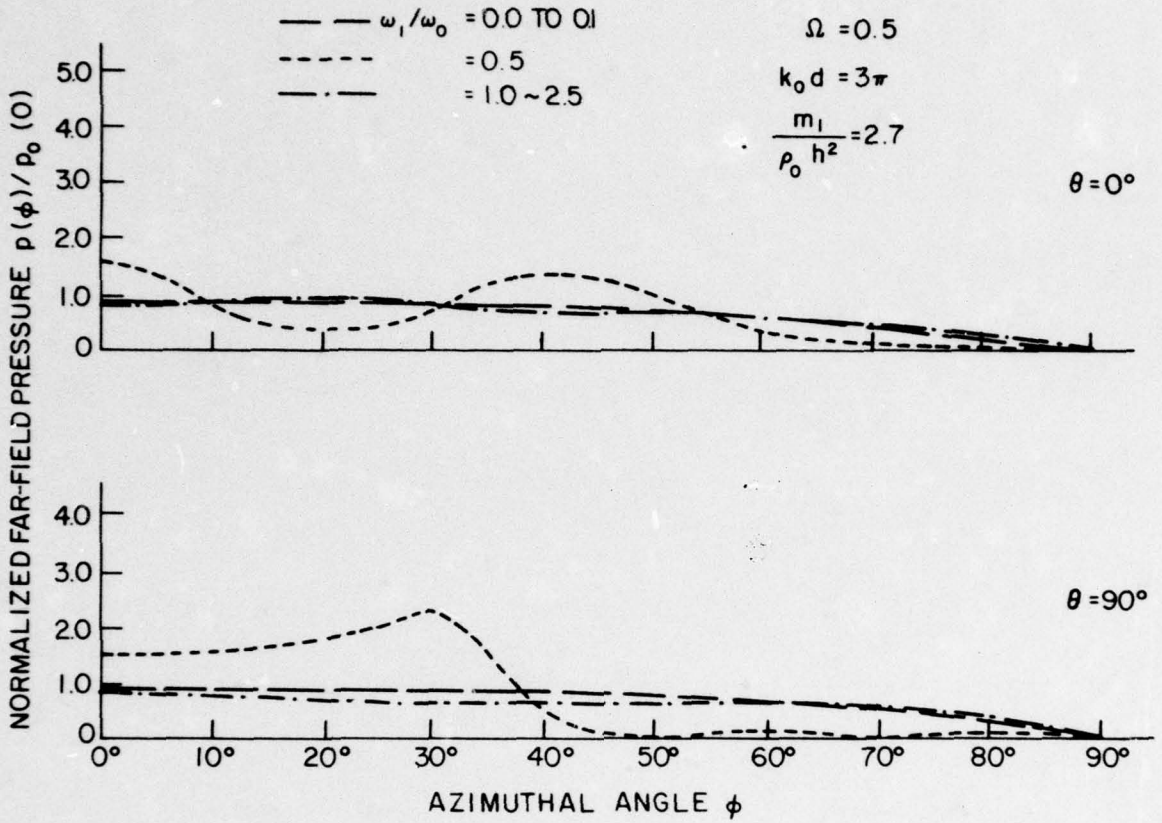

Figure 3.26 Directivity Function of Far-Field Pressure of an Acoustic Fairing Model ($\Omega = 0.5$, $k_o d = 3\pi$, $m_1/\rho_o h^2 = 2.7$)

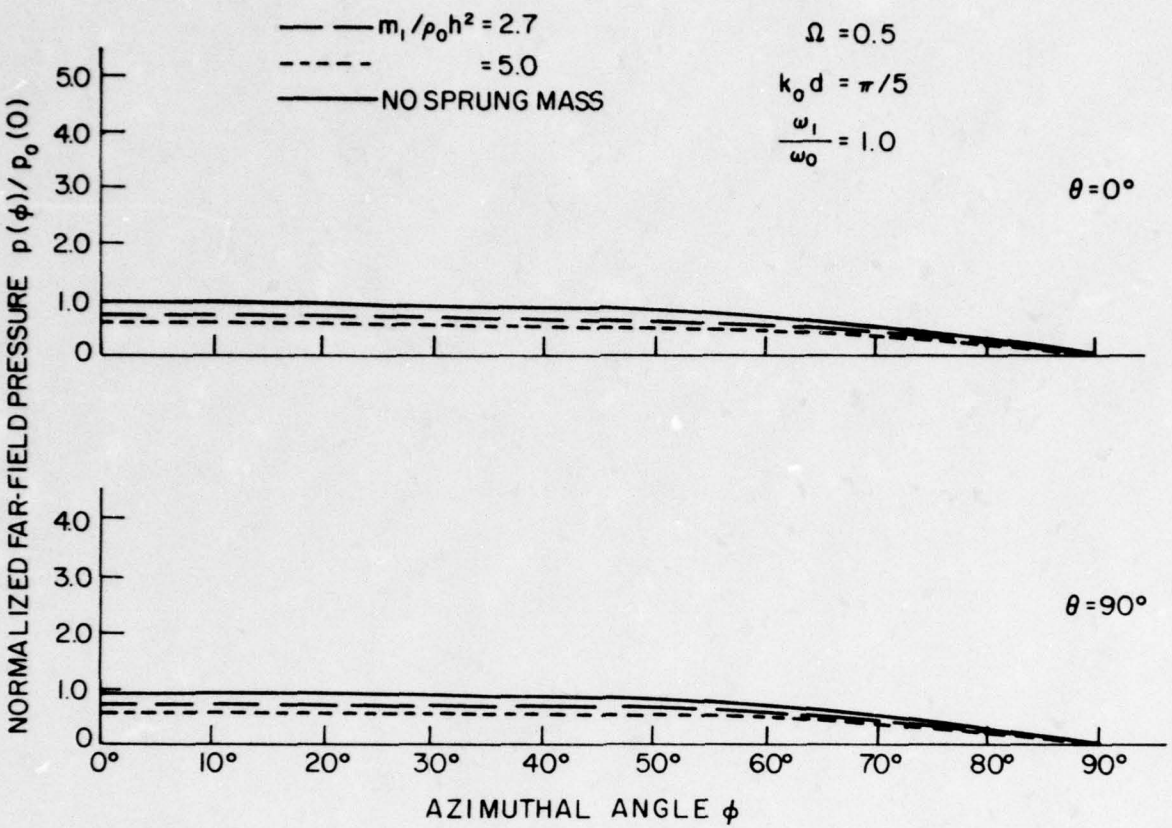

Figure 3.27 Directivity Function of Far-Field Pressure of an Acoustic Fairing Model ($\Omega = 0.5$, $k_o d = \pi/5$, $\omega_1/\omega_o = 1.0$)

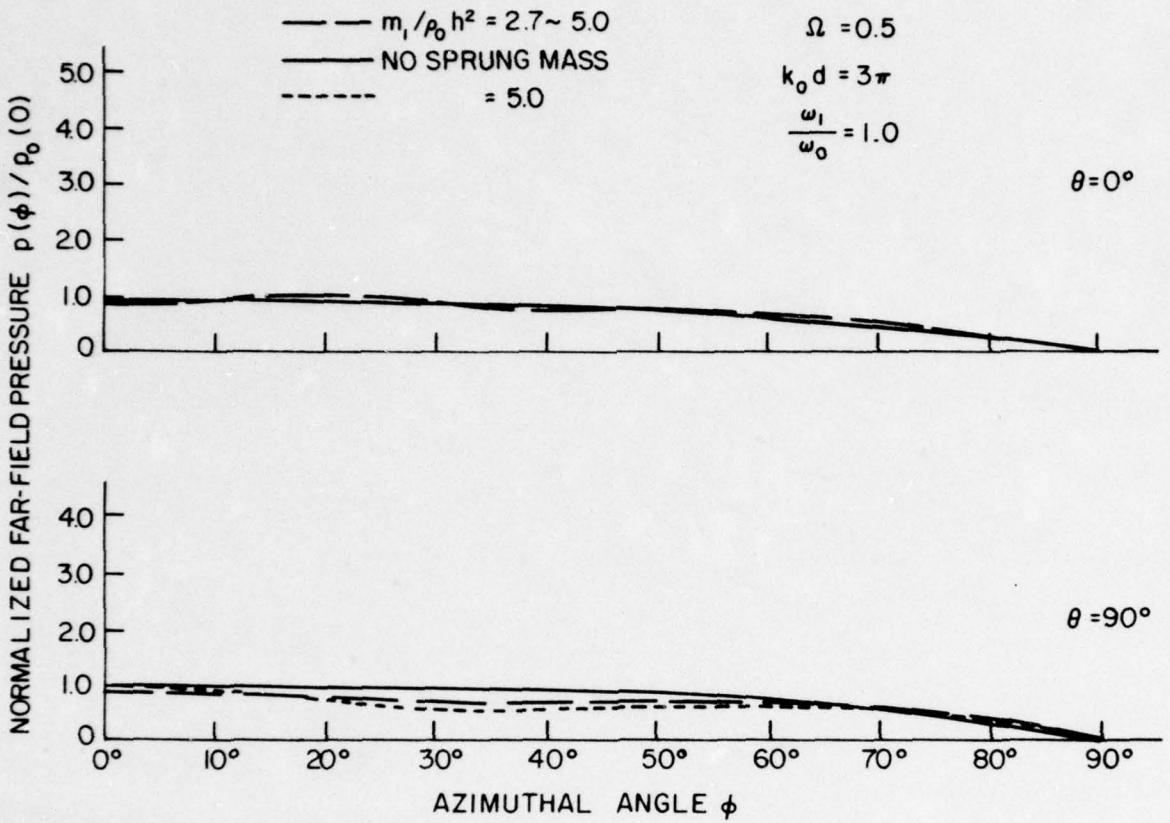

Figure 3.28 Directivity Function of Far-Field Pressure of an Acoustic Fairing Model (Ω = 0.5, $k_o d = 3\pi$, ω_1/ω_o = 1.0)

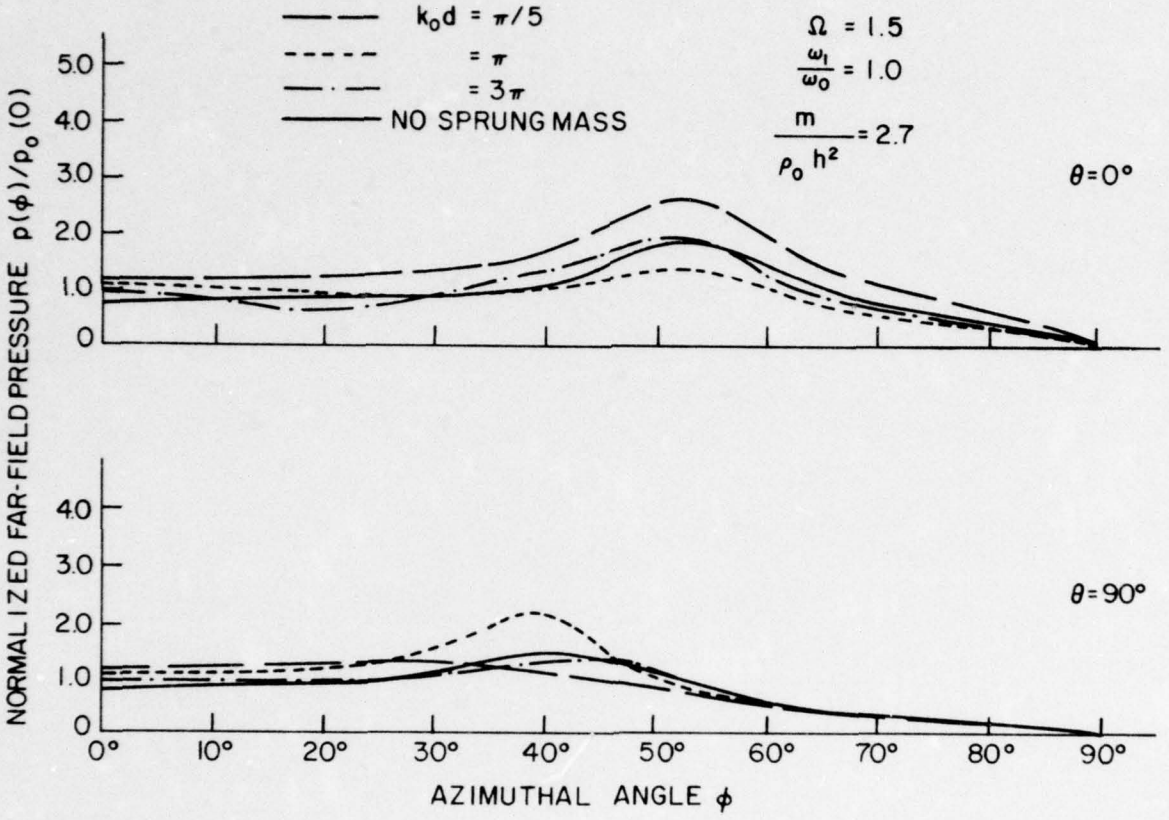

Figure 3.29 Directivity Function of Far-Field Pressure of an Acoustic Fairing Model (Ω = 1.5, ω_1/ω_o = 1.0, $m_1/\rho_o h^2$ = 2.7)

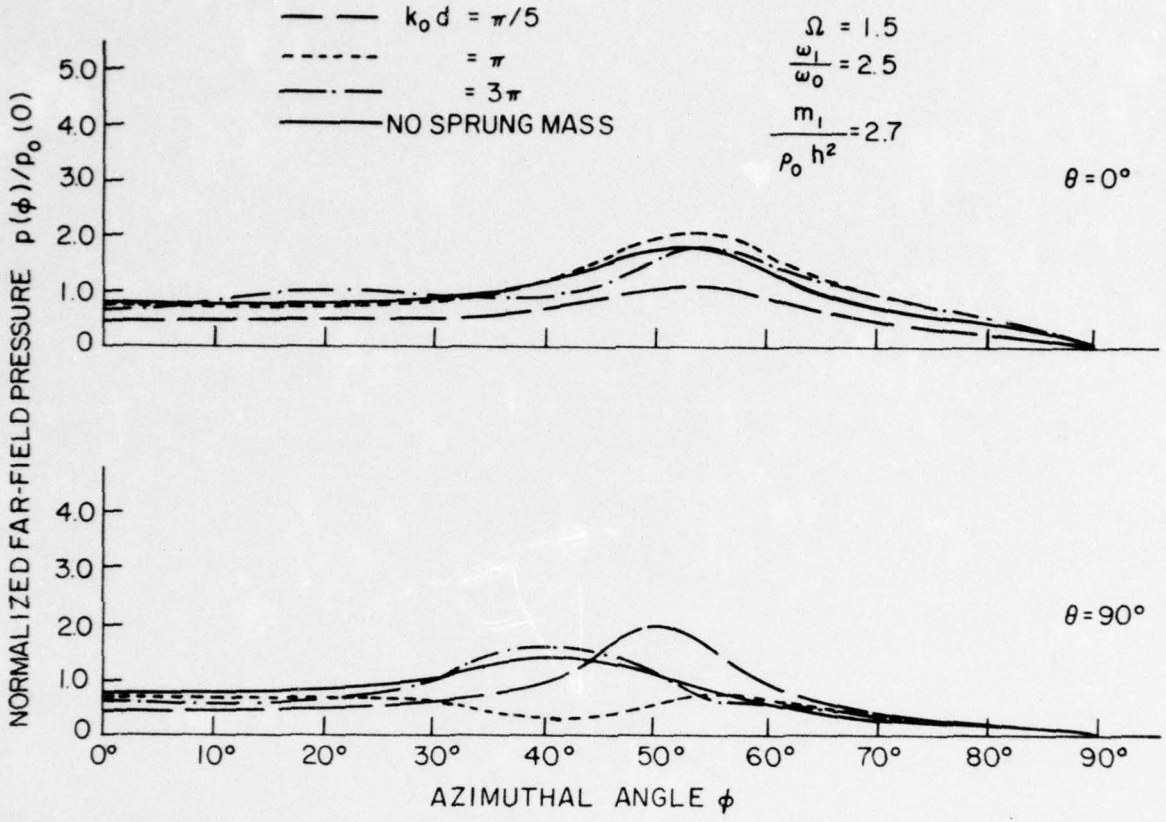

Figure 3.30 Directivity Function of Far-Field Pressure of an Acoustic Fairing Model (Ω = 1.5, ω_1/ω_o = 2.5, $m_1/\rho_o h^2$ = 2.7)

3.31 and 3.33 show the directivity function at fixed sprung mass ($m_1/\rho_o h^2 = 2.7$) and its location ($k_o d = \pi/5$, or 3π) for different spring characteristic frequencies ($\omega_1/\omega_o = 0$, 0.1, 1.0, 2.5). Figures 3.32 and 3.34 show the directivity function at the fixed spring characteristic frequency ($\omega_1/\omega_o = 1.0$) and its location ($k_o d = \pi/5$, or 3π)for different sprung masses ($m_1/\rho_o h^2 = 0$, 2.7, 5.0).

Five figures of directivity function were similarly plotted for a frequency above the coincidence frequency, i.e., at $\Omega = 2.5$, similar to those plotted for $\Omega = 1.5$. Figure 3.35 was plotted for a fixed sprung mass and its characteristic frequency for different locations; Figures 3.36 and 3.38 were plotted for a fixed sprung mass and its location for different spring characteristic frequencies; Figure 3.37 and 3.39 were plotted for a fixed spring characteristic frequency and its location for different sprung masses.

3.2.3 Power Spectrum. The radiated acoustic power (N) from a point-excited beam-reinforced plate with two additional spring-mass systems was computed relative to the driving power (N_o) of an infinite isotropic plate excited by a point force at the origin, versus the nondimensional frequencies (Ω) at different conditions.

$$\frac{N}{N_o} = g\Omega^2 \int_0^{\pi/2} \int_0^{\pi/2} \frac{\cos^2\phi \, \sin\phi \, |C_{ms}|^2 \, d\theta \, d\phi}{\sqrt{1 + \frac{\Omega^6 c^2 \rho^3}{\rho_o^2} \frac{12(1-\nu^2)}{E} \cos^2\phi \, \{\sin^4\phi - \frac{1}{\Omega^2}\}^2}} , \qquad (3.8)$$

where

$$g = \frac{8\rho c}{\pi^2 \rho_o} \sqrt{\frac{12\rho(1-\nu^2)}{E}} .$$

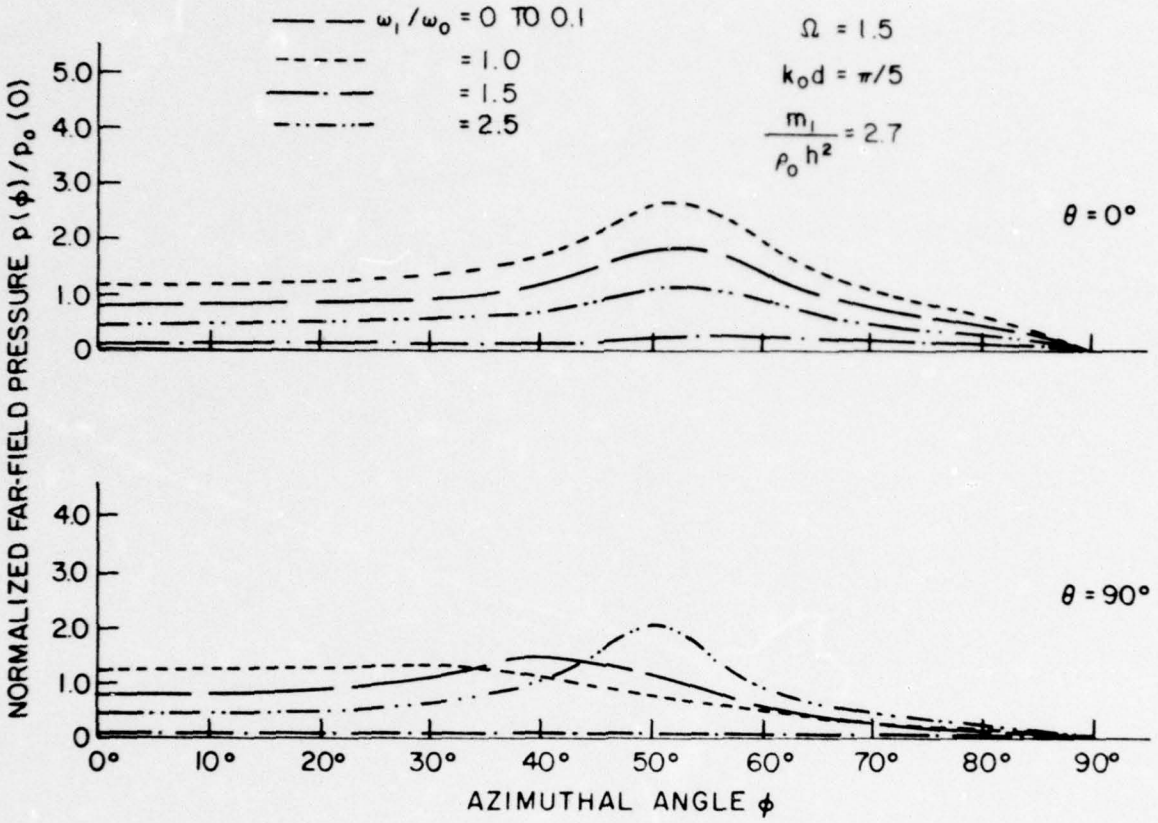

Figure 3.31 Directivity Function of Far-Field Pressure of an Acoustic Fairing Model (Ω = 1.5, $k_o d = \pi/5$, $m_1/\rho_o h^2$ = 2.7)

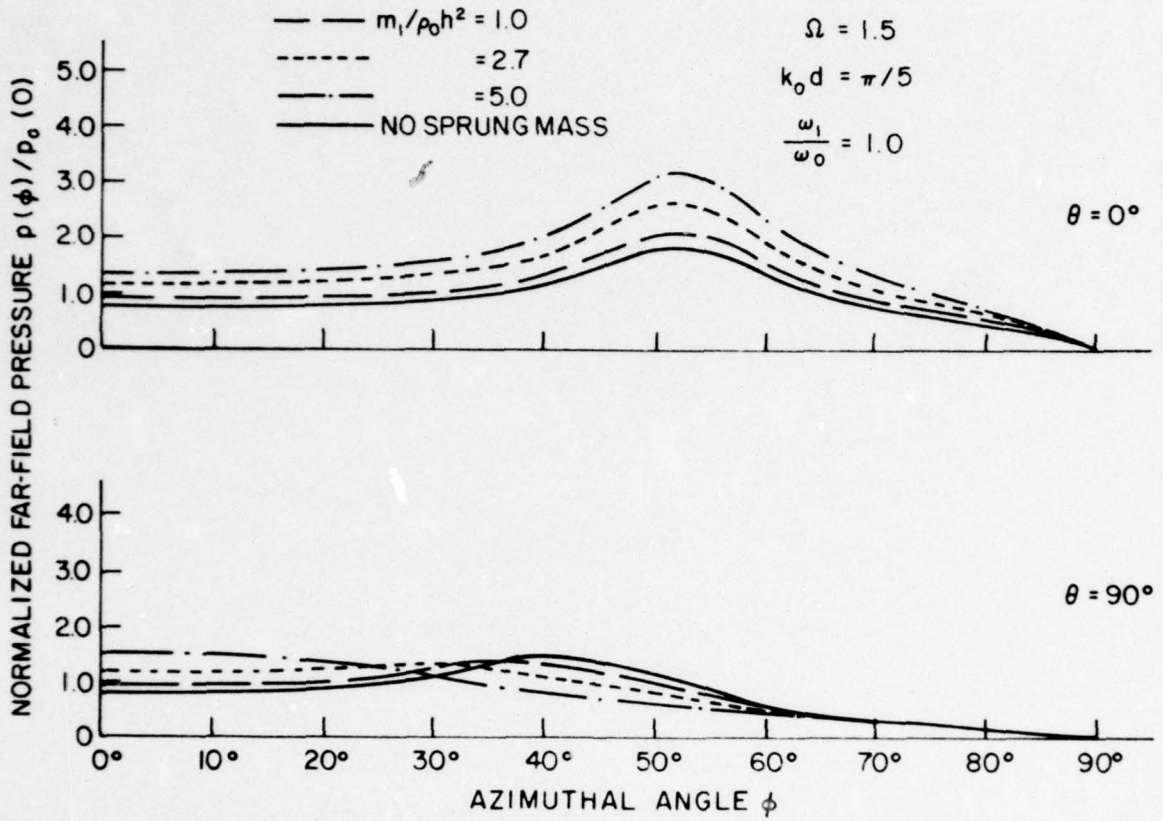

Figure 3.32 Directivity Function of Far-Field Pressure of an Acoustic Fairing Model ($\Omega = 1.5$, $k_o d = \pi/5$, $\omega_1/\omega_o = 1.0$)

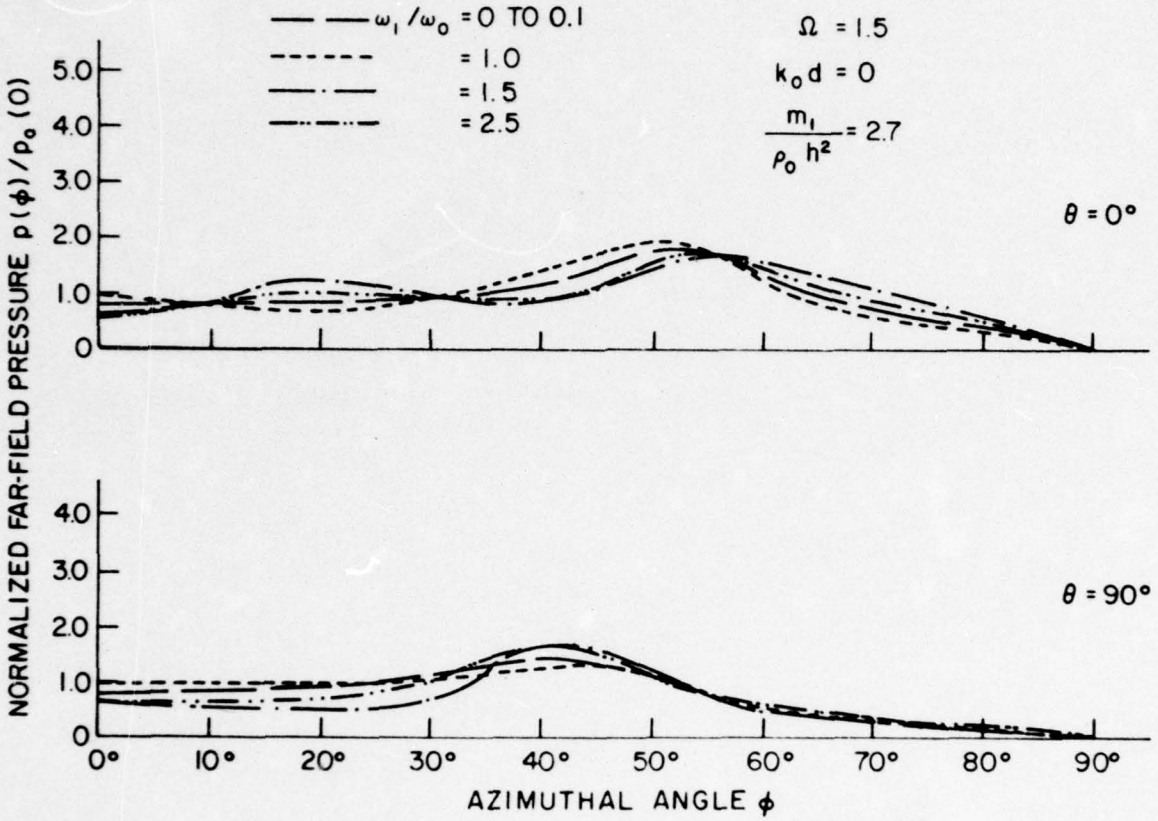

Figure 3.33 Directivity Function of Far-Field Pressure of an Acoustic Fairing Model (Ω = 1.5, $k_o d = 3\pi$, $m_1/\rho_o h^2$ = 2.7)

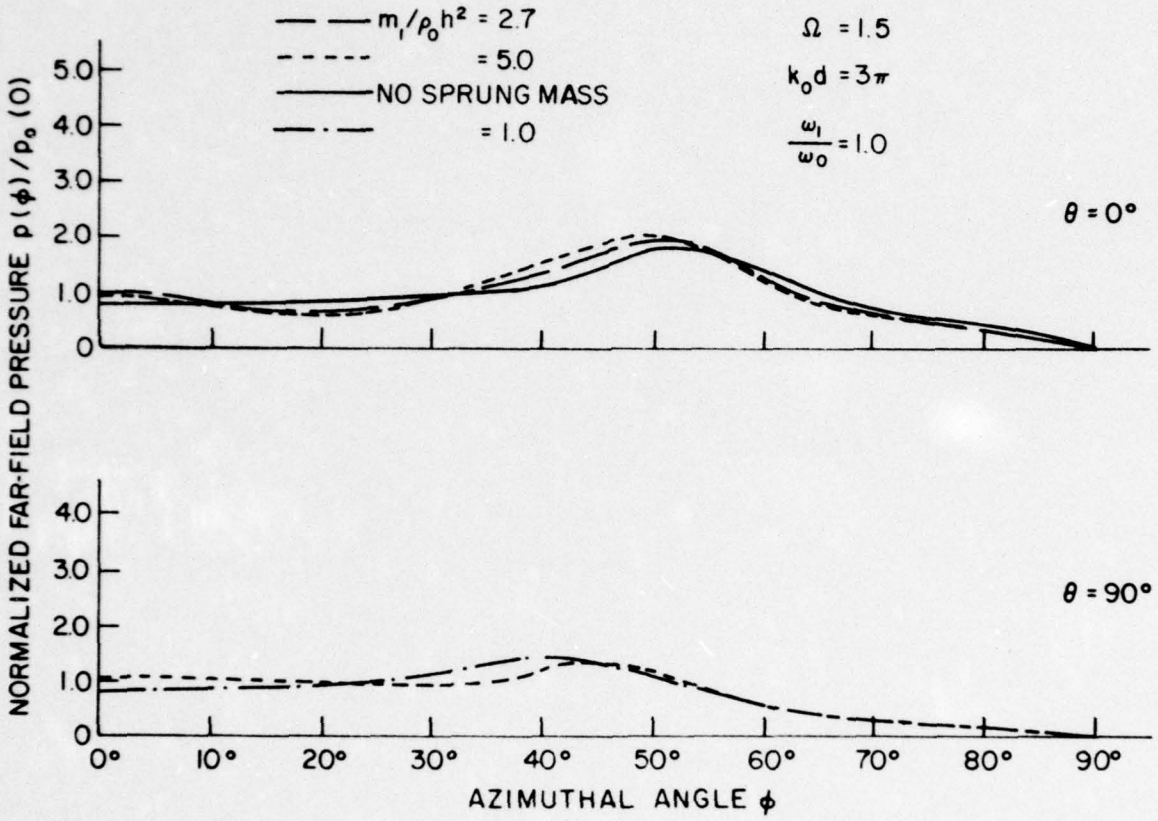

Figure 3.34 Directivity Function of Far-Field Pressure of an Acoustic Fairing Model ($\Omega = 1.5$, $k_o d = 3\pi$, $\omega_1/\omega_o = 1.0$)

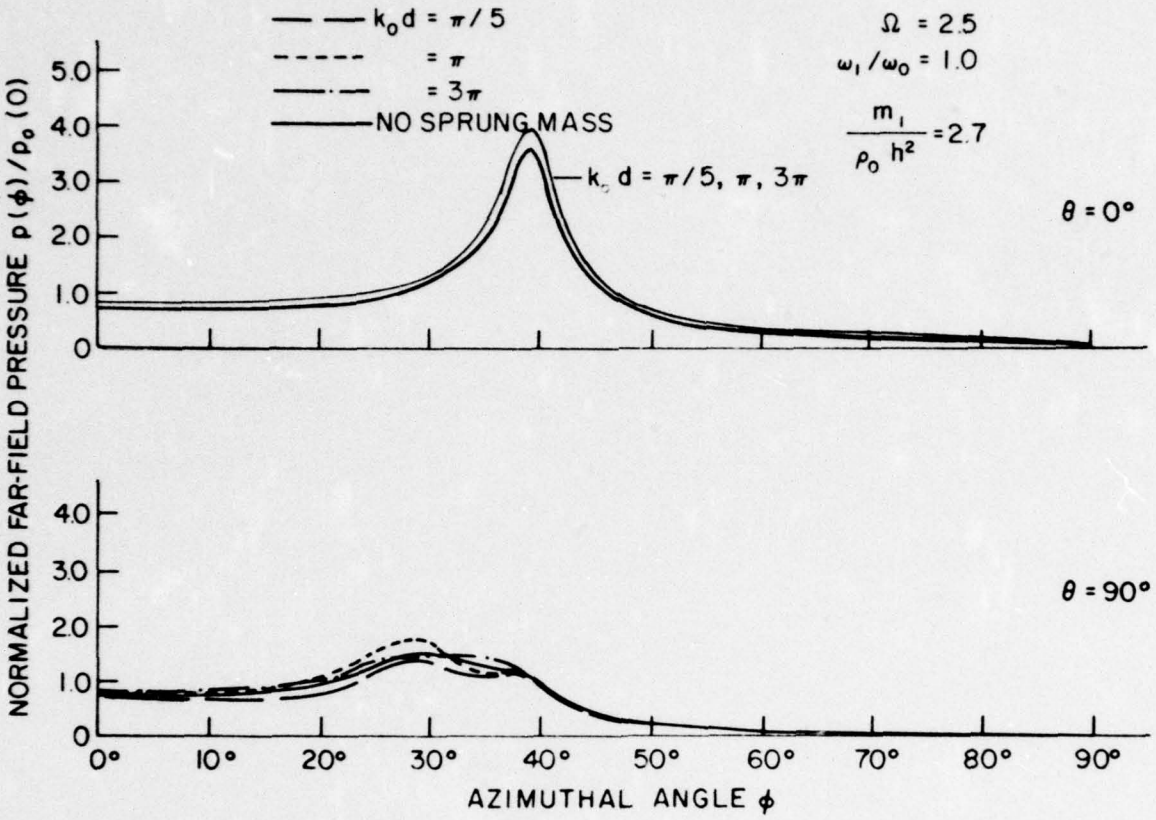

Figure 3.35 Directivity Function of Far-Field Pressure of an Acoustic Fairing Model ($\Omega = 2.5$, $\omega_1/\omega_o = 1.0$, $m_1/\rho_o h^2 = 2.7$)

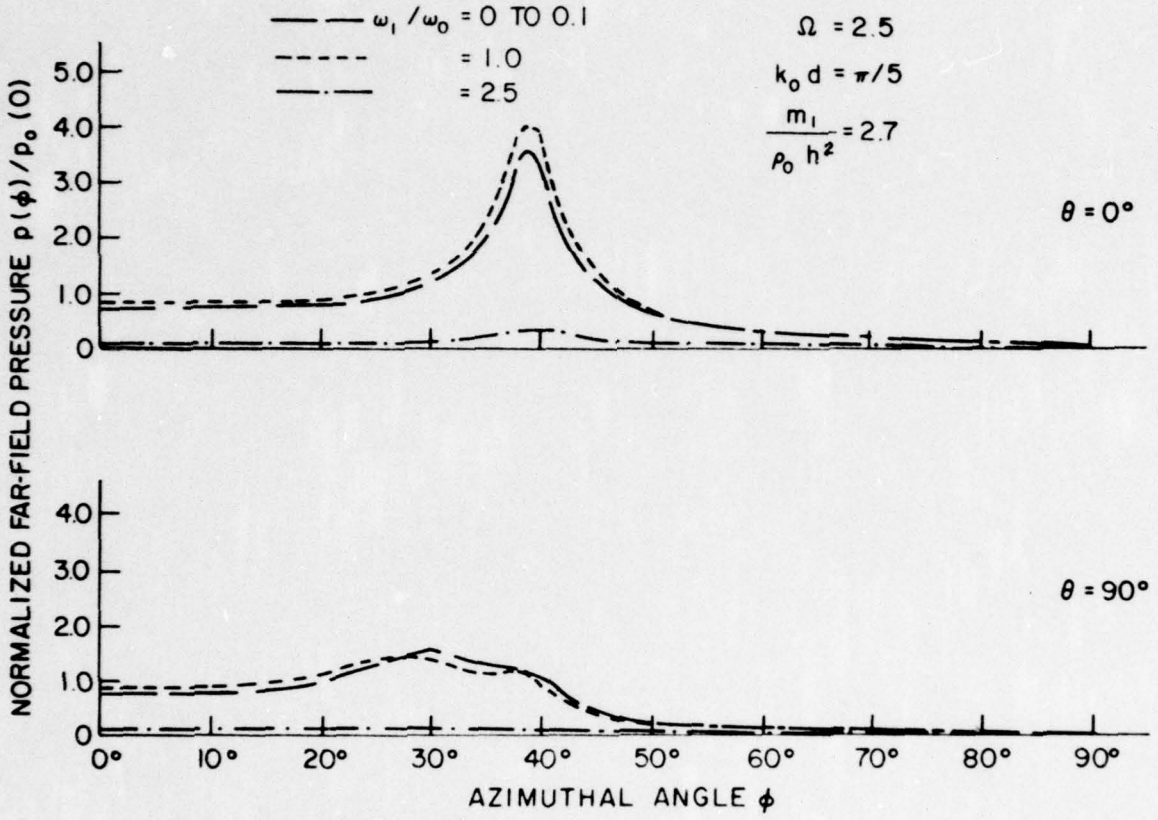

Figure 3.36 Directivity Function of Far-Field Pressure of an Acoustic Fairing Model ($\Omega = 2.5$, $k_o d = \pi/5$, $m_1/\rho_o h^2 = 2.7$)

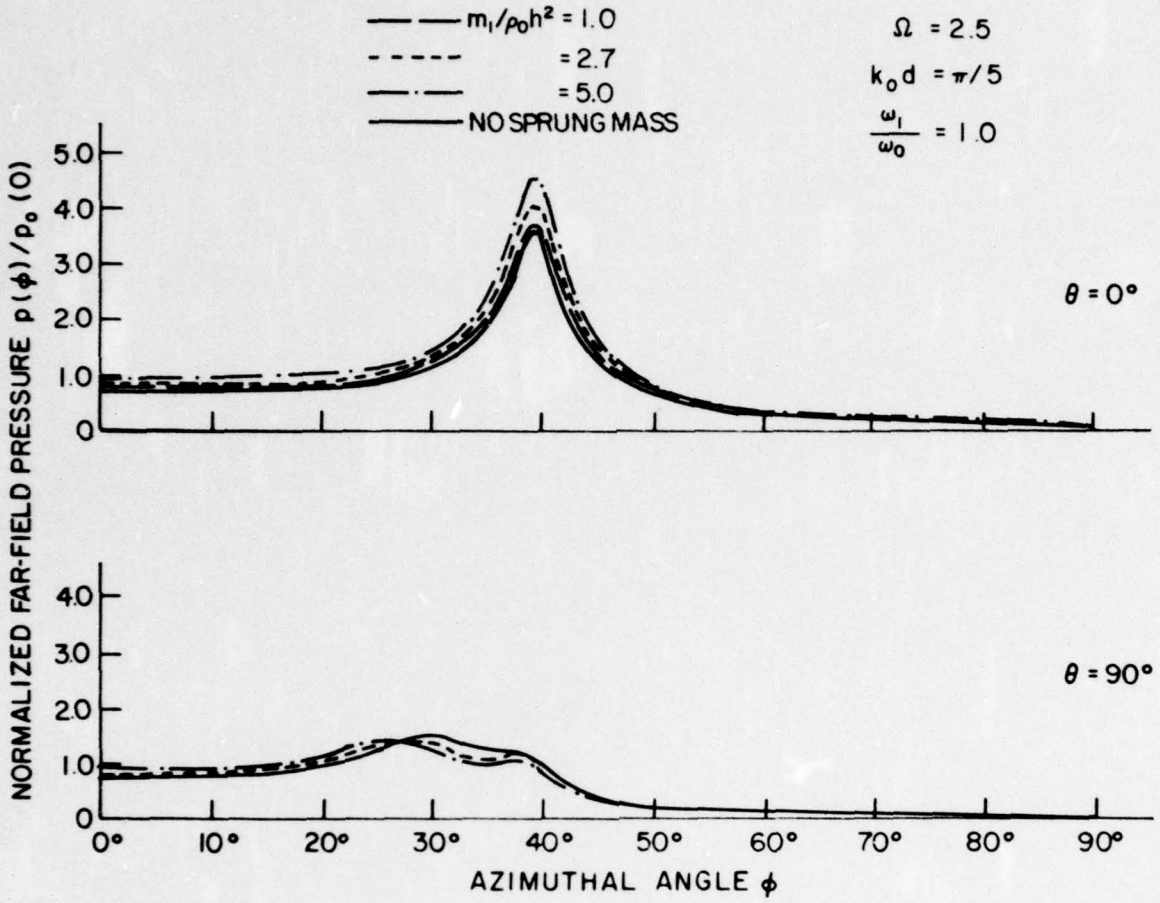

Figure 3.37 Directivity Function of Far-Field Pressure of an Acoustic Fairing Model (Ω = 2.5, $k_o d = \pi/5$, ω_1/ω_o = 1.0)

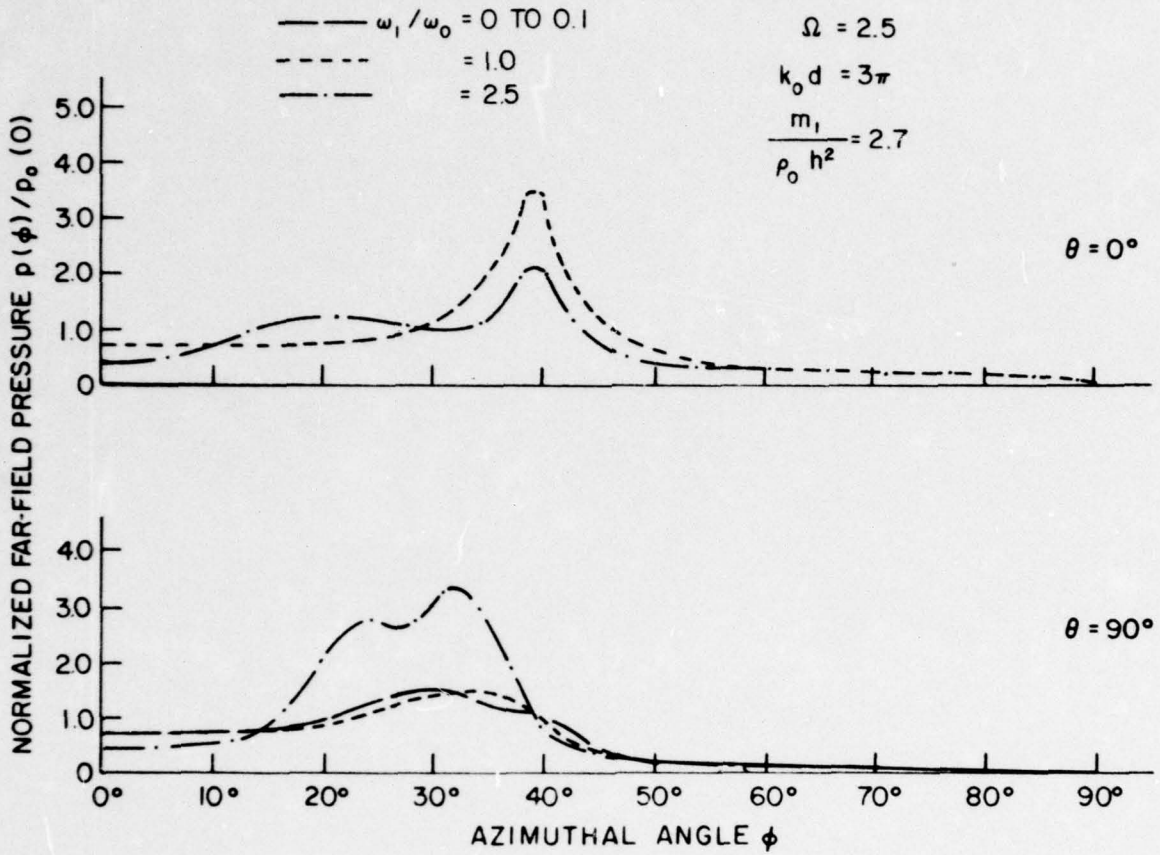

Figure 3.38 Directivity Function of Far-Field Pressure of an Acoustic Fairing Model ($\Omega = 2.5$, $k_o d = 3\pi$, $m_1/\rho_o h^2 = 2.7$)

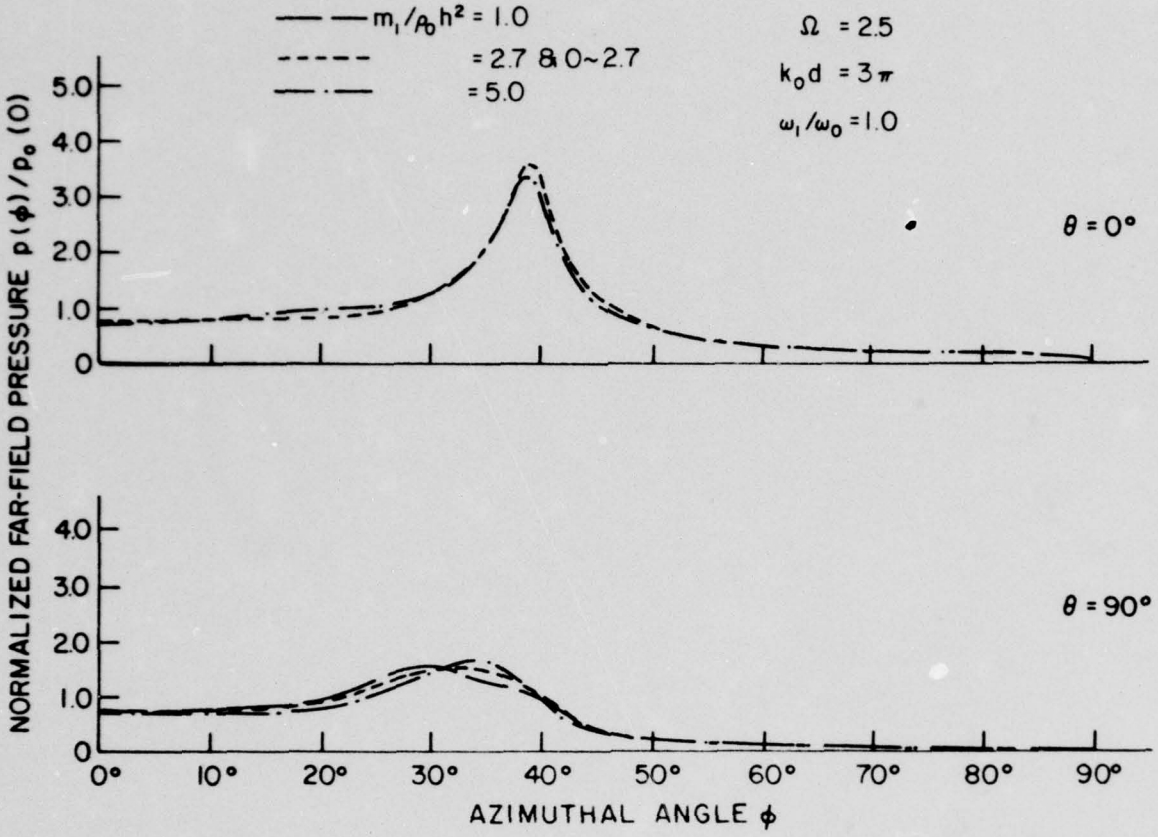

Figure 3.39 Directivity Function of Far-Field Pressure of an Acoustic Fairing Model (Ω = 2.5, $k_o d = 3\pi$, ω_1/ω_o = 1.0)

Eight figures were plotted for the power spectrum. Figure 3.40 was made at fixed spring characteristic frequency $\omega_1/\omega_o = 0.1$ and sprung mass $m_1/\rho_o h^2 = 2.7$ for different locations $k_o d = \pi/5, \pi, 3\pi$. Figure 3.40 is also valid for the case of fixed spring characteristic frequency $\omega_1/\omega_o = 1$ and location $k_o d = \pi$ for different sprung mass ratios $m_1/\rho_o h^2 = 1.0, 2.7, 5.0$. Figure 3.41 and 3.42 were made at fixed spring characteristic frequency ($\omega_1/\omega_o = 1.0$ or 2.5) and sprung mass ($m_1/\rho_o h^2 = 2.7$) for different locations ($k_o d = \pi/5, 3\pi$); Figure 3.43, 3.44, and 3.45 were made at fixed sprung mass ($m_1/\rho_o h^2 = 2.7$) and its location ($k_o d = \pi/5$ or π, or 3π) for different spring characteristic frequencies ($\omega_1/\omega_o = 0.1, 1.0, 2.5$); Figure 3.46 and 3.47 were made at fixed spring characteristic frequency ($\omega_1/\omega_o = 1.0$ or 2.5) for different sprung masses ($m_1/\rho_o h^2 = 1.0, 2.7, 5.0$).

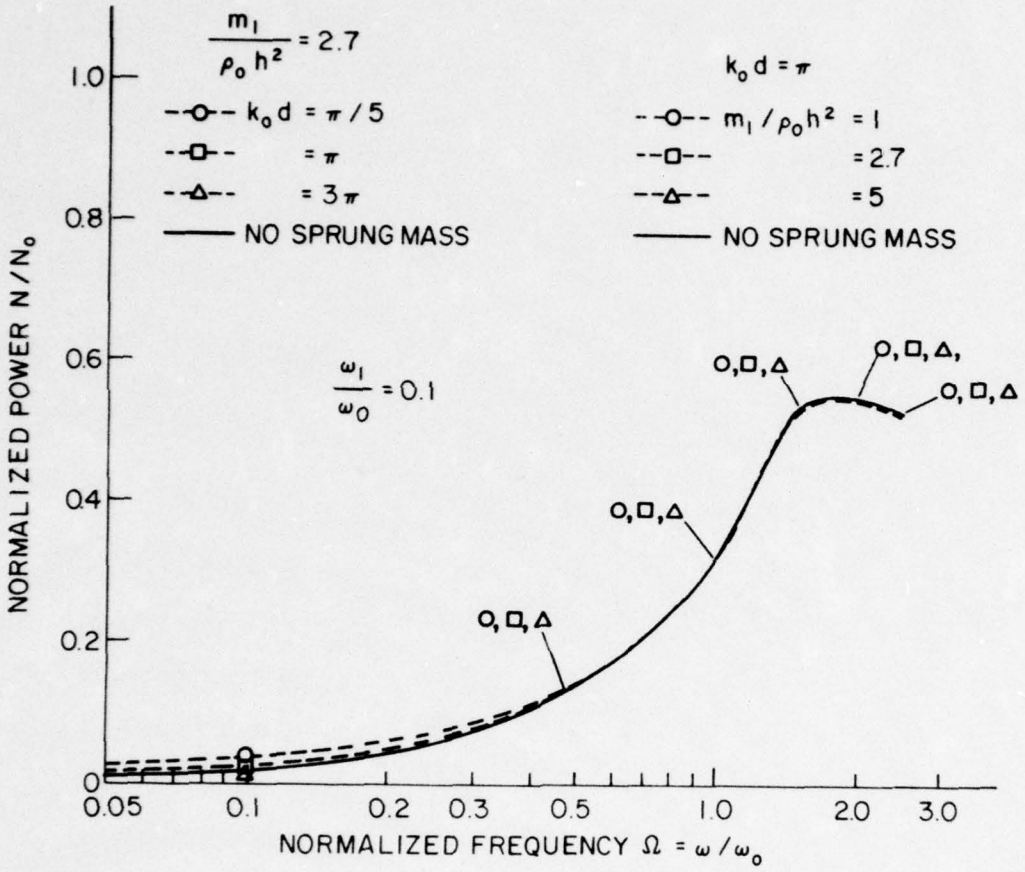

Figure 3.40 Normalized Power N/N_o of an Acoustic Fairing Model ($\omega_1/\omega_o = 0.1$ and $m_1/\rho_o h^2 = 2.7$ or $k_o d = \pi$)

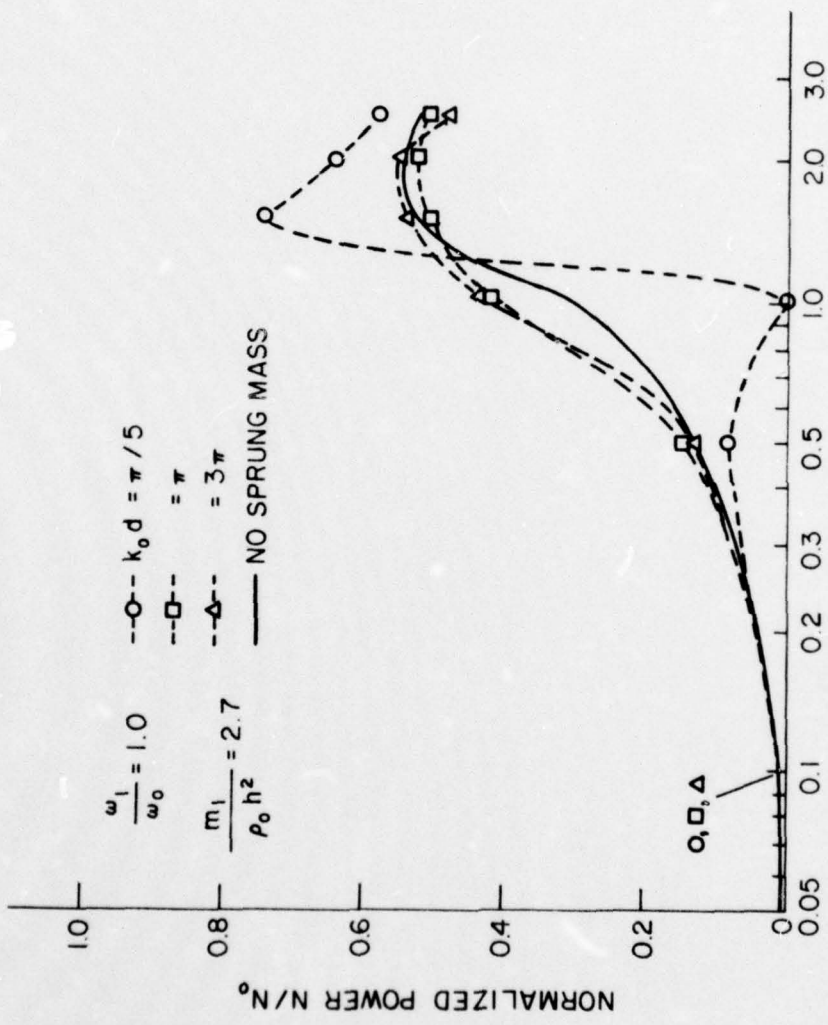

Figure 3.41 Normalized Power N/N_o of an Acoustic Fairing Model ($\omega_1/\omega_o = 1.0$, $m_1/\rho_o h^2 = 2.7$)

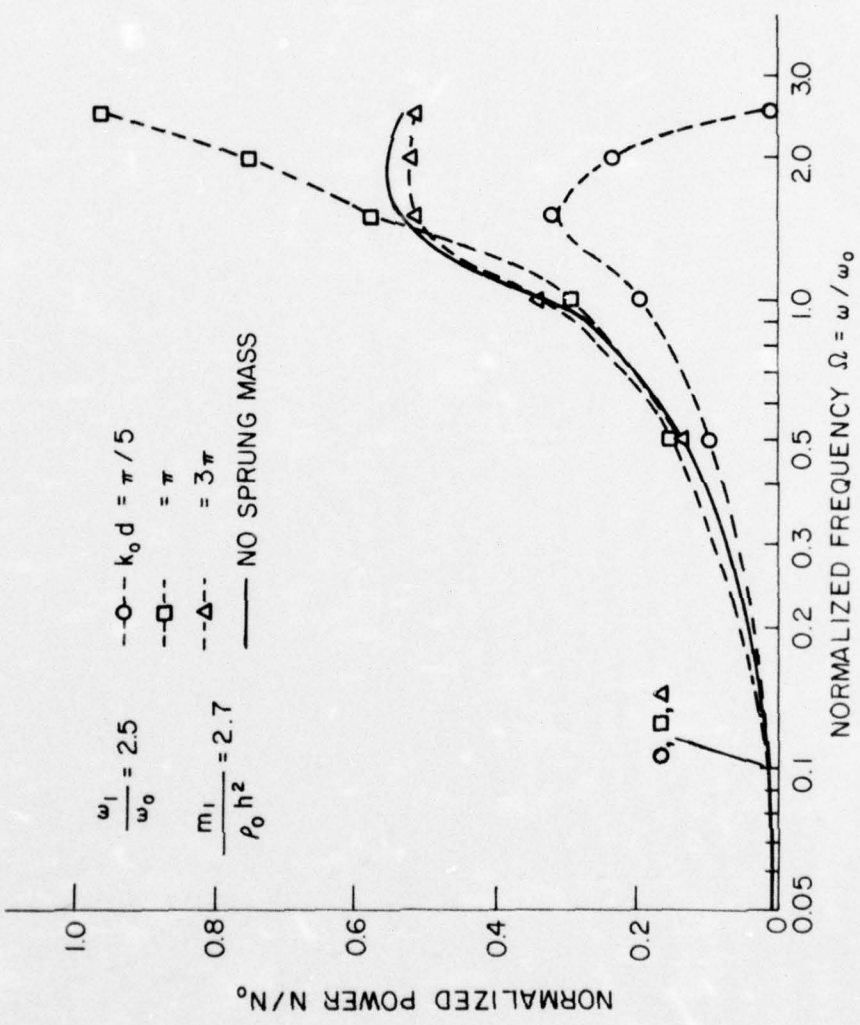

Figure 3.42 Normalized Power N/N_c of an Acoustic Fairing Model ($\omega_1/\omega_o = 2.5$, $m_1/\rho_o h^2 = 2.7$)

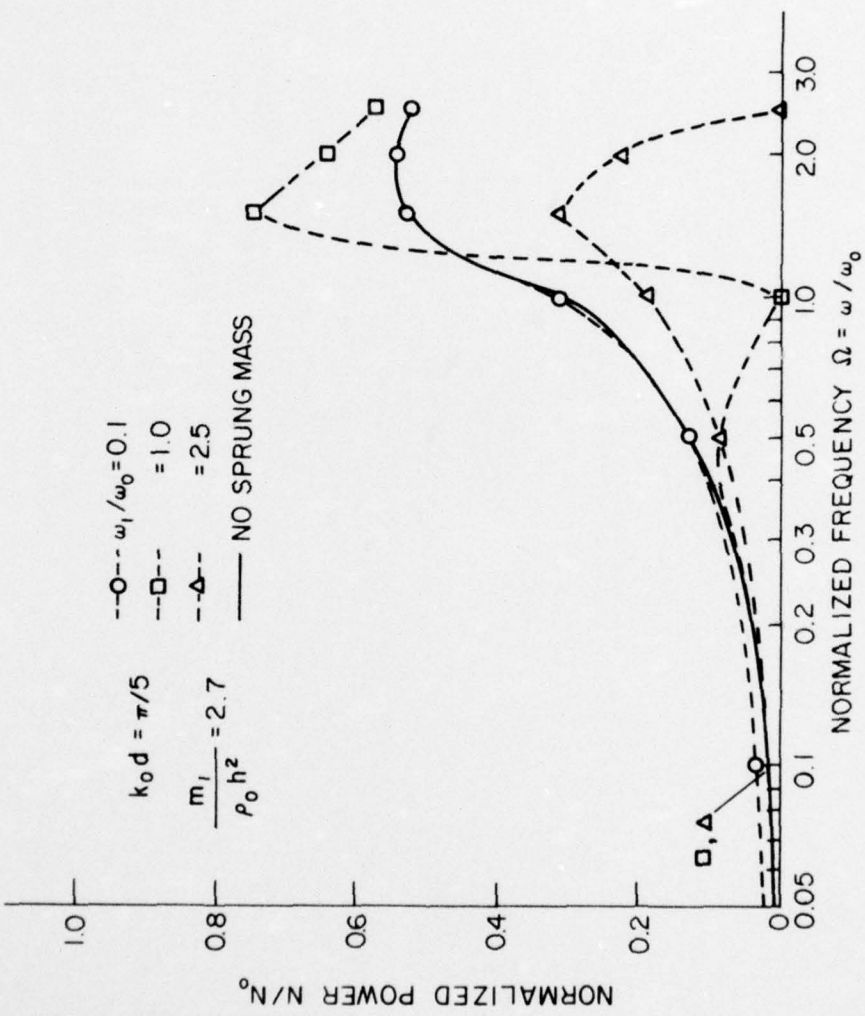

Figure 3.43 Normalized Power N/N_o of an Acoustic Fairing Model ($k_o d = \pi/5$, $m_1/\rho_o h^2 = 2.7$)

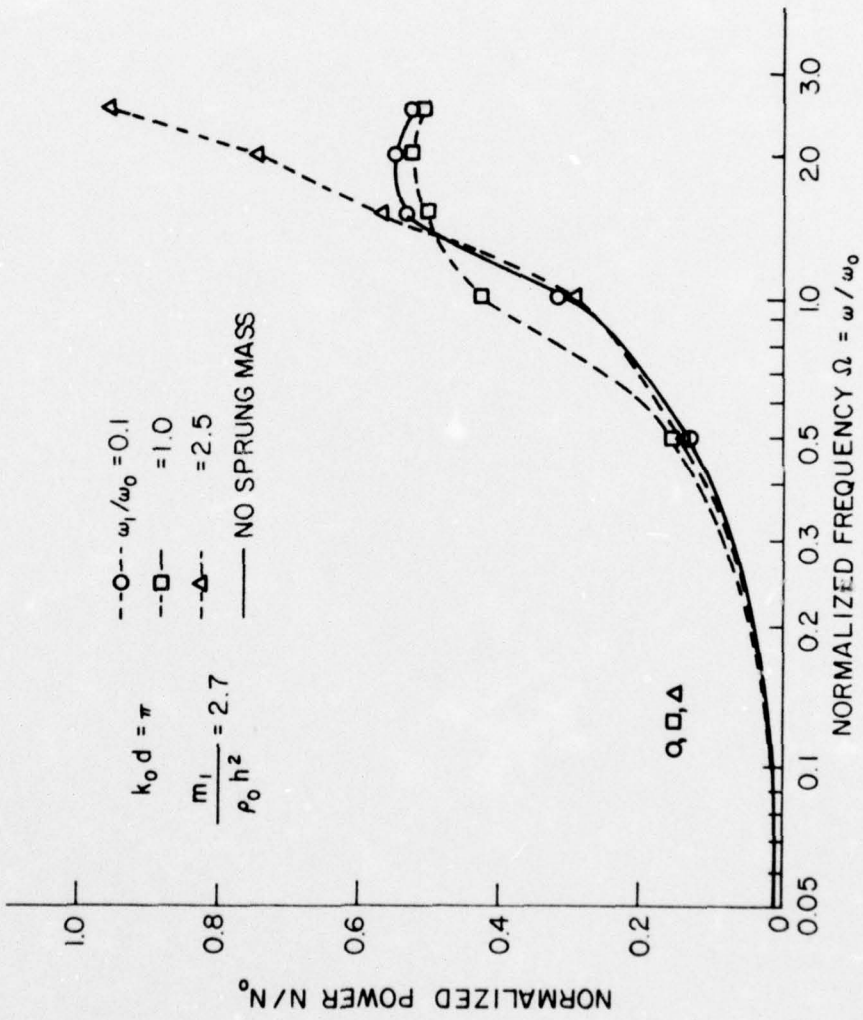

Figure 3.44 Normalized Power N/N_o of an Acoustic Fairing Model ($k_o d = \pi$, $m_1/\rho_o h^2 = 2.7$)

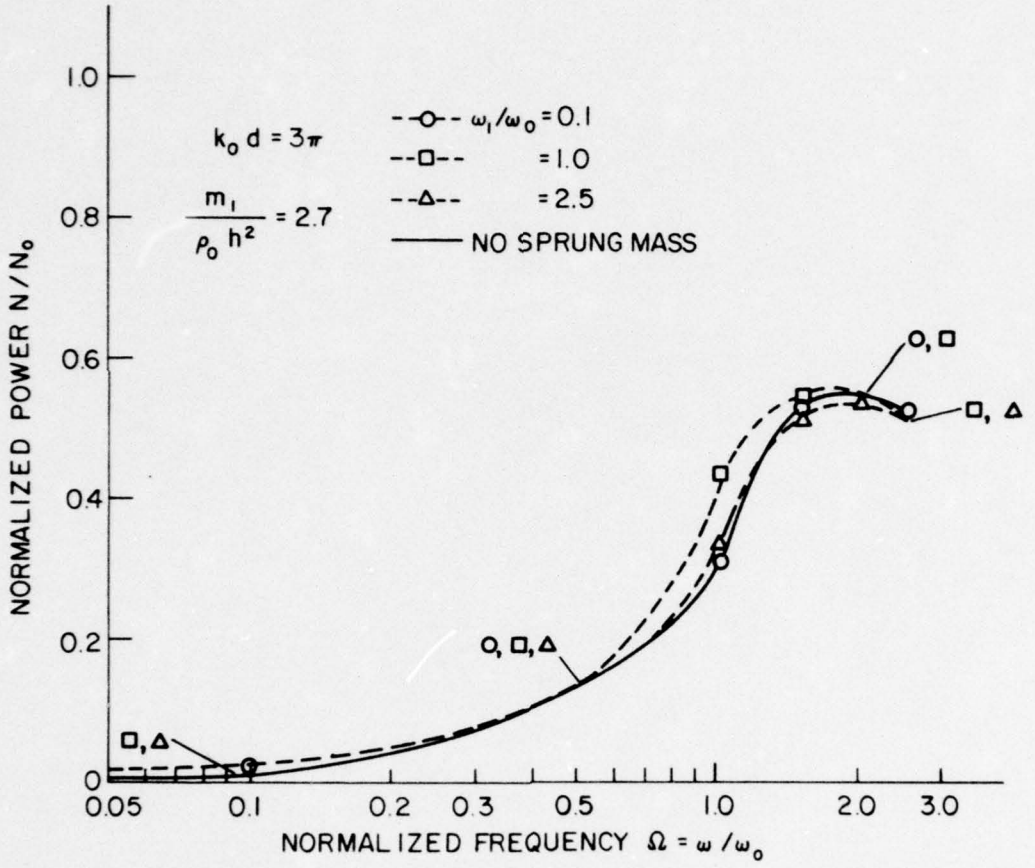

Figure 3.45 Normalized Power N/N_o of an Acoustic Fairing Model ($k_o d = 3\pi$, $m_1/\rho_o h^2 = 2.7$)

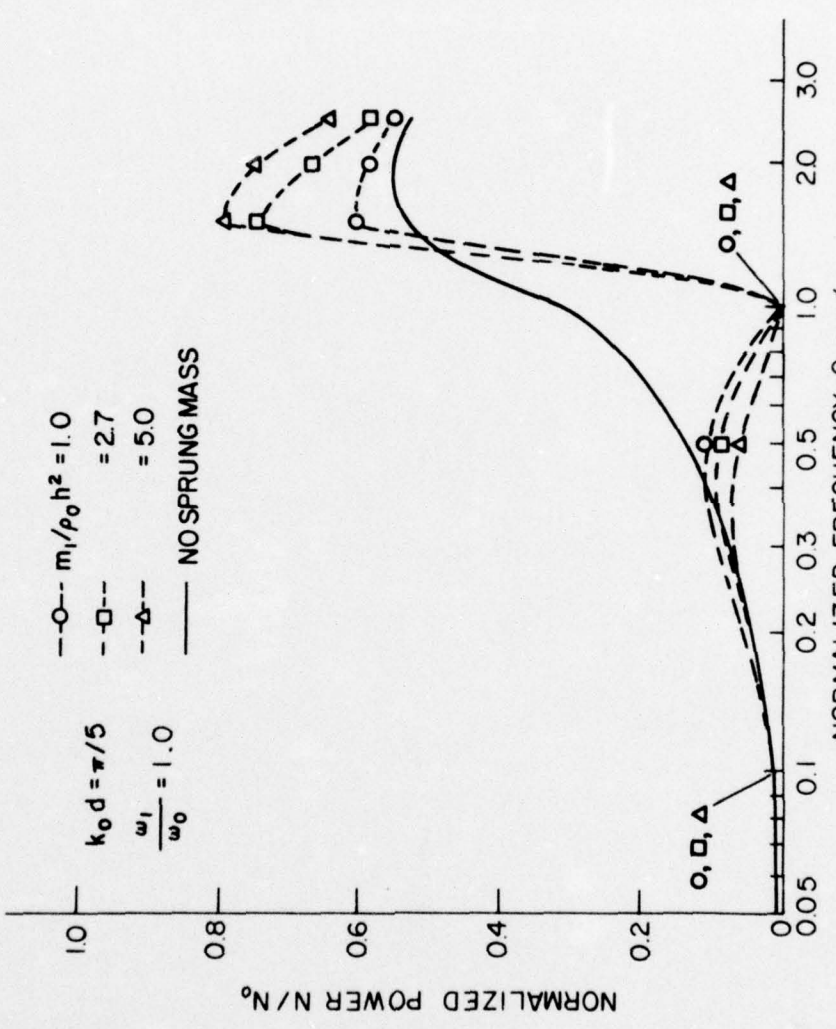

Figure 3.46 Normalized Power N/N_o of an Acoustic Fairing Model ($k_o d = \pi/5$, $\omega_1/\omega_o = 1.0$)

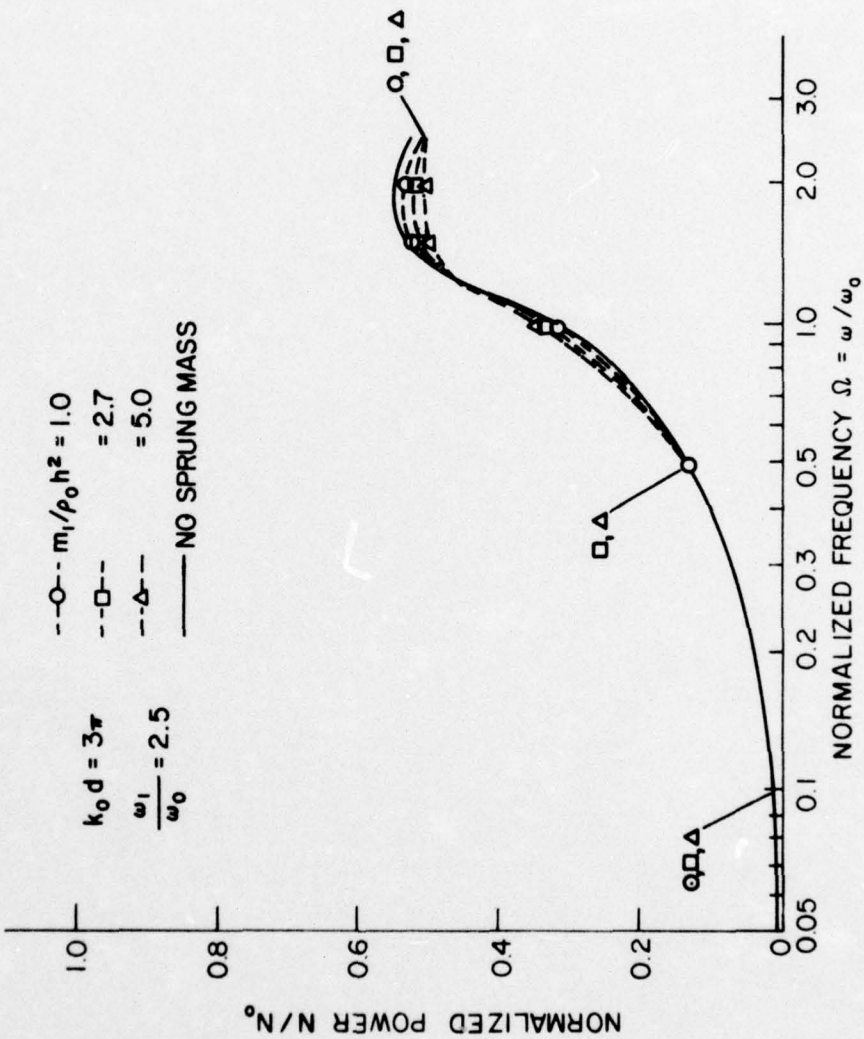

Figure 3.47 Normalized Power N/N_o of an Acoustic Fairing Model ($k_o d = 3\pi$, $\omega_1/\omega_o = 2.5$)

CHAPTER IV

DISCUSSIONS OF THE RESULTS AND CONCLUSIONS

4.1 Introduction

The initial task in the analysis of a vibrating marine structure is to initially make some simplifying assumptions about its motion and then idealize the structure so that the analysis of its motion can be made feasible. In this thesis, an idealized beam-reinforced plate will be conceived as a ship's hull reinforced by a framing element (beam), and a time-harmonic point force represents the action of a vibrating machine.

Vibrating machinery is usually supported by frames of a ship's hull due to structural design considerations. Since the reduction in the radiated noise, when a vibrating machine is attached to a reinforcing beam of a hull-plating has not been analytically proven, the first major task in this thesis was to study the acoustic fields produced by a point force excitation of an infinite beam which is welded to an infinite plate. The attached beam is considered to act as a structural discontinuity of one of the following three types: (1) a mass discontinuity which will normally act as a line mass impedance, (2) an elastic discontinuity which acts as a path of energy propagation, and (3) a beam-like discontinuity which acts as an elastic as well as mass discontinuity. This problem constitutes an initial step leading to a better understanding of the role a structural discontinuity plays in an infinite reinforced plate. Besides, a mathematical procedure for solving the sound

radiation of an infinite, reinforced plate developed for this problem can be utilized to obtain the sound radiation from other plates with more complex structural discontinuities. Numerical results of this problem were plotted and shown from Figures 3.1 to Figure 3.11. These will be subsequently discussed in detail in Section 4.2. A second major task of this thesis was to devise a simple mathematical model of acoustic fairing, i.e., by attaching two line spring-mass systems to the plate as shown in Figure 2.2, and to study their interaction with the existing attached beam. The sound radiation from an acoustically faired plate was investigated by varying the various parameters that influence it, such as the mass and the spring stiffness as well as the location of the systems with respect to the reinforcing beam. This mathematical model, though simple, yields a better understanding of the influence of the physical parameters on the application of acoustic fairing. The numerical results obtained for this second problem were plotted from Figures 3.12 to 3.47. The detailed discussions of this problem are given in Section 4.3.

4.2 Far-Field Acoustic Radiation from Point Excited Beam-Reinforced Plate

The influence of structural discontinuities on the radiated sound from plates attached to such discontinuities was assessed mathematically in Section 2.3 and many numerical examples were presented in Section 3.1.

The influence of a mass, a stiffness, or a beam on the radiated sound can be best discussed in the two frequency ranges: below and above the coincidence frequency.

4.2.1 Excitation Frequency Below the Coincidence Frequency ($\Omega < 1$). Since the frequency of excitation is below the coincidence frequency, one does not expect a peak in the radiated far-field pressure. Thus, maximum pressure is observed at points directly across the point of excitation, i.e., $\phi = 0°$.

(i) Influence of Mass: The influence of an infinitely long uniformly distributed mass on the radiated acoustic pressure is exhibited by the factor $\bar{C}_{ms}$ of Equation (3.1). If one sets $U_y = 0$ in this expression in Equation (3.1) and obtains an approximate value for $\gamma\mu_1 I_1^o$ for low frequencies, it was shown that this product increases with the frequency as $(\gamma\Omega^{0.8})$. This indicates that the factor $\bar{C}_{ms}$ will decrease in value if the frequency ratio Ω or the mass ratio γ increases. The reduction of the radiated pressure due to the addition of an infinite line mass is clearly shown in Figure 3.1. A mass ratio of $\gamma = 10$, which is equivalent to a mass whose cross-sectional area is equal to $3.7h^2$, reduces the radiated pressure by 5 dB at best, for frequencies $\Omega < 1$.

The influence of the distributed mass on the directivity function at frequencies below the coincidence frequency can be expected to be minimal. This is shown clearly by the directivity plots at $\theta = 0°$ and $90°$ in Figure 3.2.

The influence of the mass on the radiated power is shown in Figure 3.9. It is apparent that one can attain a reduction in the radiated power equivalent to that of the radiated pressure, because of the omnidirectionality of the directivity function. For a mass ratio $\gamma = 10$, the radiated power was reduced by as much as 4.5 dB for frequencies $\Omega < 1$. The reason for reduction in the radiated power can

be attributed to the fact that the mass requires additional power to accelerate; hence, a smaller portion of the input power is pumped to the acoustic medium.

(ii) Influence of Stiffness: The influence of an infinitely long line stiffness on the radiated pressure is exhibited by the factor $\bar{C}_{ms}$ in Equation (3.1). If one sets $\gamma = 0$ in Equation (3.1) and obtains an approximate expression for the products $U_y I_1^o \mu_3$ for low frequencies, it was shown that the product increases with the frequency as $(U_y \Omega^{2.8})$. This indicates that the factor $\bar{C}_{ms}$ will decrease as follows:

$$\bar{C}_{ms} = \frac{1}{1 + (...)i\, U_y\, \Omega^{2.8} \sin^4\theta \sin^4\phi} .$$

At the angle of observation $\phi = 0°$, the factor $\bar{C}_{ms}$ is not influenced by the stiffness parameter U_y and is equal to unity. Thus, the pressure spectrum in Figure 3.1 does not exhibit the influence of the stiffness.

The influence of the line stiffness on the directivity function is minimal for frequencies below the coincidence frequency, as shown by the directivity plots at $\theta = 0°$ and $90°$ in Figure 3.2.

The influence of the line stiffness on the radiated power is shown in Figure 3.10. It is apparent that a reduction of radiated power by 2.5 dB was attained when a line stiffness having a depth ratio of $q_2 = 3.7$ (or a moment of inertia ratio of 45) is attached to the plate. The reduction in the acoustic radiated power can be attributed to the additional power required by the elastic (mechanical) power of the infinite elastic stiffener and hence less of the input power is available for the acoustic medium.

(iii) Influence of a Beam: The influence of an elastic beam welded to an infinite plate on the radiated pressure is exhibited in Equation (3.1). The complicated interaction of the mass of the beam and its stiffness is shown primarily by the factor $\bar{C}_{ms}$ of Equation (3.1). However, below the coincidence frequency ($\Omega < 1$), the influence of the mass is proportional to $\Omega^{0.8}$ while that of the stiffness is proportional to $\Omega^{2.8}$, which indicates that the stiffness of a reinforcing beam of reasonable dimensions is overshadowed by the influence of its mass.

Since the stiffness of a beam has no influence on the radiated sound spectrum at $\phi = 0°$, the only factor that dominates the sound radiation at this observation point is due to its mass, as is clearly shown in Figure 3.1. Thus, the mass of the reinforcing beam does reduce the radiated pressure by 5 dB for a mass ratio $\gamma = 10$.

The influence of the beam on the directivity function can be expected to be minimal below the coincidence frequency as exhibited by the directivity plots at $\theta = 0°$ and $\theta = 90°$ in Figure 3.2.

The influence of the reinforcing beam on the radiated power is shown in Figure 3.11. The reduction of radiated sound power can reach as much as 5 dB for a beam of reasonable dimensions. Below the coincidence frequency, the radiated power reduction attained by the attachment of a beam seems to be dominated by its mass rather than by its stiffness, as indicated by the dependence of the former on the frequency as $\Omega^{0.8}$ and the latter as $\Omega^{2.8}$ for $\Omega < 1$. It is interesting to note that Howe and Heckl [Reference 13, Equation (38)] make the same point when they discuss the influence of random fluctuations of plate mass and on the radiated sound from the plate when excited by a

point force. Thus, the major part of the 5 dB noise power reduction due to the attachment of a beam can be attributed to its mass (4.5 dB) than its stiffness (2.5 dB).

An estimate of the radiated power from an excited beam-reinforced plate can be obtained by assuming that the beam is welded to the plate at only one point, the point of excitation. This obviously neglects the complex interaction of the impedance of the beam along its length with that of the plate along an infinite line. It should be expected that the coupling of the beam to the plate is minimal for shallow and strong for deep beams. Denoting the characteristic impedance of an unloaded plate and beam by Z_p and Z_b, then the portion of the force available for the excitation of the plate is given by $Z_p/(Z_p + Z_b)$. Using this force as an excitation force on an acoustically loaded isotropic plate, the ratio of the power radiated from the beam-plate to that radiated by an isotropic plate below the coincidence frequency can be expressed by the square of this ratio, see Skudryzk [15, Eq. (12.209)]. Thus,

$$\frac{N_{\text{plate-beam}}}{N_{\text{plate}}} = \left| \frac{Z_p}{Z_p + Z_b} \right|^2 . \qquad (4.1)$$

Expressions for the driving point impedance of an infinite plate and an infinite beam are given in Skudryzk [15, Equations (6.90) and (9.45)] as follows:

$$Z_p = 8\sqrt{mD} , \qquad (4.2)$$

$$Z_b = 2(1+i)\, M\sqrt{\omega} \left[\frac{E\, I_b}{M} \right]^{1/4} . \qquad (4.3)$$

The estimated power ratio as expressed in Equation (4.1) is expressed by:

$$\text{Power Ratio} = \frac{1+i}{2}\sqrt{3}\ \frac{c}{c_p}\ q_2^{3/2}\ \left(\frac{b}{h}\right)\sqrt{\Omega}\ . \qquad (4.4)$$

The expression for the power ratio in Equation (4.4) is proportional to the beam-plate depth ratio (q_2) and the beam breadth-plate depth ratio (b/h) as well as the frequency ratio $\Omega(=\omega/\omega_o)$. The estimate of power ratio given in Equation (4.4) can be compared to the exact ratio taken from Figure 3.11 as follows for the case of b = h.

Table 4.1

Power Ratios of Beam-Reinforced Plate
(Below Coincidence Frequency)

Depth Ratio $q_2 = h_b/h$	Stiffness Ratio I_b/bI	Power Ratio dB			
		Exact, $\Omega = 0.5$	Estimate, $\Omega = 0.5$	Exact, $\Omega = 1.0$	Estimate, $\Omega = 1.0$
1	1	0.6	1.4	1.0	3.0
1.8	5.6	1.0	3.3	2.2	4.4
3.7	45	2.0	6.6	5.0	8.6

The estimate of radiated power for beams which are shallow is within 2 dB of the exact solution. The plate impedance did not account for the fluid mass loading on the plate.

4.2.2 Excitation Frequency Above the Coincidence Frequency ($\Omega > 1$). The radiated acoustic pressure above the coincidence frequency has a peak at a specific azimuthal angle. The peak in the

radiated pressure from a point excited infinite isotropic plate occurs at the angle ϕ_c:

$$\sin \phi_c = \frac{1}{\sqrt{\Omega}} \text{ for } \Omega > 1 \quad . \tag{4.5}$$

The maximum pressure at the coincidence angle ϕ_c for an isotropic plate can be obtained by substituting Equation (4.5) into Equation (3.1) and setting $\bar{C}_{ms} = 1$, resulting in the following expression:

$$p_{max} = \frac{-i\, k_o\, F_o}{2\pi R} \left(1 - \frac{1}{\Omega}\right)^{1/2} e^{ik_o R} \quad . \tag{4.6}$$

When the plate is reinforced by an attached mass, stiffness or beam, the peak in the radiated pressure shifts in azimuthal angle and the maximum pressure changes in magnitude. There seems to be no closed form formulas for the prediction of the peaks or the azimuthal coincidence angles for reinforced plates.

(i) Influence of Mass: The influence of an infinite line mass on the radiated pressure is exhibited by the factor $\bar{C}_{ms}$ in Equation (3.1). If one sets $U_y = 0$ and obtains an approximate expression for the factor $I_1^o \mu_1 \gamma$, an approximate expression for $\bar{C}_{ms}$ valid for $\Omega > 1$ and $\phi = 0°$, can be obtained as follows:

$$\bar{C}_{ms} = \frac{1}{1 - \mu_1 I_1^o \gamma} \simeq \frac{1}{(1 + 0.09\gamma\Omega^{1/2}) - i(0.09\gamma\Omega^{1/2})} \quad . \tag{4.7}$$

Examination of the factor $\bar{C}_{ms}$, given in Equation (4.7), indicates tht it decreases monotonically with mass ratio and excitation frequency. This is clearly shown by the numerical results presented for the radiated pressure spectrum at $\phi = 0°$, shown in Figure 3.1. To obtain a crude estimate of the reduction in the radiated pressure at $\phi = 0°$,

one can resort to physical arguments. If the attached mass is spread over a wavelength λ and a new plate-mass surface density is computed and used in the expression for the radiation from an infinite isotropic plate, one may get a crude estimate for the pressure. Thus, the new surface mass density $\tilde{m}$ becomes:

$$\tilde{m} = m + \frac{M}{\lambda} = \rho h + \frac{\rho q_2 h^2}{\lambda} = m(1 + \frac{q_2 h}{\lambda}) \quad ,$$

where λ is the bending wavelength in the plate given by

$$\lambda = \frac{2\pi}{\sqrt{\omega_o}} \frac{1}{\sqrt{\Omega}} \alpha, \quad \alpha^4 = \frac{h^2 E}{12\rho(1-\nu^2)} \quad ,$$

$$\omega_o = c^2\sqrt{\frac{m}{D}} = \frac{\sqrt{12}}{h} \frac{c^2}{c_p} \quad \text{and} \quad c_p^2 = \frac{E}{\rho} \quad . \tag{4.8}$$

Thus, the new mass density $\tilde{m}$ becomes:

$$\tilde{m} = m(1 + \frac{\sqrt{3}}{\pi} \frac{c}{c_p} q_2 \sqrt{\Omega}) \quad . \tag{4.9}$$

The radiated pressure from an isotropic plate p_o can be written as follows:

$$p_o = \frac{-ik_o F_o}{2\pi R} \frac{e^{ik_o R} \cos\phi}{1 - \frac{ik_o m \cos\phi}{\rho_o}(1 - \Omega^2 \sin^4\phi)} \quad . \tag{4.10}$$

Thus, the ratio of the radiated pressure of a plate with an attached mass $\tilde{p}_o$ to that of an isotropic plate, p_o, computed at $\phi = 0°$ can be written as:

$$\left|\frac{\tilde{p}_o}{p_o}\right| = \left[\left(1 + \frac{k_o^2 m^2}{\rho_o^2}\right)\Big/\left(1 + \frac{k_o^2 \tilde{m}^2}{\rho_o^2}\right)\right]^{1/2} \quad . \tag{4.11}$$

The estimate given in Equation (4.11) can be compared to the exact solution shown in Figure 3.1 in the following table.

Table 4.2

Pressure Ratios of Mass-Reinforced Plate

Mass Ratio γ	$\tilde{p}_o/p_o$ in dB			
	Exact, $\Omega = 1.5$	Estimate, $\Omega = 1.5$	Exact, $\Omega = 2.5$	Estimate, $\Omega = 2.5$
1	0.8	0.6	1.0	0.8
10	6.5	4.6	8.2	5.8

Table 4.2 shows that the reduction of the radiated pressure spectrum at $\phi = 0°$ can reach 8 dB for a mass ratio of $\gamma = 10$. The table also shows that the crude estimate given by Equation (4.11) does not exceed 2.5 dB at the upper limit of mass and frequency ratios.

The directivity function for the radiated pressure has a peak at the same azimuthal angle. Since there is no way one can predict this angle analytically, a crude estimate of the coincidence angle can be made. It is clear that the mass would not alter the coincidence angle at the plane $\theta = 0°$; hence, the coincidence angle ϕ_c at $\theta = 0°$ plane is given by Equation (4.5). The directivity function will be most affected near or at the plane $\theta = 90°$. This is exhibited by Figures 3.3 and 3.6. If the attached mass is spread over a wavelength and the resulting mass density added to that of the plate, one can

obtain a new coincidence frequency $\tilde{\omega}_o$ as follows:

$$\tilde{\omega}_o = c^2 \sqrt{\frac{\tilde{m}}{D}} = \omega_o \sqrt{\frac{\tilde{m}}{m}} \quad . \tag{4.12}$$

Using the new coincidence frequency $\tilde{\omega}_o$ in the expression for the critical angle ϕ_c in Equation (4.5) results in

$$\sin \tilde{\phi}_c = \frac{1}{\sqrt{\Omega}} \left[1 + \frac{\sqrt{3}}{\pi} \frac{c}{c_p} q_2 \sqrt{\Omega}\right]^{1/4} \quad . \tag{4.13}$$

Equation (4.13) can be used to estimate the new coincidence angle $\tilde{\phi}_c$, which is then compared to the exact solution as exhibited in Figures 3.4 and 3.6. The comparison is shown in Table 4.3.

Table 4.3

New Coincidence Angles for Mass-Reinforced Plate

Mass Ratio γ	$\tilde{\phi}_c$ for $\Omega = 1.5$		$\tilde{\phi}_c$ for $\Omega = 2.5$	
	Exact	Estimate	Exact	Estimate
0	55°	55°	39°	39°
1	55°	56°	40°	40°
5	60°	62°	45°	44°
10	66°	70°	52°	48°

Comparison of the exact and estimated coincidence angles show a good agreement even at the high frequency and mass ratios. In general, an attached mass increases the magnitude of the coincidence angle $\tilde{\phi}_c$.

The magnitude of the pressure peak at the new coincidence angles decreases as γ increases at the plane $\theta = 0°$. This is due to the fact that at $\theta = 0°$, the expression for the ratio of the directivity functions of a plate with an attached mass to that of an isotropic plate is the same as that for $\phi = 0°$ given in Equation (4.7). In fact, comparison of these ratios at peak pressures gave the same dB levels as presented in Table 4.2. The magnitude of the pressure peak at $\theta = 90°$ cannot be predicted as easily as that at $\theta = 0°$. It can be seen from Figures 3.3 and 3.6 that the pressure peak for a plate with an attached mass can be higher or lower than that of an isotropic plate. It is apparent that the coefficient $\bar{C}_{ms}$ becomes very large when ϕ approaches $\tilde{\phi}_c$.

The radiated power from a plate with an attached mass is shown in Figure 3.9. The radiated power decreases with increasing attached-mass ratio γ, the reduction of the radiated power can be as high as 5 dB at $\Omega = 1.5$ and 3 dB at $\Omega = 2.5$ and $\gamma = 10$.

(ii) Influence of Stiffness: The influence of an infinite line stiffness on the radiated pressure is exhibited by the factor $\bar{C}_{ms}$ in Equation (3.1). If one sets $\gamma = 0$, and $\phi = 0°$, then $\bar{C}_{ms} = 1.0$, which indicates that the pressure spectrum at $\phi = 0°$ for a plate with an attached line stiffness, is the same as that for an isotropic plate.

The directivity function for the radiated pressure of a plate with an attached infinite line stiffness has a peak at some azimuthal angle. Since there is no way to predict this angle analytically, a crude estimate of the coincidence angle can be made. It is obvious that the line stiffness does not alter the coincidence angle at the

plane $\theta = 0°$, because the directivity function at $\theta = 0°$ is the same as that for an isotropic plate. The directivity function will be changed considerably near the plane $\theta = 90°$. This effect is exhibited in Figures 3.4 and 3.7. If the attached stiffness is spread over a wavelength λ and a new plate with a new stiffness is computed, the ratio of the stiffness of the reinforced plate $\tilde{D}$ to that of an isotropic plate D becomes:

$$\frac{\tilde{D}}{D} = 1 + q_2^2 \xi + \frac{3\xi(1+q_2^2)}{1+\xi} \quad , \tag{4.14}$$

where

$$\xi = q_2 h/\lambda = \frac{\sqrt{3}}{\pi} \frac{c}{c_p} q_2 \sqrt{\Omega} \ .$$

Using the ratio of the new stiffness $\tilde{D}$ to the isotropic stiffness D, a new coincidence frequency can be computed as follows:

$$\tilde{\omega}_o = c^2 \sqrt{\frac{\tilde{m}}{\tilde{D}}} = \omega_o \sqrt{\frac{D}{\tilde{D}}} \quad . \tag{4.15}$$

Using the new expression for $\tilde{\omega}_o$, a crude estimate of the coincidence angle $\tilde{\phi}_c$ is obtained as follows:

$$\sin \tilde{\phi}_c = \frac{1}{\sqrt{\Omega}} \left[1 + q_2^2 \xi + \frac{3\xi(1 + q_2^2)}{1+\xi}\right]^{-1/4} \quad . \tag{4.16}$$

Equation (4.16) was used to compute an estimate for the coincidence angles $\tilde{\phi}_c$ which are then compared with the exact values as presented in Figures 3.4 and 3.7. The comparison of the exact to the estimated value is presented in Table 4.4.

Table 4.4

New Coincidence Angles for Stiffness-Reinforced Plate

Stiffness Ratio q_2	$\tilde{\phi}_c$ for $\Omega = 1.5$		$\tilde{\phi}_c$ for $\Omega = 2.5$	
	Exact	Estimate	Exact	Estimate
0	55°	55°	39°	39°
0.37	50°	50°	38°	36°
1.85	25°	32°	19°	23°
3.7	17°	20°	12°	15°

Table 4.4 shows a good agreement between the estimated coincidence angles and those obtained by exact methods. It can be seen that an attached stiffness decreases the magnitude of the coincidence angle $\tilde{\phi}_c$.

The peak pressure in the directivity function generally decreases with increasing stiffness. This can be seen from Figures 3.4 and 3.7. The reduction in the peak pressure reaches 6 dB at $\Omega = 1.5$ and 11 dB at $\Omega = 2.5$ for $q_2 = 3.7$.

The radiated power from a plate with an attached infinite line stiffness was computed and shown in Figure 3.10. It can be seen that the radiated power decreases with increasing stiffness of the attached line stiffness. The reduction in radiated power reaches 4 dB at $\Omega = 1.5$ and 2.5 and $q_2 = 3.7$.

(iii) Influence of a Beam: The influence of an attached infinite beam on the radiated pressure is exhibited by the factor $\bar{C}_{ms}$ of Equation (3.1). Since the pressure spectrum at $\phi = 0°$ is only

influenced by the mass of the beam, nothing new can be added to the discussion already presented under Item (i) above, as can be seen in Figure 3.1.

The directivity function at the plane $\theta = 90°$ of the pressure has a peak at some azimuthal angle which cannot be predicted by analytical means. To obtain a crude estimate for the new coincidence angle, both the increased stiffness and mass can be distributed over a wavelength λ. The new coincidence frequency becomes

$$\tilde{\omega}_o = c^2\sqrt{\frac{\tilde{m}}{\tilde{D}}} = \omega_o\sqrt{\frac{\tilde{mD}}{mD}} \quad . \tag{4.17}$$

Thus, the new coincidence angle $\tilde{\phi}_c$ can be estimated by the equation

$$\sin\tilde{\phi}_c = \frac{1}{\sqrt{\Omega}}\left[\frac{1+\xi}{1 + q_2^2\xi + \frac{3\xi(1+q_2^2)}{1+\xi}}\right]^{1/4} , \tag{4.18}$$

where ξ was defined in Equation (4.14).

The expression in Equation (4.18) predicts an estimate of the new coincidence angles $\tilde{\phi}_c$, which is tabulated in Table 4.5. These estimates are compared to the exact values of ϕ_c obtained from Figures 3.5 and 3.8. A good agreement between estimated and exact values of $\tilde{\phi}_c$ is shown in Table 4.5. It can be seen from the results presented in Table 4.5 as well as the expression for $\tilde{\phi}_c$ in Equation (4.18) that the stiffness is more dominant than the mass of the beam. The dominance of the stiffness over the mass may be better understood in the light of Equations (4.17) and (4.18), since the mass increases linearly with the depth ratio q_2 but the stiffness increases with the third power of q_2.

Table 4.5

New Coincidence Angles for Beam-Reinforced Plate

Beam	$\tilde{\phi}_c$ for $\Omega = 1.5$		$\tilde{\phi}_c$ for $\Omega = 2.5$	
	Exact	Estimate	Exact	Estimate
$\gamma = 0$, $q_2 = 0$	55°	55°	39°	39°
$\gamma = 2.7$, $q_2 = 1.0$	40°	45°	30°	32°
$\gamma = 5$, $q_2 = 1.85$	32°	35°	23°	25°
$\gamma = 10$, $q_2 = 3.7$	25°	24°	18°	18°

The peak pressure at the coincidence angle $\tilde{\phi}_c$ cannot be predicted easily. One can observe that the peak pressure, in general, decreases with increasing mass and stiffness. The reduction in peak pressure at $\tilde{\phi}_c$ for the plane $\theta = 0°$ reaches 6.5 dB at $\Omega = 1.5$, 8 dB at $\Omega = 2.5$ for $q_2 = 3.7$. Similar reductions in the peak pressure at $\tilde{\phi}_c$ for the plane $\theta = 90°$ reaches 6 dB at $\Omega = 1.5$ and 12 dB at $\Omega = 2.5$ for $q_2 = 3.7$.

The radiated power from a plate with an attached beam was computed and shown in Figure 3.11. In general, the radiated power decreases with increasing stiffness and mass of a beam. Using the expression for the estimated radiated power given in Equation (4.4), the following results were obtained:

Table 4.6

Power Ratio of Beam-Reinforced Plate
(Above Coincidence Frequency)

Beam	Power Ratio (dB)			
	$\Omega = 1.5$		$\Omega = 2.5$	
	Exact	Estimate	Exact	Estimate
$\gamma = 2.7$, $q_2 = 1.0$	2.0	2.3	2.7	5.0
$\gamma = 5.0$ q_2 [illegible].85	3.7	5.3	4.6	6.5
$\gamma = 10.0$, $q_2 = 3.7$	6.6	9.7	7.6	13.6

The agreement between estimated and exact computation of the radiated power is within 3 dB for all beams at $\Omega = 1.5$ and within 6 dB for all beams at $\Omega = 2.5$. The deeper the beam, the worse the estimate became. However, the reduction in radiated power was shown to exceed 6 dB at $\Omega = 1.5$ and 8 dB at $\Omega = 2.5$ for the deep beam $q_2 = 3.7$.

4.2.3 Summary. In this section, a summary of the discussion in Section 4.2 is presented.

(i) Influence of an Attached Mass: In general, the attached mass reduces the radiated pressure spectrum at $\phi = 0°$ above and below the coincidence frequency by as much as 8 dB for a moderately heavy mass for $\Omega \leq 2.5$.

The directivity function is slightly influenced by an attached mass below the coincidence frequency. The directivity

function is highly influenced by the attached mass only near $\theta = 90°$, where the coincidence angle increased by as much as 13° at the upper limit of $\Omega = 2.5$. The peak of pressure could increase up to 2 dB.

The radiated power decreases with increasing mass of the attached line mass, reaching as high as 5 dB for a moderately heavy mass for $\Omega \leq 2.5$

(ii) Influence of an Attached Stiffness: The attached stiffness has no influence on the radiated pressure spectrum at $\phi = 0°$ above and below the coincidence frequency.

The directivity function is slightly influenced by an attached stiffness below the coincidence frequency. The directivity function is highly influenced by the additional line stiffness above the coincidence frequency only near $\theta = 90°$, where the coincidence angle decreased by as much as 38° at $\Omega = 1.5$ and by 27° at $\Omega = 2.5$. The peak pressure can be reduced by as much as 6 dB at $\Omega = 1.5$ and 11 dB at $\Omega = 2.5$.

The radiated power from a plate with an attached line stiffness reduces by only 2.5 dB below coincidence and by 4 dB above coincidence.

(iii) Influence of an Attached Beam: In general, the attached beam influences the radiated pressure spectrum at $\phi = 0°$ only through its mass, as was discussed in Item (ii) above.

The directivity function is slightly influenced by the attached beam below the coincidence frequency. The directivity function is highly influenced by the attached beam above the coincidence frequency, where the coincidence angle could decrease by as much as

30° at Ω = 1.5 and 21° at Ω = 2.5. It should be noted that the reason for the shift is primarily due to the stiffness of the beam (decreasing the angle) than to the mass of the beam (increasing the angle). The peak pressure can be reduced by as much as 6 dB at Ω = 1.5 and 12 dB at Ω = 2.5.

The radiated power from a plate with an attached beam generally decreases with increasing mass and stiffness of the beam. The reduction in radiated power reaches 5 dB below coincidence, which is primarily influenced by the mass of the beam rather than its stiffness. The radiated power reduction reaches 8 dB above coincidence which is primarily influenced by the stiffness of the beam rather than its mass.

4.2.4 Conclusion. The problem of reduction of the radiated noise from plates by attaching vibrating machinery to the beam was shown to be successful. This study was concerned with investigating the influence of the mass and/or stiffness of a beam on the radiated sound. Significant conclusions can be drawn from this study, especially in regard to the noise reduction problem. The main conclusions are:

(i) For excitation frequencies below the coincidence frequency, the peak pressure occurs at ϕ = 0°, which can be reduced significantly (approximately 8 dB) by using a massive beam with just the necessary stiffness dictated by structural design considerations. The radiated power was similarly reduced by this mechanism.

(ii) For excitation frequencies above the coincidence frequency, the peak pressure occurs at a new coincidence angle $\tilde{\phi}_c$. The peak pressure can be reduced significantly (approximately 12 dB)

by increasing the stiffness of the beam. The angle shift is not important, considering the large decrease in the peak pressure accompanying this shift. The reduction in radiated power can be reduced by as much as 8 dB by the use of a moderately stiff beam.

4.3 Far-Field Acoustic Radiation from Acoustically-Faired Beam-Reinforced Plate

The beam-reinforced plate discussed in Section 4.2 is now being acoustically faired to further reduce the radiated sound. The particular method of fairing employed in this study is done by attaching an infinite line sprung mass to each side of the reinforcing beam. Each sprung mass consists of a uniformly distributed mass per linear length m_1 and spring constant per unit length k_1 and located at a distance d from the beam. Thus, a parametric study of the radiated sound from an acoustically faired beam-reinforced plate can be made with the parameters defined by $m_1/\rho_o h^2$ representing the non-dimensional sprung mass, ω_1/ω_o ($\omega_1^2 = k_1/m_1$) the nondimensional natural frequency of the spring-mass system and $k_o d$ the nondimensional distance to the beam.

The expression for the radiated sound from an acoustically faired beam-reinforced plate is given in Equation (2.74). The expression contains a factor C_{ms} which takes into account the beam as well as the spring-mass systems. Since the sprung masses are symmetrically located with respect to the beam, they vibrate in phase with each other and give off a sound pressure similar to two line monopoles separated by distance 2d. The directivity of such a source term is exhibited by the term $\cos (k_o d \cos \theta \sin \phi)$.

If the forcing frequency ω is not close to the natural frequency ω_1, and if the separation distance is small compared to a wavelength, the two monopole line sources merge into one and the cosine term can be approximated by unity. The integrals I_3^o and I_2^o are approximately equal to I_1^o if $k_o d << 1$. Thus, the effect of the sprung masses on the directivity function is very minimal when $k_o d << 1$. If the distance between the sprung masses is much larger than a wavelength, i.e., $l_o d >> 1$, the integrals I_2^o and I_3^o become negligible and the cosine function oscillates rapidly. Thus, the effect of the sprung masses on the directivity function is again minimal. It is expected that, if $k_o d >> 1$, the sprung masses are too far to influence the near-field of the force and, hence, the radiated pressure field must be that of a vibrating beam-reinforced plate. This can be shown analytically if one neglects I_2^o and I_3^o with respect to I_1^o in Equation (2.74), where the expression for C_{ms} becomes $\bar{C}_{ms}$ of Equation (3.1).

If the excitation frequency ω is close to the tuning frequency ω_1, the expression for the radiated sound is given by Equation (3.5). At such a frequency, the line sprung masses become simple supports for the plate, allowing complete freedom of rotation but no transverse motion. Thus, the influence of sprung masses is very strong. If $k_o d << 1$, then the sprung masses, acting as simple supports, approach the excitation point and, consequently, the radiated sound becomes negligible. If $k_o d >> 1$, the supports are too far from the excitation point to influence the radiated field. The expression for $\bar{\bar{C}}_{ms}$ in Equation (3.5) reduces to $\bar{C}_{ms}$ for an excited beam-reinforced

plate given in Equation (3.1) if one lets I_2^o and I_3^o vanish. It is expected that when $k_o d \sim 0(1)$ the radiated power will increase because of the scattering of elastic waves at the supports.

Due to complexity of the acoustic fairing problem, and the large number of independent parameters that need varying, the geometry of the beam-reinforced plate was made constant. The beam parameters used in the numerical computations are $q_2 = 1$ and $\gamma = 2.7$.

In the subsequent discussions, numerical results for the acoustically faired beam-plate were compared to those for the beam-plate only.

The influence of the three parameters can be best discussed in the two frequency ranges: below and above the coincidence frequency.

4.3.1 Excitation Frequency Below the Coincidence Frequency ($\Omega < 1$). The influence of the parameters ω_1/ω_o, $m_1/\rho_o h^2$ and $k_o d$ on the radiated sound will be discussed in relation to ω/ω_1, where ω_1 is the tuning frequency of the spring-mass system. In the frequency range below $\Omega = 1.0$, the sprung mass located at $k_o d = \pi/5$ is always within, those at $k_o d = \pi$ and 3π are always outside a half-structural wavelength from the point of excitation.

(i) $\Omega < \omega_1/\omega_o \leq 1$: In this frequency range, the excitation frequency is below the tuning frequency ω_1, where the action of the sprung mass is mass controlled and the force transmitted to the plate is proportional to $m_1\omega^2$.

The influence of the separation distance $k_o d$ on the radiated pressure spectrum at $\phi = 0°$ is exhibited in Figures 3.13 and 3.14. It can be seen that a modest reduction is attainable when $k_o d = \pi/5$, but actually increases when $k_o d = \pi$ or 3π. The influence of the

separation distance $k_o d$ on the directivity function, shown in Figure 3.24, is predictably very marginal. The influence of the separation distance $k_o d$ on the radiated power is shown in Figures 3.41 and 3.42. The radiated power is somewhat reduced (1 to 2 dB) when $k_o d = \pi/5$, but raised even by a smaller amount when $k_o d = \pi$ or 3π.

The influence of the sprung mass $m_1/\rho_o h^2$ on the radiated pressure spectrum at $\phi = 0°$ is shown in Figures 3.18 and 3.20. Increasing the sprung mass ($m_1/\rho_o h^2 = 1$ to 5) generally decreases the pressure when $k_o d = \pi/5$ (Figure 3.18), the reduction reaches 3 dB when the sprung masses are close to the beam. The sprung masses have little influence on the pressure when their distance is far from the beam, as is shown in Figures 3.19 and 3.20. The influence of the sprung mass on the directivity function is minimal, as is shown in Figures 3.27 and 3.28. The influence of the sprung mass on the radiated power is shown in Figures 3.46 and 3.47. The radiated power decreases with increasing sprung mass (Figure 3.46) by as much as 4 dB when the sprung mass is close to the beam ($k_o d = \pi/5$). No noticable change in the radiated power is observed when the sprung masses are increased and their distance from the beam is far ($k_o d = 3\pi$) as shown in Figure 3.47.

The influence of the stiffness k_1 is indicated by the value of the tuning frequency ω_1. The influence of the stiffness on the pressure spectrum at $\phi = 0°$ is shown in Figures 3.15 and 3.17. The pressure decreases by 3 dB with increasing stiffness for $k_o d = \pi/5$, while it increases by 3 dB for $k_o d = \pi$ or 3π. The influence of the spring stiffness on the directivity function is minimal as shown in Figures 3.25 and 3.26. The influence of the spring stiffness on the

radiated power is shown in Figures 3.43 to 3.45. In general, increasing stiffness decreases the radiated power by 2 dB for $k_o d = \pi/5$, while no noticable reduction was observed when $k_o d = \pi$ or 3π, as anticipated earlier in Section 4.3

(ii) $\Omega \sim \omega_1/\omega_o \leq 1$: When the excitation frequency ω is close to the natural frequency ω_1, the expression for radiated sound is given by Equation (3.5). The discussion in Section 4.3 concluded that if $k_o d << 1$, the radiated sound is negligible and if $k_o d >> 1$, the radiated sound is independent of the sprung mass system.

The influence of the separation distance $k_o d$ on the radiated sound spectrum at $\phi = 0°$ when $\omega \sim \omega_1$ is shown in Figure 3.13. It can be seen that the reduction of pressure for $k_o d = \pi/5$ reaches 15 dB at $\Omega = \omega/\omega_1 = 1.0$. The pressure reduction is broadband, where at least a 6 dB reduction is achieved for frequencies $0.5 < \Omega < 1.2$. The radiated pressure actually increases when $k_o d = \pi$ or 3π, where a 6 dB increase is noticable. The influence of $k_o d$ on the directivity function is shown in Figure 3.21. While the directivity function is not affected at $k_o d = \pi/5$, except for a reduction in amplitude, the directivity functions for $k_o d = \pi$ or 3π have new peaks. These peaks in the azimuthal plane of the directivity function can be traced to the minor lobes of the directivity function of the cosine term. The influence of the separation distance $k_o d$ on the radiated power near $\omega \sim \omega_1$ is exhibited in Figure 3.41. The radiated power was reduced by as much as 20 dB when $k_o d = \pi/5$, and $\Omega = \omega/\omega_1 = 1.0$. The reduction is broadband, where 3 dB reduction in power can be

achieved for frequencies, $0.5 < \Omega < 1.2$. The radiated power actually increases (1 dB) when $k_o d = \pi$ or 3π.

Since the spring-mass systems act as rigid supports when $\omega = \omega_1$, they do not influence the radiated sound at all.

(iii) $\omega_1/\omega_o < \Omega \leq 1$: In this frequency range, the excitation frequency ω is above the tuning frequency ω_1, where the action of the sprung mass is stiffness controlled, and the force transmitted to the plate is proportional to displacement at $x = \pm d$.

The influence of the separation distance $k_o d$ on the radiated pressure spectrum at $\phi = 0°$ is shown in Figure 3.12. In this case, the radiated sound is reduced appreciably by as much as 10 dB when $k_o d = \pi$, but the radiated sound spectrum increased by as much as 10 dB when $k_o d = \pi/5$ or 3π. The influence of $k_o d$ on the radiated power is minimal in this frequency range, as is shown in Figure 3.40.

The influence of the sprung mass on the radiated pressure in this frequency range should be minimal, since the action of the sprung mass is stiffness controlled. This was borne out by the numerical computations for $\omega_1/\omega_o = 0.1$ and $m_1/\rho_o h^2 = 1$ to 5 at $k_o d = \pi/5$, π and 3π. These results are not presented in this thesis for lack of interesting phenomena and brevity, and similar calculations on the radiated power were computed and found not to vary when m_1 was increased fivefold.

The influence of the stiffness k_1 on the radiated sound spectrum at $\phi = 0°$ is exhibited in Figures 3.15 to 3.17. For ω_1/ω_o to increase from 0.1 to 1.0, the stiffness k_1 increased by a factor 100. The pressure spectrum increased by as much as 10 dB when $k_o d = \pi$, but decreased by as much as 8 dB when $k_o d = \pi/5$ or 3π. The influence

of the stiffness k_1 on the radiated power is shown in Figures 3.43 to 3.45, for $\omega_1/\omega_o = 0.1$. In the frequency range $0.1 < \Omega < 1$, the stiffness seems to have little influence on the radiated power.

4.3.2 Excitation Frequency Above the Coincidence Frequency ($\Omega \geq 1$): The influence of the three parameters of the sprung-mass on the radiated sound will be discussed in relation to ω/ω_1 again.

(i) $\omega_1/\omega_o > \Omega \geq 1$: In this frequency range, the sprung mass action is mass controlled and the transmitted force is proportional to the inertia of the sprung mass.

The influence of the separation distance $k_o d$ on the radiated pressure spectrum at $\phi = 0°$ is shown in Figure 3.14. For $\Omega < 2.5$, the separation distance $k_o d = \pi/5$ is within a half structural wavelength from the point of excitation in the plate. Thus, the radiated pressure spectrum is reduced by as much as 10 dB for $k_o d = \pi/5$. The influence of the separation distance on the directivity function is exhibited in Figure 3.30. The coincidence angle did not change in the plane $\theta = 0°$ as expected, and there is a reduction in the peak pressure by 4 dB when $k_o d = \pi/5$, but no major change when $k_o d = \pi$ or 3π. A major change in the coincidence angle and the peak pressure occurred at the plane $\theta = 90°$. The coincidence angle shifted up by 10° for $k_o d = \pi/5$ and by 14° for $k_o d = \pi$, both of which are within half a structural wavelength from the beam. The cause of the increase is the same as that of an attached mass, as discussed in Section 4.2.2. When the mass is outside a wavelength, as is the case for $k_o d = 3\pi$, one expects no change in the coincidence angle, as is shown in Figure 3.30. The influence of $k_o d$ on the radiated power is exhibited in Figure 3.42. The radiated power decreased when $k_o d = \pi/5$ by as much as 4 dB

for $\Omega \leq 2$. The radiated power for $k_o d = \pi$ and 3π at $\Omega = 1.5$ does not change noticeably.

The influence of the mass in the radiated pressure spectrum at $\phi = 0°$ is similar to the case when $\Omega < 1$. Similar reductions were attained (approximately 4 dB) when the sprung mass increased five times at $\Omega = 1.5$, $\omega_1/\omega_o = 2.5$ and $k_o d = \pi/5$. The influence of the sprung mass on the directivity function is minimal as to the shift in the angle of coincidence as well as the peak pressure. These numerical results were computed, but are not presented in the thesis. Increasing the sprung mass reduces radiated power at $\Omega = 1.5$, $\omega_1/\omega_o = 2.5$ and $k_o d = \pi/5$ by as much as 4 dB, while no such reduction is attained when $k_o d = \pi$ or 3π. These numerical results are not presented in the thesis.

The influence of the stiffness k_1 on the radiated pressure spectrum at $\phi = 0°$ is shown in Figures 3.15 to 3.17. The radiated pressure reduced by 14 dB at $\Omega = 1.5$ and 2.0 when $k_o d = \pi/5$ and the stiffness increased six fold. The pressure decreased by only 2 dB when $k_o d = \pi$ and 3π for the same increase in the stiffness. The influence of the stiffness is exhibited in Figures 3.31 and 3.33. In both figures, one can see that the coincidence angle did not shift at $\theta = 0°$. The coincidence angle did increase at $\theta = 90°$, due to the additional mass carried by the plate, especially when the sprung mass fell within a structural wavelength ($k_o d = \pi/5$, Figure 3.31) while it did not change much when $k_o d = 3\pi$, see Figure 3.33. The influence of the stiffness k_1 on the radiated power is shown in Figures 3.43 to 3.45. The radiated power decreased by as

much as 4 dB at $\Omega = 1.5$ when $k_o d = \pi/5$ but changed very little when $k_o d = \pi$ or 3π.

(ii) $\omega_1/\omega_o \sim \Omega \geq 1$: When the excitation frequency approaches the tuning frequency ω_1, each sprung mass becomes a simple line support for the plate. The discussion follows the same lines as the one given in Section 4.3.1. The radiated pressure is then independent of the mass or stiffness of the system but is dependent on the value of $k_o d$. If $k_o d \ll 1$, the radiated sound becomes negligible, and if $k_o d \gg 1$, even the distance $k_o d$ does not influence the radiated sound.

The influence of $k_o d$ on the radiated pressure spectrum at $\phi = 0°$ when $\omega \sim \omega_1$ is exhibited in Figures 3.13 and 3.14. In each case, the radiated pressure was reduced considerably when $k_o d = \pi/5$, by as much as 15 and 22 dB at $\omega_1/\omega_o = \Omega = 1.0$ and 2.5, respectively. The radiated pressure increased when $k_o d = 3\pi$, where the system is located well outside a structural wavelength for all frequencies up to $\Omega = 2.5$, by as much as 8 dB.

The influence of the separation distance $k_o d$ on the directivity function is exhibited in Figures 3.22 and 3.23. The coincidence angle and peak in the pressure is completely absent from the case $k_o d = \pi/5$ at $\theta = 0°$ and $\theta = 90°$ and the frequencies $\Omega = 1.5$ and 2.5. The influence of larger values of $k_o d$ is negligible when $\theta = 0°$ but can shift up or down depending on the value of $k_o d$. One should note that, unlike the discussion in Item (i) above, the sprung mass no longer contributes to the surface mass density of the plate and, hence, a physical reasoning cannot be made to account for the shift in the angle of coincidence. The peak pressure reduced by as

much as 18 dB for $\theta = 0°$ and 25 dB for $\theta = 90°$ when $k_o d = \pi/5$ and $\Omega = 1.5$ or 2.5, while it increased by 1 dB at $\Omega = 1.5$ and 7 dB at $\Omega = 1.5$ for $k_o d = 3\pi$. The influence of $k_o d$ on the radiated power is shown in Figures 3.41 and 3.42. The radiated power generally decreased by 16 dB at $\Omega = 1$ and 23 dB at $\Omega = 2.5$ when $k_o d = \pi/5$. The radiated power actually increased when $k_o d = \pi$ or 3π by as much as 3 dB at $\Omega = 1.5$ and 2.5.

(iii) $\Omega > \omega_1/\omega_o \geq 1$: In this frequency range, the sprung masses are stiffness controlled. As ω/ω_1 increases without limit, it can be seen from Equation (2.74) that the effect of the sprung masses will be negligible and the acoustically faired reinforced plate will behave as if the sprung masses are absent.

The influence of the separation distance $k_o d$ on the radiated spectrum at $\phi = 0°$ is illustrated in Figure 3.13. Comparison of the spectra when $\omega_1/\omega_o = 1.0$ shows that regardless of the distance $k_o d$, they all approach the spectrum for beam-reinforced plates from above as Ω increases. The influence of $k_o d$ on the directivity function is shown in Figure 3.35. In this case, when $\Omega = 2.5$ and $\omega_1/\omega_o = 1.0$, the distance $k_o d$ has negligible effect on the angle of coincidence as well as the peak pressure. The influence of the distance $k_o d$ on the radiated power is shown in Figure 3.41. Again, the radiated power is not altered significantly for all values of $k_o d$.

The influence of the sprung mass m_1 on the radiated pressure spectrum at $\phi = 0°$ becomes minimal as $\Omega >> \omega_1/\omega_o$, as can be seen in Figures 3.18 through 3.20, where the spectra for m_1 approach the beam-plate spectrum from above. The influence of the mass m_1 on the directivity function is exhibited in Figures 3.37 and 3.39.

In each case, the mass has no influence on the angle of coincidence or on the peak pressure. The influence of the sprung mass on the radiated power also diminishes as Ω increases, as is shown in Figure 3.46, where the power spectrum for the sprung mass approaches the power spectrum for the beam-plate from above.

The influence of the stiffness on the radiated pressure spectrum at $\phi = 0°$ also becomes negligible as Ω becomes larger then ω_1/ω_o, as is shown in Figures 3.16 and 3.17. The influence of the stiffness k_1 on the directivity function is exhibited by Figures 3.36 and 3.38. The directivity function for $\omega_1/\omega_o = 1.0$ is very close to that for $\omega_1/\omega_o = 0$ (no sprung mass), where the angle of coincidence and the peak pressure changed very little. The influence of the stiffness on the radiated power is shown in Figures 3.44 and 3.45 where the comparison is to be made on the power spectrum for $\omega_1/\omega_o = 1.9$. In each case, the power spectrum approaches that of a beam-reinforced plate from above as Ω increases.

4.3.3 Summary. In this section, a summary of the discussions carried out in Section 4.3 is presented. The summary will be present in the three frequency ranges $\omega_1/\omega < 1$, ~ 1, and > 1.

(i) $\omega_1/\omega_o > \Omega$: In this frequency range, the sprung mass's action is mass like.

Below the coincidence frequency, the most important parameter that influences the radiated sound is the separation distance $k_o d$. If $k_o d = \pi/5$ is well within half a structural wavelength for $\Omega > 0.1$, the radiated pressure and power spectrum decreases with increasing mass m_1 or stiffness k_1. If $k_o d = 3\pi$, well outside a structural wavelength for $\Omega < 2.5$, the radiated sound

usually increases with increasing sprung mass m_1 or stiffness k_1. The influence of all the parameters on the directivity function is minimal.

Above the coincidence frequency, the same can be said for the radiated sound pressure and power spectrum. The only change that is different is the influence of the sprung mass on the angle of coincidence. The angle usually increases if $k_o d$ is within a structural wavelength from the beam, primarily due to the added mass effect, and is negligible if $k_o d$ is outside a structural wavelength.

(ii) $\omega_1/\omega_o \sim \Omega$: If the excitation frequency ω is close to the natural frequency of the sprung mass ω_1, the sprung masses become simple supports. Hence, the mass m_1 and stiffness k_1 has no influence on the radiated pressure. Thus, if the distance $k_o d$ is small compared to structural wavelength, then the radiated pressure spectrum can decrease by as much as 15 dB below coincidence and by 22 dB above coincidence. The reduction is broadband about the frequency $\omega = \omega_1$, extending to over an octave for a 6 dB reduction. The radiated pressure actually increases by as much as 6 dB if $k_o d$ represents a distance outside a half structural wavelength. The reduction in the pressure is achieved over the whole azimuthal plane, so that the radiated power does reduce by as much as 20 dB below coincidence and 16 dB above coincidence.

(iii) $\omega_1/\omega_o < \Omega$: In this frequency range, the sprung mass's action is stiffness controlled. As the frequency of excitation Ω increases over the tuning frequency ω_1/ω_o, the influence of the sprung mass diminishes, as was expected when the analytical solution was examined. Thus, the radiated pressure and power spectra for an

acoustically faired beam-reinforced plate approach those for a beam-reinforced plate from above as $\Omega >> \omega_1/\omega_o$. The directivity function is also unaffected when $\Omega >> \omega_1/\omega_o$.

4.3.4 Conclusion. The problem of reduction of the radiated noise from reinforced structures was attempted by employing a method of acoustic fairing where an infinite line sprung mass is added to each side of the reinforcement. After an exhaustive number of parametric numerical results were computed, only a small portion of which were presented in this thesis, the main conclusions are presented below:

(i) To achieve a reduction in the radiated pressure and power spectra, it is recommended that the acoustic fairing is applied to within half a structural wavelength from the reinforcing beam.

(ii) To achieve a broadband noise reduction, the sprung-mass system employed in the acoustic fairing must be tuned, such that its natural frequency is close to the frequency around which a reduction is desired. This tuning provides as much as 25 dB noise reduction at the desired frequency. The tuning normally provides for almost an octave, (centered) at the desired frequency, where at least 6 dB noise reduction is achieved.

(iii) Structural discontinuities of any kind usually increase the radiated pressure and power in the frequency range below $\Omega = 2.5$ if they are located outside a structural half wavelength. Thus, such discontinuities are to be avoided if at all possible, if one desires to reduce the radiated noise below $\Omega = 2.5$.

BIBLIOGRAPHY

1. G. L. Lamb, Jr., Input Impedance of a Beam Coupled to a Plate, J. Acoust. Soc. Amer., 33:5, 1961.

2. E. E. Ungar, Transmission of Plate Flexural Waves Through Beams: Dynamic Stress Concentrations, J. Acoust. Soc. Amer., 33:5 1961.

3. R. H. Lyon, Sound Radiation from a Beam Attached to a Plate, J. Acoust. Soc. Amer., 34:9, 1962.

4. E. L. Shenderov, Transmission of Sound Through a Thin Plate with Interjacent Supports, Sov. Phys.-Acoust., 9:3, 1964.

5. D. D. Plakhov, Transmission of a Sound Wave Through a Laminated Plate Reinforced with Stiffness Members, Sov. Phys.-Acoust., 14:1, 1968.

6. I. I. Klyukin and Y. D. Sergeev, Scattering of Flexural Waves by Anti-Vibrators on a Plate, Sov. Phys.-Acoust., 10:1, 1964.

7. V. T. Lyapunov, Flexural Wave Propagation in a Liquid-Loaded Plate with an Obstruction, Sov. Phys.-Acoust., 14:3, 1969.

8. I. P. Konovalyuk, Diffraction of a Plane Sound Wave by a Plate Reinforced with Stiffness Members, Sov. Phys.-Acoust., 14:4, 1969.

9. V. N. Romanov, Investigation of a Plate T-Junction in a Diffuse Flexural Wave Field, Sov. Phys.-Acoust., 15:2, 1969.

10. G. Maidanik and E. M. Kerwin, Jr., Acoustic Radiation from Ribbed Plates Including Fluid-Loading Effects, BBN Rpt. No. 1024, Contract No. Nobs 86680, 1963.

11. E. S. Jarmul, Sound Radiation from Simple and Ribbed Plates, M.S. Thesis, The Pennsylvania State University, 1970.

12. D. S. Pallett, Application of Statistical Methods to the Vibration and Acoustic Radiation of Fluid Loaded Cylindrical Shells, Ph.D. Thesis, The Pennsylvania State University, 1972.

13. M. S. Howe and M. Heckl, Sound Radiation from Plates with Density and Stiffness Discontinuities, J. Sound and Vibration, 21:2, 1972.

14. M. C. Junger, and D. Feit, Sound, Structures, and Their Interaction, The MIT Press Cambridge, Massachusetts, and London, England, 1972.

15. E. J. Skudrzyk, Simple and Complex Vibratory Systems, The Pennsylvania State University Press, University Park, Pennsylvania, 1968.

16. E. J. Skudrzyk, Foundation of Acoustics, The Pennsylvania State University Press, University Park, Pennsylvania, 1972.

17. M. C. Junger, Normal Modes of Submerged Plates and Shells, Part II Acoustic Interaction Problems in Fluid-Solid Interaction, The Am. Soc. of Mech. Engrs., 1967.

18. V. S. Vladimirov, Equations of Methamtical Physics, Marcel Dekker, Inc., New York, 1971.

19. P.A.M. Dirac, The Principles of Quantum Mechanics, Clarendon Press, Oxford, 1947.

20. L. Schwartz, Theorie des Distributions, Hermann and Cie, Paris, 1950.

21. B. Friedman, Principles and Techniques of Applied Mathematics, John Wiley and Sons, Inc., New York, 1956.

22. D. Pilkey, Integrals of Singularity Functions and Applications to the Mechanics of Deformable Solids, Ph.D. Thesis, The Pennsylvania State University, 1962.

23. L. M. Brekhovskikh, Waves in Layered Media, Academic Press Inc., New York, 1960.

24. E. T. Copson, Asymptotic Expansions, Cambridge University Press, 1967.

25. A. Erdelyi, Asymptotic Expressions, Dover Publications, New York, 1956.

26. A. Sommerfeld, Partial Differential Equations in Physics, Academic Press, New York, 1964.

27. A. D. Stuart, Acoustic Radiation from a Point Excited Infinite Elastic Plate, Ph.D. Thesis, The Pennsylvania State University, 1972.

28. G. F. Carrier, M. Krook, and C. E. Pearson, Functions of a Complex Variable, McGraw-Hill Book Company, 1966.

29. W. M. Ewing, W. S. Jardetzky, and F. Press, Elastic Waves in Layered Media, McGraw-Hill Book Company, 1957.

UNCLASSIFIED

Security Classification

DOCUMENT CONTROL DATA - R & D

(Security classification of title, body of abstract and indexing annotation must be entered when the overall report is classified)

1. ORIGINATING ACTIVITY (Corporate author)	2a. REPORT SECURITY CLASSIFICATION
Applied Research Laboratory University Park, Pennsylvania	Unclassified
	2b. GROUP

3. REPORT TITLE

Acoustic Fairing - An Application to Beam Reinforced Plates

4. DESCRIPTIVE NOTES *(Type of report and inclusive dates)*

Ph.D. Thesis, Engineering Mechanics, December 1973

5. AUTHOR(S) *(First name, middle initial, last name)*

Gau. F. Lin

6. REPORT DATE	7a. TOTAL NO. OF PAGES	7b. NO. OF REFS
August 23, 1973	175	29

8a. CONTRACT OR GRANT NO.	9a. ORIGINATOR'S REPORT NUMBER(S)
N00017-73-C-1418	TM 73-196
b. PROJECT NO.	
c.	9b. OTHER REPORT NO(S) *(Any other numbers that may be assigned this report)*
d.	

10. DISTRIBUTION STATEMENT

Approved for Public Release. Distribution unlimited.
Per NAVORD - September 11, 1973

11. SUPPLEMENTARY NOTES	12. SPONSORING MILITARY ACTIVITY
	Naval Ordnance Systems Command Department of the Navy

13. ABSTRACT The radiated sound from a beam reinforced plate excited by a point force is investigated. The point force is located on the reinforcing beam, simulating a standard method of supporting vibrating machinery by plate structures. The radiated pressure spectrum of excited reinforced plates was reduced by as much as 6 dB for moderately stiff beams. The radiated power generally decreased with increasing mass and stiffness of the reinforced beam, reaching by as much as 8 dB for excitation frequencies above the coincidence frequency. The angle of coincidence usually increased with increasing mass and decreased with increasing stiffness of the reinforcing beams. The peak pressure at the coincidence angle could be reduced by as much as 12 dB by judicious choice of the geometry of a reinforcing beam, whose dimensions are generally dictated by structural design considerations.

A method of adding other structural discontinuities to further reduce the radiated noise was also investigated. This is referred to as Acoustic Fairing in this thesis. The procedure thus employed consists of a pair of infinite line sprung masses, where one is located on each side of the reinforcing beam. The radiated sound from point excited reinforced plates with acoustic fairing was investigated and a parametric study was completed. It was found that a modest 2-4 dB reduction in the radiated pressure and power can be attained if the sprung mass is located within a half structural wavelength from the beam. In addition, if the tuning frequency of the sprung mass is close to the excitation frequency, reduction of the radiated pressure and power of the order 15-22 dB were realized. The reduction thus achieved was also broad band, extending over an octave centered at the tuning frequency. If the sprung mass is located outside a structural wavelength from the beam, an increase in the radiated pressure and power

DD FORM 1 NOV 65 1473 (PAGE 1) PLATE NO. 21856

S/N 0102-014-6600

UNCLASSIFIED

Security Classification

14. KEY WORDS	LINK A		LINK B		LINK C	
	ROLE	WT	ROLE	WT	ROLE	WT
ACOUSTIC FAIRING	8					
BEAM-REINFORCED PLATES	8					
PRESSURE SPECTRUM	8					
RADIATED NOISE	8					
STRUCTURAL DISCONTINUITIES	8					
VIBRATION	8					

13. ABSTRACT (continued):

results, primarily through scattering of elastic waves at the sprung mass junctions. The effectiveness of the sprung masses, regardless of their location with respect to the beam, is vastly reduced when the excitation frequency is much higher than the tuning frequency. The effectiveness of the sprung masses also diminishes when they are located too many wavelengths away from the beam.

DISTRIBUTION

Commander (ORD 632)
Naval Ordnance Systems Command
Department of the Navy
Washington, D. C. 20360 — Copies 1 and 2

Commander (ORD 34B)
Naval Ordnance Systems Command
Department of the Navy
Washington, D. C. 20360 — Copies 3 and 4

Defense Documentation Center
5010 Duke Street
Cameron Station
Alexandria, Virginia 22314 — Copies 5 through 16

Via: Commander (ORD 632)
Naval Ordnance Systems Command
Department of the Navy
Washington, D. C. 20360